

FUNCTIONAL MATERIALS – SYNTHESSES, CHARACTERISATION AND CATALYTIC APPLICATIONS

PhD Dissertation

MÓNIKA SIPICZKI



Supervisors:

DR. PÁL SIPOS

DR. ISTVÁN PÁLINKÓ

Doctoral School of Chemistry

Material and Solution Structure Research Group

Department of Inorganic and Analytical Chemistry

Department of Organic Chemistry

Faculty of Science and Informatics | University of Szeged

Szeged

2013

TABLE OF CONTENTS

1.	Introduction.....	4
2.	Literature review	5
2.1.	Structure of the layers	6
2.2.	Iron-based layered double hydroxides	8
2.3.	Interlamellar anions.....	10
2.4.	Preparative chemistry of anion-intercalated layered double hydroxides	11
2.4.1.	Co-precipitation methods	11
2.4.2.	The urea hydrolysis method	13
2.4.3.	Anion-exchange method	13
2.4.4.	Dehydration-rehydration (reconstruction) method	14
2.5.	Applications of layered double hydroxides	16
2.5.1.	Catalytic applications	16
2.5.2.	Environmental applications.....	19
2.5.3.	Additives for polymers.....	20
2.5.4.	Pharmaceutical and cosmetic applications.....	21
3.	The main aims of the dissertation	23
4.	Experimental part.....	24
4.1.	Materials.....	24
4.2.	Preparation of concentrated and carbonate-free NaOH solution	25
4.3.	Synthesis of the layered double hydroxides.....	25
4.4.	Intercalation of the layered double hydroxides.....	25
4.5.	Immobilisation of L-proline in functionalised chloropropylated silica gel	26
4.6.	Heterogeneous catalytic reactions.....	26
4.7.	Instrumentation and characterisation methods.....	27
4.7.1.	X-ray diffractometry	27
4.7.2.	Thermal analytical measurements.....	27
4.7.3.	ICP–OES measurements	27
4.7.4.	Microscopic techniques.....	27
4.7.5.	Mössbauer spectroscopy	28

4.7.6.	XAS measurements	28
4.7.7.	UV-Vis spectroscopy	32
4.7.8.	FT-IR spectroscopy	32
4.7.9.	Molecular modelling	32
4.7.10.	Gas chromatography	32
5.	Results and discussion	33
5.1.	Preparation and characterisation of Ca(II)Fe(III)- and Mg(II)Fe(III) layered double hydroxides	33
5.2.	Intercalation into the Ca ₃ Fe-LDH	46
5.3.	The application of pristine CaFe-LDH as a catalyst in an epoxidation reaction	60
5.4.	Preparation of immobilised organocatalysts and their application in cross-aldol dimerisation.....	65
5.4.1.	Composite materials as catalysts for aldol dimerisation reactions	67
6.	Conclusions.....	72
7.	References	75

1. INTRODUCTION

Synthetic inorganic materials with well-defined structures and tailor-made functionalities exhibit useful properties for the solution of today's environmental and industrial problems and for the design of novel composites used in advanced technological processes. Among the several classes of lamellar solids, layered double hydroxides are of particular interest since they qualitatively resemble the conventional intercalation compounds with nanoscale periodicity and complete charge separation between the gallery ions and the layers. Significant progress has been made in the synthesis of layered double hydroxides with new compositions and morphologies over the last decade allowing improved applications in many areas. In this work, the catalytic properties of the uncalcined and intercalated varieties are demonstrated. Other functionalised solids like those displayed in this work can also have many applications. Once again their catalytic properties are highlighted in the dissertation.

2. LITERATURE REVIEW

Layered double hydroxides (LDHs) are a group of anion-intercalated inorganic functional materials which are also known as anionic clays. These materials are not so prevalent in nature as the well-known cationic clays, but are very easy to prepare and they are inexpensive. The first natural mineral belonging to this family of materials was discovered in Sweden in 1842, and is known as hydrotalcite.¹ It has the formula of $\text{Mg}_6\text{Al}_2(\text{OH})_{16}\text{CO}_3 \cdot 4\text{H}_2\text{O}$. Since hydrotalcite is one of the most representative minerals of the group, the LDHs are also called ‘hydrotalcite-like compounds’ (HTlc), even though other natural as well as artificial structural varieties also exist. The structure of hydrotalcite is related to that of brucite, $\text{Mg}(\text{OH})_2$ which consists of Mg^{2+} ions octahedrally surrounded by hydroxide ions. These octahedral units form infinite layers by sharing edges, with the O–H bond perpendicular to the plane of the layers.² In the lattice of LDHs, trivalent M(III) cations (*i.e.*, Al^{3+} in hydrotalcite) substitute some of the Mg^{2+} cations in the brucite layers resulting in positively charged host layers, while in the interlamellar area A^{n-} anions are located in hydrated interlayer galleries to maintain electroneutrality. The host layers are stacked on top of one another to form a three-dimensional structure. The general formula for other members of the family, based on a combination of divalent and trivalent metal cations, can be written as $[\text{M}(\text{II})_{1-x}\text{M}(\text{III})_x(\text{OH})_2]^{x+}[\text{X}^{m-}_{x/m} \times n\text{H}_2\text{O}]^{x-}$, where $[\text{M}(\text{II})_{1-x}\text{M}(\text{III})_x(\text{OH})_2]^{x+}$ represents the layer, and $[\text{X}^{m-}_{x/m} \times n\text{H}_2\text{O}]^{x-}$ the interlayer compositions (*Figure 1*). The divalent and trivalent metal cations found in layered double hydroxides belong mainly to the third and fourth periods of the table of elements (divalent cations: Mg, Mn, Fe, Co, Ni, Cu, Zn; trivalent cations: Al, Mo, Fe, Co, Cr, Ga) The ionic radii are mostly in the range 0.65–0.80 Å for divalent cations and 0.62–0.69 Å for trivalent ones (there are some exceptions like Al: 0.50 Å and Ba: 1.49 Å).³ Tetravalent cations such as Zr^{4+} and Sn^{4+} can also be incorporated into the layers.⁴ Only one example is known of LDH structure with monovalent cation, the LiAl_2 -LDH that is. It has been speculated that the ionic radii of M(II) and M(III) and the difference between them,^{5,6} as well as the solubility products⁷ of $\text{M}(\text{II})(\text{OH})_2$ and $\text{M}(\text{II})\text{CO}_3$, play roles in defining the boundaries of the range of metal cations that can form LDHs.

Many researchers have suggested^{5,8} that pure LDH phases can only be formed for stoichiometries in the

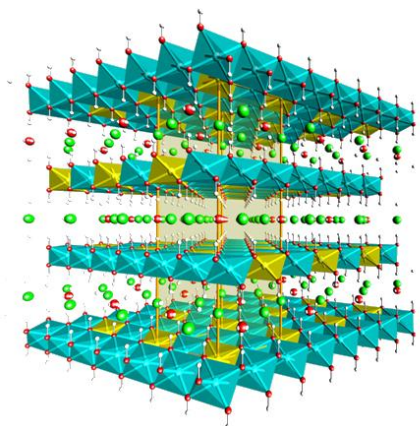


Figure 1. The schematic structure of a layered double hydroxide (LDH).

range $0.20 < x < 0.33$, corresponding to M(II)/M(III) molar ratios in the range 2–4. For $x > 0.33$, the presence of M(III)–OH–M(III) linkages is unavoidable and this is energetically unfavourable due to the strong repulsion between the adjacent trivalent cations.^{9,10}

2.1. Structure of the layers

In layered double hydroxides, the octahedral environment of metallic cations is far from being a regular polyhedron. The octahedra are significantly flattened along the stacking direction, lowering the symmetry from O_h to D_{3d} , as illustrated in *Figure 2* for a ZnAl-LDH. The higher is the metal ionic radius, the more flattened are the octahedra with lowering of the layer thickness h and an increase of the distance a between metals – which is the same as the one between the OH groups on the same side of the layer.¹¹ All brucite-like metal hydroxides show this type of distortion,^{12,13} which results in hexagonal symmetry (space group P-3m1). The weak forces between the layers of brucite have been attributed to contributions from dispersion forces and hydrogen bonding.^{2,14}

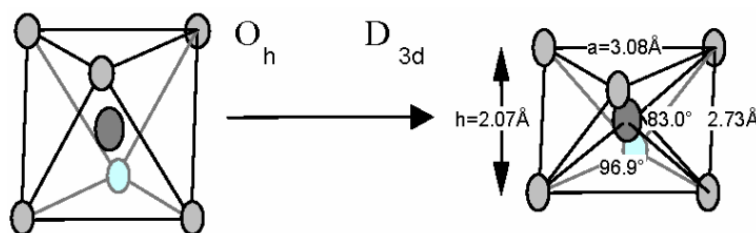


Figure 2. Flattening of the $M(OH)_6$ octahedron in a ZnAl-LDH.

Layered materials are characterised by strong polar covalent bonding along two dimensions and weak bonding along the third dimension, which is also the stacking direction. Given the weak bonding between layers, the layers can stack, in a multiplicity of patterns, called stacking sequences, to yield different polytypes. Polytypism is best defined as polymorphism in one dimension. All polytypes can be classified in the frame of the number of stacked sheets along the c axis in the unit cell. The brucite-like layers in LDHs may be stacked in various ways, giving rise to a variety of possible polytype structures. If the opposing OH groups lie vertically above one another; an interlayer with a trigonal prismatic arrangement is resulted, whilst an octahedral arrangement is formed if they are offset.¹⁵ There are three possible two-layer polytypes with hexagonal stacking of the layers, denoted as $2H_1$, $2H_2$, and $2H_3$ where the $2H_1$ polytype has all prismatic interlayers and the $2H_2$ polytype has all octahedral interlayers while both types of interlayers are present in the $2H_3$ polytype. There are nine possible three-layer polytypes of which two have rhombohedral symmetry— $3R_1$ and

$3R_2$ – while the remaining seven ($3H_1$ – $3H_7$) have hexagonal symmetry. The $3R_1$ polytype has all prismatic interlayers; $3R_2$, $3H_1$, and $3H_2$ have all octahedral interlayers and other polytypes involve both types. The various possible six-layer polytypes with rhombohedral ($6R$) and hexagonal symmetry ($6H$) have also been described.^{15,16} Hydrotalcite [$MgAl(CO_3)$ -LDH] has the $3R_1$ polytype structure, which most other carbonate-containing LDHs also adopt,¹¹ since the prismatic arrangement of hydroxyl groups facilitates hydrogen bonding with the oxygen atoms of the CO_3^{2-} anion and the interlayer water molecules. It is difficult to distinguish between the various polytypes, since the intensities of reflections in the XRD pattern of an LDH are sensitive to the interlayer anion.

If the radius of one of the metallic cations becomes too high, the octahedral coordination is lost by opening one side of the octahedron on the interlamellar domain leading to additional coordination with one interlamellar water molecule. The symmetry around the metal is lowered from D_{3d} to C_{3v} . Such behaviour is observed in minerals from the hydrocalumite group. For CaAl-based layers, three different short range distances are observed¹¹ around calcium: 3 Ca–OH at 2.375 Å, 3 Ca–OH at 2.455 Å, and 1 Ca–OH₂ at 2.497 Å. The structure is based on corrugated brucite-like main layers with an ordered arrangement of Ca(II) and M(III) ions, seven- and six-coordinated, respectively, the seventh apex of the Ca-polyhedron is a water molecule from the interlayer. The composition of the hydroxide layer of this structure type is limited; the divalent and trivalent cations are typically Ca^{2+} and Al^{3+} . These lamellar calcium aluminium hydroxides salts have been studied in detail, for they occur in the hydration process of cement compounds.¹⁷ The replacement of Al^{3+} by Fe^{3+} , Cr^{3+} , Ga^{3+} , and Ca^{2+} by Cd^{2+} have been reported but only few data are available on these phases.¹⁸ Several rhombohedral space groups, a monoclinic one and the two triclinic space groups have been observed for synthetic monoanionic tetracalcium aluminates. In the rhombohedral space groups $R-3$ and $R-3c$, the water molecules linked to Ca atoms are on the straight line passing through the Ca atoms and perpendicular to the (001) plane (Figure 3).

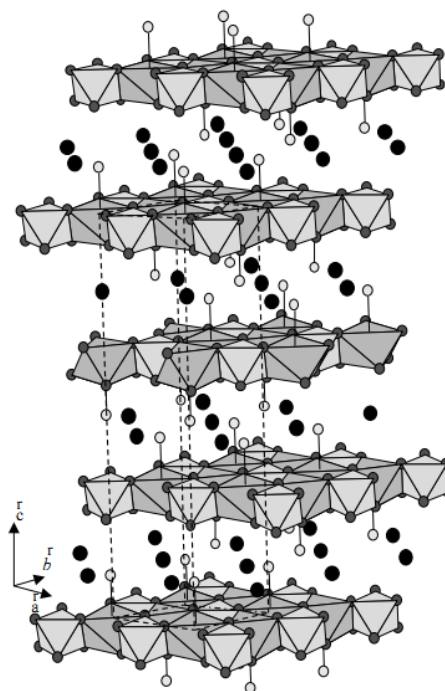


Figure 3. Crystal structure of $Ca_2Al(OH)_6Cl \cdot 2H_2O$, in $R-3$ space group.

The neighbouring brucite-like layers may be stacked in two different ways building two kinds of interlayers: either OH groups form prisms resulting in a three-layer polytype (3R) and the R-3 unit cell or they form octahedra resulting in a six-layer polytype (6R) and the R-3c unit cell. As already noticed,¹⁹ the change of space group from R-3 to R-3c depends on the size of the anions. Indeed, chloride compound crystallizes in the space group R-3c, larger anions like iodine and sulphate compounds crystallize in R-3 while intermediate anions like bromide exhibit both unit cells.

The replacement of Al^{3+} cations by larger M^{3+} cations in hydrocalumites results in a linear variation of the unit-cell parameters: a increases and c decreases as the $\text{M}^{3+}\text{--OH}$ bond length increases. In the octahedral layer, the accommodation of longer $\text{M}^{3+}\text{--OH}$ distances proceeds like in hydrotalcite-like compounds, *i.e.*, by flattening the $\text{M}^{3+}(\text{OH})_6$ octahedra along the c -axis in order to minimise the repulsion between cations.²⁰ This distortion evidenced by the HO--M(III)--OH bond angle values given by Rousselot *et al.*²¹ The overall effect on these octahedral layers is thus a compression in the c direction and an elongation in the (a, b) plane.

2.2. Iron-based layered double hydroxides

For natural LDHs the chemical composition is the main fundamental characteristic feature to distinguish individual minerals and to name them. At present, the following major cation compositions have been recognized among natural layered double hydroxide minerals: MgAl (hydrotalcite-manasseite), MgFe (pyroaurite-sjögrenite), NiFe (honessite-reevesite), NiAl (takovite), CuAl (woodwardite), MgCr (stichtite), *etc.* A particular type of LDHs which contains only iron as a cation in the brucite-type layers is called green rust, Fe(II)Fe(III)-LDH that is. If we focus on the layered double hydroxides synthesised in laboratory, we found that a diverse combination of $\text{M}^{2+}\text{--M}^{3+}$ cations in the LDH host sheets has been extensively pursued, and can be routinely attained through a convenient co-precipitation of corresponding di- and trivalent metal salts under alkaline conditions. This in fact yields a large family of LDHs. Nevertheless, the research interest on LDH materials has been traditionally driven and predominated by M(II)–Al(III) category, particularly $\text{Mg}^{2+}\text{--Al}^{3+}$, partly due to the fact that hydrotalcite is a widely known anionic clay found in nature. In addition, the amphoteric feature of Al^{3+} also plays a very favourable role in promoting the precipitation and crystallisation of Al-based LDHs. By virtue of this amphoteric feature, well-crystallized M(II)Al(III)-LDH crystallites have been readily synthesised.

Without the incorporation of amphoteric Al^{3+} into the host sheet, it is more difficult to synthesise LDH in a highly crystalline form. Consequently, non-Al(III) LDHs remain as the least explored category. Relatively few articles describe the structures of the layers in iron-containing layered double hydroxides.^{22,23,24,25} It is surprising, since Fe(III)-based layered double hydroxides can be prosperous, especially if used in catalysis. In aqueous media the iron(III) ion is water-soluble in a much narrower pH range than aluminium(III) ions. Al^{3+} ion is considered toxic (*e.g.*, thought to be related to the development of Alzheimer-disease), thus its biological applications are highly restricted. The variable valence of iron is well-known and, therefore, the iron-containing layered double hydroxides may be important in catalysis. Another advantage of iron-containing layered double hydroxides, that they can be converted into magnetisable materials, which can lead some non-conventional applications. It has to be noted, however, that in industrial applications the amphoteric properties of aluminium may also play a role, since in highly alkaline medium the Al(III)-containing layered double hydroxides are not stable.

It is worth mentioning that many of the experimental methods (for example Mössbauer spectroscopy, ESR, UV-Vis) can be employed for studying double hydroxides containing iron, but not that of aluminium. Among them let me detail ^{57}Fe Mössbauer spectroscopy. Relatively few articles describe the structures of the layers in iron-containing LDHs with the assistance of Mössbauer spectroscopy. ^{57}Fe Mössbauer spectroscopy has been used to investigate the mechanisms of oxidation of Ni(II)Fe(II) hydroxides and its role in the synthesis of pyroaurite-type NiFe-LDH,²⁶ the oxidation state of iron in complexes such as $[\text{Fe}(\text{CN})_6]^{3-/4-}$ intercalated in layered double hydroxides²⁷ and ferrocene sulphonates intercalated in LDHs.²⁸ Numerous studies focussing on the examination of the layers, deal with green rust-type Fe(II)Fe(III)-LDH. One explanation may be that the structural features of this LDH can be established completely from the ^{57}Fe Mössbauer spectrum presenting two ferrous quadrupole doublets D_1 and D_2 and one ferric doublet D_3 in the paramagnetic state.²⁹ In addition, the ferromagnetic behaviour of green rust³⁰ and the effect of intercalation of linear C9–C16 carboxylates into layered Fe(II)Fe(III)-hydroxides have also been reported.³¹ It is clear from these few examples that ^{57}Fe Mössbauer spectroscopy has been used to study the structure of layers at a scarce, but it is not entirely unprecedented.^{23,24,25,32}

2.3. Interlamellar anions

In LDHs the interlamellar domains contain anions, water molecules and sometimes other neutral or charged entities. One major characteristic of LDHs is that in most cases only weak bondings occur between these interlamellar ions or molecules and the host structure. A great variety of anionic species can therefore be introduced between the layers during the formation of the lamellar structure or by further anionic exchange. The following families of anions can be found within the layers:

- halides (F^- , Cl^- , Br^- , I^-),
- non-metal oxoanions (BO_3^{3-} , CO_3^{2-} , NO_3^- , $\text{Si}_2\text{O}_5^{2-}$, HPO_4^{2-} , SO_4^{2-} , ClO_4^- , AsO_4^{3-} , SeO_4^{2-} , BrO_4^- *etc.*),
- oxo- and polyoxometallate anions (VO_4^{3-} , CrO_4^{2-} , MnO_4^- , $\text{V}_{10}\text{O}_{28}^{6-}$, $\text{Cr}_2\text{O}_7^{2-}$, $\text{Mo}_7\text{O}_{24}^{6-}$ *etc.*),
- anionic complexes of transition metals ($\text{Fe}(\text{CN})_6^{2-}$ *etc.*),
- organic anions (CH_3COO^- , $\text{C}_6\text{H}_5\text{COO}^-$, $\text{C}_{12}\text{H}_{25}\text{COO}^-$, $\text{C}_2\text{O}_4^{2-}$, $\text{C}_6\text{H}_5\text{SO}_3^-$ *etc.*),
- anionic polymers (PSS, PVS, polyacrylate, *etc.*).

The structure of interlamellar domains is more difficult to characterise than the main layers. With small anionic species, such as halides and carbonates, and up to sulphate-containing LDHs with a basal spacing of 1.1 nm, a regular stacking of the layers is observed in the X-ray diffractograms. With bulky anions, in most cases the stacking of the layers does not display long-range ordering any more (turbostratic effect) and the diffractograms show only lines related to the basal spacing and the structure of the main layers.

Most of the articles on the intercalation chemistry of LDH describe the fully exchanged products, while only a few report on mixed ion-exchanged forms. In one, the competitive intercalation of ClO_4^- and NO_3^- into ZnCr-LDH has been investigated.³³ The two phases coexist, implying that the formation of phases with mixed anions in the interlayer space is energetically unfavourable. Theoretical models would suggest that regular stacking, referred to as 'staging', as commonly observed in graphite, does not occur in LDH due to the rigidity of the layers.³⁴ However, using *in situ* time-resolved XRD, it was demonstrated³⁵ that LiAl-LDH can form second-stage intermediates, *i.e.*, every second layer is filled by dicarboxylate anions. Layer interstratification has been observed during the interlayer exchange of terephthalate with chloride and nitrate anions.³⁶ This is ascribed to two orientations of terephthalate anions, vertical and horizontal they are, which can be controlled by varying the layer charge density and the extent of drying. Thus, it is possible that staging in LDH can occur either during the

exchange process, or by direct synthesis, and is associated with different interlayer contents or different orientations of the same molecule.

The anions orient themselves in such a way that they maximise their interaction with the positively charged hydroxide layer. This feature is reflected in the interlayer spacing and is normally valid for 3R stacking, also denoted by the $d(003)$ value. In pristine LDH, CO_3^{2-} anions lie parallel to the hydroxide layer to ensure intimate interaction between the oxygen atoms and the layer by forming hydrogen bonds.³⁷ Organic anions always interact *via* their anionic groups being strongly hydrogen bonded to the surface hydroxyl groups, while their hydrophobic hydrocarbon chains are pushed far away from the hydrophilic layer surface, and adopt the lowest energy conformation.³⁸

2.4. Preparative chemistry of anion-intercalated layered double hydroxides

Layered double hydroxides are simple and inexpensive to synthesise both on laboratory and industrial scales. Many methods allow the preparation of materials with tailored physical and chemical properties suitable for many applications.

2.4.1. Co-precipitation methods

This is the most common preparative method of LDHs. It is based on the slow addition of a mixed solution of divalent and trivalent metal salts in appropriate ratio. A second (alkaline) solution is added to the reactor in order to maintain the pH at a selected value leading to the co-precipitation of the two metallic salts. The mechanism of co-precipitation is ideally based on the condensation of hexa-aqua complexes in solution, leading to the build-up of the brucite-like layers with close to evenly distributed metallic cations and with solvated interlamellar anions. Observation of the precipitates and X-ray diffraction characterisation show that the co-formation of the main layers and interlamellar domains takes place at a very early stage of the process without clear "delaminated" state of the layers.¹¹

The metal cations in the layers of the obtained material are originated from the metal salt solution, but the provenance of interlamellar anions has to be discussed. If these anions are the counter anions of the metal salts they come from the same solution. If the preparation is performed at very high pH values, the interlamellar anion can be the hydroxyl anion coming from the alkaline solution. When the alkaline solution is a sodium or potassium carbonate, the intercalated anion is likely the carbonate ion because of its high selectivity for LDHs interlamellar domains. Moreover, when the preparation is performed at relatively high pHs, one has to exclude air borne CO_2 in order to avoid carbonate contamination. Another way to

Depending on the precipitation conditions, it is possible to obtain well-crystallised LDH phases or quasi amorphous materials. Some of the influencing experimental parameters are obvious, like:

- temperature in the reactor,
- pH of the reaction medium,
- concentration of metal salt solution,
- concentration of alkaline solution,
- flow rate of reactants,
- ageing of the precipitate,

- accumulation of electrolytes in the reaction medium,
- hydrodynamics of the dilution of reactive species, related to the stirring mechanism,
- geometry of the reactor including reactants injection pipes,
- complexation state of the metal cations.¹¹

The diagram is a ternary plot with the x-axis representing the ratio $x = n(\text{M}^{\text{III}}) / [n(\text{M}^{\text{III}}) + n(\text{M}^{\text{II}})]$ ranging from 0 to 1. The y-axis represents the ratio $R = n(\text{OH}^-) / [n(\text{M}^{\text{II}}) + n(\text{M}^{\text{III}})]$ ranging from 0 to 3. The plot is divided into three main regions by red arrows: 'Coprecipitation' (top), 'Oxidation' (middle), and 'LDH[M^{II}-M^{III}]' (bottom). Key points and lines include:

- Point B at (0,0) labeled $\text{M}^{\text{II}}_{\text{aq}}$.
- Point C on the y-axis at $R \approx 1.8$ labeled $\text{M}^{\text{II}}(\text{OH})_2$.
- Point D at $x \approx 0.25, R \approx 2.0$ labeled $\text{LDH}[\text{M}^{\text{II}}-\text{M}^{\text{III}}]$.
- Point A on the x-axis at $x \approx 0.33$ labeled $x = 0.33$.
- Point M^{III} at (1,0).
- Point M^{II}M^{III}O₄ at $x \approx 0.67, R \approx 2.6$.
- Point M^{III}OOH at (1,3).
- Lines connect B to C, C to D, D to A, A to M^{III}, and M^{II}M^{III}O₄ to M^{III}OOH.

Figure 4. *M(II)(MIII)* mass-balance diagram showing the co-precipitation and oxidation synthesis routes.³⁹

A procedure using (hydro)thermal treatment following co-precipitation is often necessary to increase yields and/or the crystallinity of amorphous or poorly crystallised materials. A conventional ageing procedure is performed by heating the LDH suspension at temperatures in the range of 0–100 °C during several hours or even days. Two main co-precipitation methods have been commonly employed: (i) precipitation at constant pH value and (ii) at variable pH values.

In order to obtain well-defined phases, the operating conditions have to be optimised for each system.

2.4.2. The urea hydrolysis method

By using a base retardant as precipitating agent, the nucleation step can be separated from particle growth, and ageing is prevented from the beginning. Urea is a very weak Brønsted base ($pK_b = 13.8$) and can be employed as a reagent for "homogeneous" precipitation from solution. The hydrolysis of urea results in a solution with $pH = 9$, depending on the temperature, which is suitable for precipitating many metal hydroxides and a variety of LDHs. The urea hydrolysis method is suitable for the preparation of MgAl-LDHs with high layer charge densities.⁴⁰ This method results in LDH crystallites with a relatively large size (microns in diameter) and a well-defined hexagonal shape due to a low supersaturation during precipitation.⁴¹ The particle size can be controlled by altering the reaction temperature which affects the hydrolysis rate of urea and larger particles are formed at lower temperatures due to the lower nucleation rate.⁴² The disadvantages of this method are that the as-synthesised LDHs usually contain carbonate ions, which generally cannot be deintercalated and that the LDHs containing metal ions that precipitate at higher pH are not possible to obtain.

2.4.3. Anion-exchange method

The anion-exchange method is based on the exchange properties of the interlayer anions.⁴³ This method is especially useful when the co-precipitation method is inapplicable, for example, the divalent or trivalent metal cations or the anions involved are unstable in alkaline solution, or the direct reaction between metal ions and guest anions is more favourable, or there is no suitable soluble salt of the guest anions. In thermodynamic terms, anion exchange in LDHs depends mainly on the electrostatic interactions between the host sheets and the exchanging anions and, to a lesser extent, on the free energy associated with the changes of hydration.^{43,44} Another important remark is that the equilibrium constant increases when the ionic radius of the bare anion decreases. Exchange is therefore favoured

for in-going anions with a high charge density. From calculations of the equilibrium constant of various exchange reactions, Miyata⁴⁵ gave a comparative list of ion selectivities for monovalent anions: $\text{OH}^- > \text{F}^- > \text{Cl}^- > \text{Br}^- > \text{NO}_3^- > \text{I}^-$ and for divalent anions: $\text{CO}_3^{2-} > \text{C}_{10}\text{H}_4\text{N}_2\text{O}_8\text{S}^{2-} > \text{SO}_4^{2-}$. Moreover, it appears that the selectivities of divalent anions are higher than those of the monovalent anions. According to these results, nitrate- and chloride-containing LDHs appear to be among the best precursors for ion-exchange reactions. From a kinetic point of view, the rate-determining step of the reaction is the diffusion of the in-going anions within the interlayer, provided that the "infinite solution conditions" are respected. The diffusion of big anions inside the interlayer can be prevented by a too small basal spacing of the precursor. Exchange reactions *via* organic-anion-pillared precursors are then used. It has been verified that the favourability of the anion-exchange process is related to the following five main factors. (1) The exchange ability of incoming anions increases with increasing charge and decreasing ionic radius. The co-intercalation of a second anion was found to have no effect on the order of anion-exchange preference.⁴⁶ (2) Appropriate choice of solvent will favour the swelling and anion exchange of an LDH precursor.⁴⁷ (3) The pH value should generally be greater than 4, in order to preserve the host hydroxyl layer against damage. A low pH value favours the liberation of anions of weak conjugate acids and incorporation of a less basic anion.⁴⁸ (4) In some cases, the chemical composition of the LDH host layer affects the anion-exchange process. (5) Generally, higher temperatures favor anion exchange.⁴⁹

2.4.4. Dehydration-rehydration (reconstruction) method

Miyata was the first to describe in 1980 the reconstruction of the original LDH structure by hydration of the calcined LDH.⁵⁰ This unique property, ascribable to a structural memory effect, can be used as a general preparation method of LDH. In the first step the LDH is calcined into a mixture of oxides and then to rehydrated in an aqueous solution containing the anion to be intercalated (*Figure 5*).

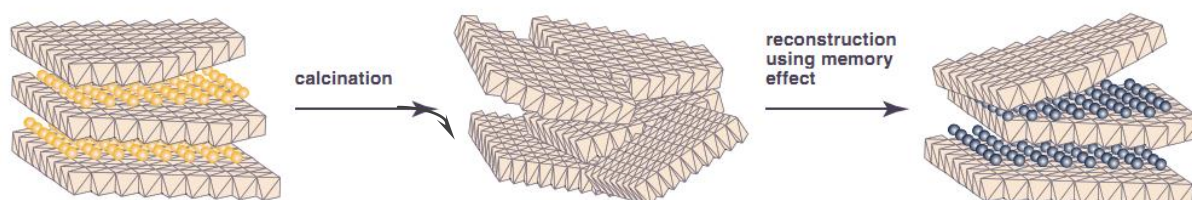


Figure 5. A simplified representation of the calcination/reconstruction method.

The calcination conditions (temperature, rate, and duration of treatment) are important parameters determining structure recovery. Some limits of reversibility were observed. Repeated calcination/hydration cycles with hydrotalcite decrease the content of interlayer carbonate anions and increasing extraction the Al^{3+} from the brucite layers.⁵¹ The reconstruction method cannot be used for all M(II)–M(III) combinations. Reconstruction of Fe^{3+} -containing hydrotalcites is limited by the formation of MgFe_2O_4 spinel, which appears even at low Fe^{3+} content.

For most LDHs, during progressive calcination, four larger thermal events can be identified in general, and experimental evidence suggests that they can be resumed as follows: (1) continued dehydration process and dehydroxylation of layers between room temperature and 250 °C, (2) interlayer anion decomposition, between 250 and 350 °C, with notable increases in the activation energy values, revealing the existence of different and simultaneous processes, (3) shrinkage and then collapse of the layered structure, between 350 and 550 °C and (4) the crystallisation of new phases.⁵² Spinel formed at temperatures around 1000 °C will not convert back to LDH by the memory effect, regardless of how hard one tries. The complexity of these stages implies that the separation of the contributory rate processes is difficult and kinetic analyses are complicated. The condensation of OH groups to form water molecules imply strong local reorganization leading to the collapse of the layered structure. This is probably a high-energy consuming step, which should be favoured by nucleation and growth of new phases at some local critical dehydration extension. After dehydroxylation quasi-amorphous mixed oxides are obtained, which crystallise progressively at higher temperatures, generally as a $\text{M(II)M(III)}_2\text{O}_4$ spinel-like phase and the divalent metal oxide. The ill-organised mixed oxides display three broad X-ray diffraction peaks generally corresponding to the future strongest lines of the spinel-like phase; they are therefore called pre-spinel oxides and it is not impossible that the transformation from the layered structure to this oxide phase could be topotactic. Generally, these mixed oxides display generally a relatively high specific surface ($100\text{--}300\text{ m}^2\text{g}^{-1}$) compared to the as-prepared LDHs ($\approx 15\text{ m}^2\text{g}^{-1}$).

This method is suitable for the preparation of hybrid LDH with large organic anions. An inert N_2 atmosphere is required during the rehydration process when an anion other than carbonate is to be incorporated. It is difficult to obtain pure crystalline intercalated products because the lamellar structure of LDHs can often only be partially restored during the reconstruction stage.⁵³ It has been found that the extent of intercalation observed using this method depends on (i) the reaction medium, (ii) the composition of the host layer, and (iii) the

geometric and electronic structures of the anions. A wide range of anions, *inter alia* amino acids have been incorporated into layered double hydroxides using this method.⁵⁴

Besides the methods for preparation discussed above, various other ways have been developed for the synthesis of LDHs, such as hydrothermal synthesis,⁵⁵ the sol-gel process,⁵⁶ a method involving separate nucleation and aging steps (SNAS),⁵⁷ the salt-oxide (or salt-hydroxide) method,⁵⁸ electrochemical synthesis,⁵⁹ reverse microemulsion method⁶⁰ *etc.* but they are used infrequently and only in special cases.

2.5. Applications of layered double hydroxides

Compositional diversity in the layers and in the interlayer anions leads to a functional diversity that allows LDHs to be used for a variety of material science applications.

2.5.1. Catalytic applications

As a result of their relative ease of synthesis, LDHs represent an inexpensive, versatile and potentially recyclable source for a variety of catalyst supports, catalyst precursors or actual catalysts. In particular, mixed metal oxides obtained by controlled thermal decomposition of LDHs have large specific surface areas, basic properties, a homogeneous and thermally stable dispersion of the metal ion components, synergetic effects between the elements, and the possibility of structure reconstruction under mild conditions. The thermal treatments at low temperature lead to synergetic effects between the elements in spinel-like or mixed oxide structures (*e.g.*, Mg(Al)O mixed oxide with strong basic properties). The opportunity is thus offered for the fine control of the nature of the active sites and their environment, and the texture and the stability of the catalysts. This tailoring is supported by the lamellar structure, resulting from the moderate-temperature dehydration. In this case both the intercalated anion and the amount of remaining H₂O determine the reactivity⁶¹ and the LDH behaves as a Brønsted-type catalyst and as such, it has been applied to aldol and Knoevenagel condensations,^{62,63} epoxidation of olefins,⁶⁴ halide exchanges,⁶⁵ phenol hydroxylation,⁶⁶ Michael additions⁶⁷ and transesterification.⁶⁸ In these reactions the catalysts are mixed oxides obtained through the thermal decomposition of the LDH precursors. Those of the Mg(Al)O-type have attracted much attention due to the presence of Mg²⁺-O²⁻ acid-base pairs leading to specific catalytic properties. They find applications in reactions as diverse as aldol, Claisen-Schmidt and Knoevenagel condensations, transesterification, alkylation of phenol by alcohols, oxidation of thiols, Baeyer-Villiger oxidation of ketones, polymerization of lactones, methanol synthesis, epoxidation of activated olefins with H₂O₂, and reduction of

aldehydes and ketones by hydrogen transfer from alcohols.^{61,69} Some examples are detailed in the followings.

Industrial processes have hitherto used large amounts of liquid bases as catalysts for C–C bond formation in condensation reactions. The replacement of these liquid bases by environmentally friendly basic solids with similar activities and selectivities is a real challenge. Basic oxides such as MgO, CaO and BaO are very active in these reactions. The mechanism generally accepted for the aldol condensation of aldehydes and ketones involves first a hydrogen abstraction leading to the formation of an enolate-type species, then its condensation with another molecule, then the dehydration of the aldol thus formed to yield an α,β -unsaturated compound. This mechanism shows that, aside from the basic sites of adequate strength, acid sites are also required for stabilising the enolate species, and for the dehydration.⁷⁰ The balance between basic and acidic sites is thus a key parameter for the catalytic properties. Illustrations of the versatility of acid-base properties for catalytic application are, *e.g.*, the aldolisation of acetone, Michael addition of nitromethane and cyclo-2-en-1-one, and cross-condensation of heptanal and acetaldehyde.⁷¹

There are a lot of examples when the active catalyst results from the intercalation of specific anionic species in the interlayer space of the LDH, which is acting as the host structure. In the field of catalysis, their preparation has been claimed in order to fulfill the following objectives: (i) to obtain shape-selective chemical, electrochemical or photocatalysts, (ii) to stabilize homogeneous or biomimetic catalysts in order to increase their service life and allow easy recovery and recycling, and (iii) to prepare supported catalysts with concentrations of the active phase and activities higher than those obtained with conventional supports. Although an LDH is seemingly a weak base, intercalation of acidic anions (such as many polyoxometallate – POM anions) makes it simultaneously possess acidity, which has been well demonstrated in the epoxidation of various olefins. Most interesting is the variation of transition metal ions in the brucite-like layer that enables LDHs to show a spread spectrum of catalytic activity for oxidation and reduction, which has been exemplified in the applications for total oxidation of volatile organic compounds, H₂ production, DeNO_x and DeSO_x reactions and CNT formation.⁷² It has been demonstrated that both calcined and uncalcined LDHs are effective supports for noble metal catalysts.^{73,74} For example, palladium supported on calcined MgAl-LDH has been used for the one-pot synthesis of 4-methyl-2-pentanone (methyl isobutylketone) from acetone and hydrogen at an atmospheric pressure.⁷⁵ Choudary *et al.*⁷⁶ studied Pd(0) catalysts supported on MgAl-LDHs prepared by ion-exchange with PdCl₄²⁻, followed by reduction. They observed that the catalysts, used in ionic liquids, not

only exhibited higher activity and selectivity than the homogeneous PdCl_2 system in the Heck olefination of electron-poor and electron-rich chloroarenes, but also showed superior activity in the C–C coupling reactions of chloroarenes compared with other heterogeneous catalysts involving $\text{Pd}(0)$ on supports such as silica, alumina or Merrifield's resin. Intensively investigated polyoxometallate-based (POM) and sulphonato-salen-based (Salen) catalysts have been intensively investigated for oxidising C=C double bonds with H_2O_2 or oxygen over a homogeneous or heterogeneous catalyst in systems free of organic solvent. These two catalytic anions can be intercalated and thus confined in the interlayer spacing of LDHs, which leads to high activity and selectivity for epoxidation of various olefins.³⁷ Since POMs are restricted in the interlayer or on the surface, only part of the anion is exposed to reactants, which probably causes the regioselective epoxidation of one C=C bond over another in the same organic molecule, and stereoselective epoxidation of a C=C bond to form a specific stereostructure. Stereo- and regioselectivities have been observed in the epoxidation of terpene, 3-carene, squalene and (–)-carveol.⁷⁷ ZnAl -LDHs intercalated with sulphonato-salen-Mn, Fe or Co complex anions have also demonstrated high activity and selectivity in the epoxidation of various olefins. These catalysts are able to convert 95–100% of (+)-limonene and (–)- α -pinene with nearly 90% selectivity to the relevant epoxides in various solvents with O_2 or air as the oxidant at room temperature.⁷⁸ The secondary and tertiary amines can be oxidised with various oxidising reagents over the catalyst with a certain alkalinity. MgAl -LDH is a weak base, and can be made stronger by intercalating OBU^- anion.⁷⁹ It showed an activity similar or superior to KOBU and NaOH for N-oxidation of N-methylmorpholine and dibutylamine using H_2O_2 as the oxidant in benzonitrile-methanol. Several secondary and tertiary amines were readily N-oxidized with high yields (72–98%). It seems that N-oxidation of tertiary amines is much faster than secondary amines, since the tertiary amines are almost quantitatively N-oxidised with H_2O_2 over $\text{WO}_4\text{--MgAl}$ -LDH under similar conditions (95% yield).⁸⁰ These LDH-based catalysts are all recyclable, without any obvious loss of activity.

Research involved coating LDH particles onto magnetic Fe_3O_4 particle surface to form a core-shell structure. The calcined LDH/ Fe_3O_4 composite particles were then immersed in $\text{W}_7\text{O}_{24}^{6-}$ solution to load this POM during reconstruction of the LDH phase. This magnetically recoverable POM-LDH/ Fe_3O_4 composite catalyst showed high photocatalytic activity for the decomposition of hexachlorocyclohexane under visible light emitted from high-pressure mercury lamp, and the activity was unchanged even after cycling for 6 times.⁸¹ Layered double hydroxides may also be useful support precursors^{8,82,83} of Ziegler–Natta catalysts for ethylene polymerization or DESO_x additives to FCC catalysts, showing high

stability also under severe reaction conditions, and excellent catalytic properties as well as easy regeneration. The more detailed description of the chosen reactions for catalytic testing studies is given in Chs. 5.3. and 5.4., pp. 60–71.

2.5.2. Environmental applications

Recently, since serious contamination of water arises from various anionic compounds, and cultivated soils extensively develop acidic property, attempts to remove anionic ions and pesticides by adsorption to LDHs have steadily increased. LDH can take up a variety of contaminants and toxic substances directly from the environment through anion exchange, reconstruction, and adsorption.

Phosphate, a causative factor in surface water eutrophication, can be captured by the chloride or nitrate forms of LDH through ion exchange.^{84,85} Competing anions affect phosphate uptake. For example, nitrate causes only a slight decrease in phosphate removal whereas sulphate brings about 12–13%, and carbonate does 33%, reduction.

A few studies have been carried out to develop the potential of LDHs as plant nutrients, pesticides, growth regulators, and active component in animal feeds.^{86,87}

Only a few of natural antibiotic substances are available for pest control mainly because of their inherent properties such as easy degradability, high minimum inhibition concentration for practical application and often extremely low availability. The hybridisation of natural antibiotic substances with layered double hydroxides could be an alternative for green formulation of pesticides.⁸⁸

Humic substances constitute a major fraction of organic matter in natural water and effluents from lakes and rivers. Their presence has been a problem in the water industry and in environmental purification such as soil remediation. During the removal process of heavy metal contaminants in soil remediation and the removal process of organic pollutants in drinking water treatment, humic acids often reduce the removal of the target substances through their adsorption onto adsorbents and/or a formation of a complex with the target substances. The removal of the humic compound by conventional adsorbents is, however, difficult due to their good solubility in water and their wide range of distribution in molecular weight and size. Layered double hydroxides are ideal choice for the removal of the humic substances, their removal occurs by both the intercalation into the positively charged innerlayer (ion-exchange) and the adsorption onto hydroxyl groups of the layers.⁸⁹ The main advantages of LDHs over the conventional anion exchange resins include their higher anion-

exchange capacity for certain oxy anions and their good thermal stability. Furthermore, LDHs can be fully regenerated in a short time for reuse.

Adsorption of carbon dioxide onto LDH was investigated as a possible method for recovery of CO₂ from hot gas streams.^{90,91} The recovery of CO₂ from power-plant flue gases is considered to be the first step in reducing total CO₂ emission. The carbon dioxide adsorption capacity of LDH is dependent on the micropore volume, interlayer spacing, and layer charge density of the material.

2.5.3. Additives for polymers

The incorporation of a polymer in the interlayer galleries may proceed *via* various pathways such as co-precipitation, ion exchange, surfactant-mediated incorporation, hydrothermal treatment, reconstruction, or delamination followed by restacking.⁹² Alternatively, various monomers can be intercalated and polymerised *in situ* within the interlamellar space of LDH. This method requires appropriate monomers. To date, intercalation of polyacrylate, polyaniline, poly(aminobenzoate) and poly(α,β -aspartate) have been reported.^{93,94,95} The spatial confinement is believed to increase the degree of polymerisation, and, in addition, this type of *in situ* radical polymerisation process makes it possible to tune the tacticity and the molecular weight of the resulting polymer by varying the layer-charge density and the particle size of the host structure, respectively.

From several studies, it has been observed that the multicomponent LDH/polymer systems are thermally more stable than the pristine inorganic compounds, leading to potential applications such as flame-retardant composites. From an environmental standpoint, LDH-based flame retardants are preferable to their halogen-based counterparts. Many flame retardants are considered harmful, having been linked to liver, thyroid, reproductive or developmental, and neurological effects. In flame-retardancy tests, LDHs are superior to other inorganic hydroxides, such as magnesium and aluminium hydroxides.⁹⁶ A throughout review on the topic was given by Taviot-Guého and Leroux.⁹⁷

The literature regarding polymers with LDH additives is even more extensive. Now, the LDHs are the guest materials (in previous paragraphs they were the matrices) and many mechanical properties of the resulting polymer-nanocomposite (*e.g.*, strength and heat resistance, gas permeability and flammability, biodegradability, *etc.*) did improve with the modification.⁹⁸ These nanocomposites are prepared from the delamination of the hydroxide sheets in a polymer matrix.⁹⁹ Synthetic LDHs are commercially used as acid neutralisers or HCl scavengers in stabiliser packages for poly(vinylchloride) (PVC). PVC undergoes

autocatalytic dehydrochlorination when exposed to heat or UV light, becoming brittle and changing colour. Mori *et al.*¹⁰⁰ reported that adding LDH to PVC in the presence of 6-anilino-1,3,5-triazine-2,4-dithiol and zinc stearate, jointly used as a stabiliser, reduces the rate of PVC discoloration. From the viewpoint of this work these type of applications have lower importance, if a deeper insight is needed, please consult with the review of Kumar *et al.*¹⁰¹

2.5.4. Pharmaceutical and cosmetic applications

Pharmaceutical applications of LDHs mainly rely on their acid buffering effect and anion-exchange properties. Hydrotalcite-derived antacidic and antipeptic formulations are representative of their applications in pharmaceuticals. Hydrotalcite has also found pharmaceutical applications as an ingredient in sustained-release pharmaceuticals containing nifedipine, for stabilising pharmaceutical composition, and for preparing aluminium magnesium salts of antipyretic, analgesic and anti-inflammatory drugs.¹⁰² One principal area that has been the focus of intense research in recent years is the use of LDH hosts as storage and delivery devices for biologically important species. A number of important bioactive species are based on carboxylic acids, and hence are suitable for intercalation into LDHs. Furthermore, the wide variety of cations that can comprise an LDH mean that it is facile to produce biocompatible materials. A variety of drugs have been incorporated into LDHs.^{103,104} It is a long-term goal of pharmaceutical scientists to develop so-called ‘controlled release formulations’ (CRFs). These are advantageous over current methods of drug delivery: instead of taking doses of the drug regularly at given time intervals, CRFs allow the patient to take only tablets far less frequently. Delivery of the drug is slow and sustained, and an effective and non-toxic concentration of the drug may be retained in the body over a long period of time. With traditional formulations, the drug concentration is in the effective region for a relatively short period of time, at either side the concentration may be dangerously high or ineffectively low. Choy *et al.* have made very significant contributions to this area. Mg₂Al-LDH was successfully employed to intercalate folic acid and methotrexate (MTX), both commonly used to treat cancer sufferers.¹⁰⁴ An *in vitro* bioassay was used to demonstrate that in the initial stages after administration of the drug, MTX–Mg₂Al-LDH has a significantly higher efficacy against tumor cells than MTX alone. This could be because the LDH matrix allows MTX to pass through the cell membrane more effectively, and also prevents decomposition of the drug in the cell plasma. However, it is not exactly clear how this could occur. The LDH is not simply acting as a delivery matrix, but is also improving the efficiency of the drug. Another recent development is the synthesis of LDHs intercalated with β-

cyclodextrins.¹⁰⁵ These bowl-like molecules can be used to contain lipophilic drug molecules, thereby increasing their stability, water solubility and bio-availability. LDHs can intercalate many important negatively charged biomolecules such as oligomers, single or double stranded DNA, and simple molecules like nucleotides.^{106,107} Especially, the single or double stranded DNAs have a great deal of application potentials in various fields, expanding from gene therapy to biosensing and even high density information storage. However, DNA strands are very susceptible to degradation and denaturation occurring during manufacture processes and storage. The intercalated DNA on the other hand was safely protected against harsh condition including strong alkaline, weak acidic environments and DNase attack.¹⁰⁷ It could also be recovered very easily by exposing DNA-LDH hybrids to an acidic condition due to the solubility of LDHs in acid, implying promising potential of LDHs in biological applications. Further experiments have shown that vitamins may also be intercalated and discharged in a controlled fashion.¹⁰⁸ *In vivo* studies have demonstrated that LDH particles have little systematic effect at low doses, and thus are likely to be suitable as drug delivery matrices.¹⁰⁹

LDHs possess many fascinating features to be also applied in cosmetics like high adsorption capacity, excellent anion-exchange ability and stabilising potentials. For example, the high adsorption capacity can be used to remove skin exudates and to encapsulate skin sensitive colouring and UV-screening agents, while the anion-exchange ability can be useful to protectively deliver active substances for anti-wrinkling and skin regeneration. LDHs stabilise unstable molecules such as retinoic acid, ascorbic acid, tocopherol, *etc.* often used in cosmetics and can improve rheological properties of various formulations, especially emulsions. Even if the practical application of LDHs in cosmetics is not much developed, there are some studies in which the potentials of LDHs for cosmetic purposes were explored.^{110,111,112}

3. THE MAIN AIMS OF THE DISSERTATION

Layered double hydroxides have a wide range of compositions which give rise to the possibility of fine-tuning their properties in a variety of ways, allowing improved applications in many areas. At the beginning of my work several goals were set out:

- Exploring and finding the optimum experimental conditions for the synthesis of pristine Ca(II)Fe(III)- and Mg(II)Fe(III)-LDHs, representatives of hydrocalumite and hydrotalcite structural types, respectively.
- Characterising these materials with as many methods as it is possible.
- Studying the catalytic activity of the pristine, uncalcined CaFe-LDH.
- Functionalising CaFe-LDH *via* intercalating aromatic, partially or fully saturated N-containing heterocycles – studying the effects of changing the solvents on the intercalation and characterising the obtained organic-inorganic hybrid substances.
- Functionalising chloropropylated silica gel at the N- or the C-terminal.
- Comparing the catalytic activities of the L-prolinate– and DL-pipecolate–CaFe-LDH samples with those of the L-proline-functionalised silica gel samples and (a purchased) L-prolinol-functionalised resin.

4. EXPERIMENTAL PART

4.1. Materials

All materials used for experiments [calcium chloride (CaCl_2 , Molar Chemicals, *puriss*), magnesium chloride ($\text{MgCl}_2 \cdot 6\text{H}_2\text{O}$, Molar Chemicals, *a.r.* grade), iron chloride ($\text{FeCl}_3 \cdot 6\text{H}_2\text{O}$, Molar Chemicals, *puriss* special) hydrogen chloride (HCl), sodium hydroxide (NaOH , VWR, *a.r.* grade) potassium hydroxide (KOH , Reanal, *a.r.* grade), (*S*)-pyrrolidine-2-carboxylic acid (L-proline, Sigma-Aldrich, $\geq 99\%$), DL-2-piperidine-carboxylic acid (DL-pipecolinic acid, Sigma-Aldrich, $\geq 99\%$), (*S*)-(-)-indoline-2-carboxylic acid (dihydroindole-2-carboxylic acid, Sigma-Aldrich, $\geq 99\%$), indole-2-carboxylic acid (Sigma-Aldrich, $\geq 98\%$), sodium dodecylbenzenesulphonate (DBS, Sigma-Aldrich, technical grade) *tert*-butoxy-carbonyl-L-proline (Boc-Pro-OH, Sigma-Aldrich, *a.r.* grade), L-proline methylester (H-Pro-OMe, Sigma-Aldrich, *a.r.* grade) chloropropylated silica gel (SG, Sigma-Aldrich, *a.r.* grade, particle size: 230–400 mesh, BET surface area: $500 \text{ m}^2/\text{g}$, functionalisation: 8%)] were used as received without further purification. The resin-anchored L-prolinol-2-chlorotrityl ether was also a commercial product (Sigma-Aldrich, particle size: 200–400 mesh, extent of labeling: 0.3–1 mmol/g loading). The resin in the acid-labile chlorotrityl resin is polystyrene cross-linked with 1% divinyl benzene. Dichloromethane (CH_2Cl_2 , Reanal), trifluoroacetic acid (CF_3COOH , Reanal) and sulphuric acid (H_2SO_4 , CarloErba 96%) were used for removing the protecting groups. The solvents [acetone (Sigma-Aldrich, $\geq 99.5\%$), methanol (Sigma-Aldrich, 99.93%), ethanol (VWR, $\geq 96\%$), 2-propanol (Molar Chemicals, *a.r.* grade) 2-methyl-2-propanol (Sigma-Aldrich, $\geq 99.5\%$), formamide (Reanal, *a.r.* grade), 1,4-dioxane (Reanal, *a.r.* grade), cyclohexene (Reanal, *a.lt.* grade), n-hexane (Reanal, *a.lt.* grade), dimethyl sulphoxide (DMSO, Merck, 99.7%)] were also used without further purification. Filtered and ion exchanged water (Millipore) was applied throughout the experiments.

The reagents used for the catalytic reactions [hydrogen peroxide (H_2O_2 , 30 wt%), 2-cyclohexen-1-one, benzaldehyde, 2-nitrobenzaldehyde, 4-nitrobenzaldehyde and 2-thiophene carbaldehyde] were Sigma-Aldrich products. All these compounds were of analytical grade and were used without further purification except the liquid aldehydes, which were freshly distilled before use.

4.2. Preparation of concentrated and carbonate-free NaOH solution

The preparation of the concentrated [$c \approx 20$ M] and carbonate-free sodium hydroxide solution was carried out by dissolving solid NaOH in water ($\sim 1:1$ mass ratio). After precipitating the sodium carbonate, the solution was filtered on polysulphone Nalgene filter.¹¹³ The exact density of the solution was determined by a pycnometer. The concentration of the solution was calculated from the known density vs. concentration curve of sodium hydroxide.¹¹⁴ NaOH solutions of various concentrations were made from this stock solution just before the synthesis.

4.3. Synthesis of the layered double hydroxides

The Ca(Mg)Fe-LDHs were prepared by the co-precipitation method *via* dropwise addition of the two metal salt solutions with various molar ratios (M(II):Fe(III)) ranging from 6 to 2) to hot (*ca.* 80 °C), vigorously stirred and N₂-blanketed NaOH solution. The precipitates formed were rapidly filtered until air dry in a CO₂-free atmosphere, with the aid of a caustic resistant vacuum filter unit (Nalgene) equipped with an appropriate membrane (Versapor, 0.45 μ m). The solid material was washed and filtered and the obtained crystals were kept at room temperature in a desiccator over P₂O₅.

4.4. Intercalation of the layered double hydroxides

The anions of various N-containing carboxylic acid, aromatic (indol-2-carboxylate), partially ((*S*)-(-)-indoline-2-carboxylate) or fully saturated (L-prolinate, DL-pipecolate) heterocycles were intercalated into Ca₃Fe-LDH with the dehydration-rehydration method, utilising the memory effect of the layered double hydroxides (for the structures of organic anions, see *Figure 6*).

A typical recipe is as follows. The pristine CaFe-LDH was heat-treated at 773 K for 5 h in N₂ atmosphere. A portion of the obtained dehydrated material was suspended in 80 cm³ solvent mixture (ethanol/H₂O/NaOH or acetone/H₂O/NaOH both with 1:5:1 volume ratios), which also contained the heterocyclic compounds in a high excess (usually 10 : 1 molar ratio for the Fe(III)-content of the LDO), after inert N₂ was bubbled through the mixture. The reaction mixture was stirred for a week at 60 °C. The solid catalyst was filtered and washed with water. The crystals obtained were kept at room temperature in a desiccator over P₂O₅.

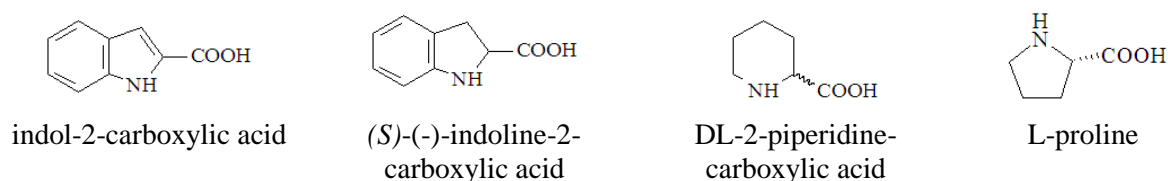


Figure 6. The structures of the intercalated organic anions (for simplicity, protons are uniformly shown to be attached to the carboxylate groups).

4.5. Immobilisation of L-proline in functionalised chloropropylated silica gel

The N-protected or C-protected L-proline was covalently grafted onto the modified silica gel surface with esterification (*tert*-butoxycarbonyl-L-proline) or N-alkylation (L-proline methylester) reactions. After 24 h reflux in a basic isopropanolic suspension (KOH was used) the materials obtained were filtered washed and dried. Then, the protecting groups were removed. The ester was hydrolysed with sulphuric acid (2 h reflux), while the *tert*-butoxycarbonyl group was removed via a 2 h reflux under vigorous stirring at moderate temperature (338 K) in a 1:1 mixture of CH_2Cl_2 and CF_3COOH .

4.6. Heterogeneous catalytic reactions

The pristine as-prepared layered double hydroxides were tested in the epoxidation of electron-deficient carbon–carbon double bonds of an α,β -unsaturated ketone (2-cyclohexen-1-one) using 30 wt% aqueous hydrogen-peroxide as oxidant under mild reaction conditions (vigorous stirring at 298 K for 2 h) applying various solvents (methanol, ethanol, 2-methyl-2-propanol, acetone, formamide, 1,4-dioxane, cyclohexene, n-hexane). Temperature dependence (288–343 K range) was also examined. The catalytic properties of intercalated derivatives (indole-2-carboxylate– $\text{Ca}_3\text{Fe-LDH}$ and L-prolinate– $\text{Ca}_3\text{Fe-LDH}$) were also examined. The general conditions for the reactions were as follows: 1 mmol 2-cyclohexen-1-one, 4 mmol H_2O_2 , 2.5 mL solvent, 0.075 g catalyst. Recycling and time dependence were also studied.

The catalytic activities of the L-prolinate– and DL-pipecolate– $\text{Ca}_3\text{Fe-LDH}$, the functionalised chloropropylated silicagel and functionalised resin samples were tested in the intermolecular cross-aldol dimerisation–condensation of acetone with various aldehydes (benzaldehyde – on all the solid materials, 2-nitro- and 4-nitrobenzaldehyde and 2-thiophene carbaldehyde – on the functionalised silica gel and resin samples). The reactions were run for 24 h at room temperature under vigorous stirring. Various solvents were used like water, DMSO or the acetone reactant itself. The composition of the initial mixture was generally as

follows: 4-5 cm³ of solvent, 1-1 cm³ of the reactants (if the aldehydes were liquid) or 0.15 g when they were solid and 0.3 g of catalyst. Recycling study with the L-prolinate–Ca₃FeLDH sample was also performed.

4.7. Instrumentation and characterisation methods

4.7.1. X-ray diffractometry

Powder X-ray diffraction (XRD) patterns of the air-dried and heat-treated solid samples were registered in the $2\Theta = 3\text{--}60^\circ$ range on Rigaku Miniflex II and DRON-2 instruments, using CuK α and FeK α ($\lambda = 1.5418 \text{ \AA}$ and 1.9374 \AA , respectively) radiations in Bragg-Brentano geometry. Reflection positions were determined *via* fitting a Gaussian function. They were found to be reproducible within 0.05° (2Θ), therefore the uncertainty of the basal spacing was estimated as $\pm 0.01 \text{ nm}$.

4.7.2. Thermal analytical measurements

Thermal analytical measurements (TG/DTG) were performed using a Setaram Labsys derivatograph working under N₂ flow at $2^\circ\text{C}/\text{min}$ heating rate. Both the weight loss *vs.* temperature (thermogravimetric – TG) and the differential weight loss *vs.* temperature (differential thermogravimetric – DTG) curves were recorded. Approximately 20 mg sample (measured accurately into a ceramic crucible sample holder) was applied in each experiment. Measurements were started right after removing the samples from the desiccators.

4.7.3. ICP–OES measurements

Determination of the Fe(III) content of the LDH samples was done using a Thermo's IRIS Intrepid II ICP-OES spectrometer. The instrument was externally calibrated with a calibration solution series prepared from ICP Multielement standard solution XXIII made by CertiPUR.

4.7.4. Microscopic techniques

The morphology of the samples was examined with scanning electron microscope (SEM – Hitachi S-4700 microscope with varying acceleration voltage). The samples were ground before fixing them on a double-sided adhesive carbon tape. They were coated with gold in order to obtain images with more contrast, using a sputter coater (Quorum Technologies SC7620). The thickness of the gold layer was a few nanometers. The approximate

composition and the elemental map of the substances were investigated by a Röntec QX2 energy dispersive X-ray fluorescence spectrometer (EDX) coupled to the microscope.

The layer thickness of the $\text{Ca}_3\text{Fe-LDH}$ sample was estimated from a transmission electron microscopic (TEM) dark-field image taken by a FEI TECNAI G²20 X-TWIN microscope at 200kV accelerating voltage. Samples of the material to be analysed were suspended in absolute ethanol by means of and ultrasound bath, the mixture placed on a lacey carbon 200 mesh copper grid, and the solvent allowed to evaporate.

4.7.5. Mössbauer spectroscopy

^{57}Fe Mössbauer spectra of the samples were recorded with conventional Mössbauer spectrometers (Wissel and Ranger) in transmission geometry at 78 K or 295 K. A $^{57}\text{Co/Rh}$ γ -radiation source of 3×10^9 Bq activity was used. The spectrometers were calibrated with α -iron at room temperature. Spectrum evaluation was carried out using the MOSSWIN code *via* fitting Lorentzian curves.

4.7.6. XAS measurements

The X-ray absorption spectra (XAS) were measured at beamline I511-3 (*Figure 7*) at the MaxLab facility, Lund, Sweden. The station is based on a superconductive undulator injection device connected to the 1.5 GeV MAX II storage ring. X-ray radiation in the 50–1500 eV energy range can be obtained from this system.

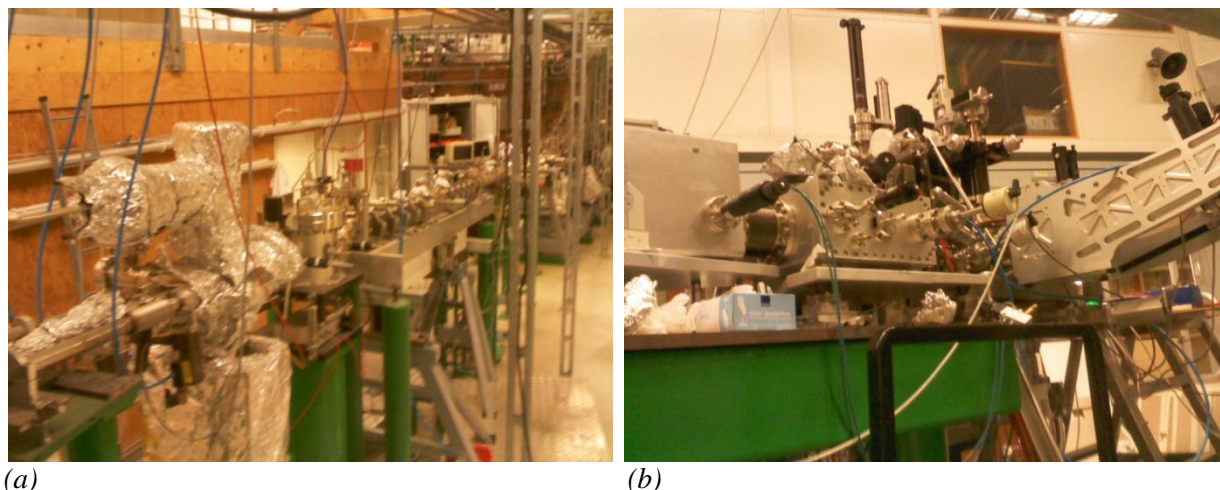


Figure 7. The I511-3 station at MaxLab:(a) the beamline and (b) the spectrometers (for X-ray absorption emission).

Since this is not the method one uses on an every-day basis (except one is working at a synchrotron facility), the major characteristics of the method is described briefly in the followings. The fundamental phenomenon underlying XAS is the absorption of an X-ray

photon by a core level of an atom in a solid and the consequent emission of a photoelectron. The absorption of the X-ray photon is based on the photo effect, *i.e.*, the absorbed photon pushes out an electron from the inner shell of the bombarded atom or ion. The absorption coefficient decreases with the increase in energy, until it reaches the bonding energy of an inner electron. At this point a sharp peak appears in the spectrum. The corresponding energy is the so-called threshold energy. Beyond this energy a fine structure in the spectrum is seen up to even 10000 eV. The various regions of the X-ray absorption provide different information.

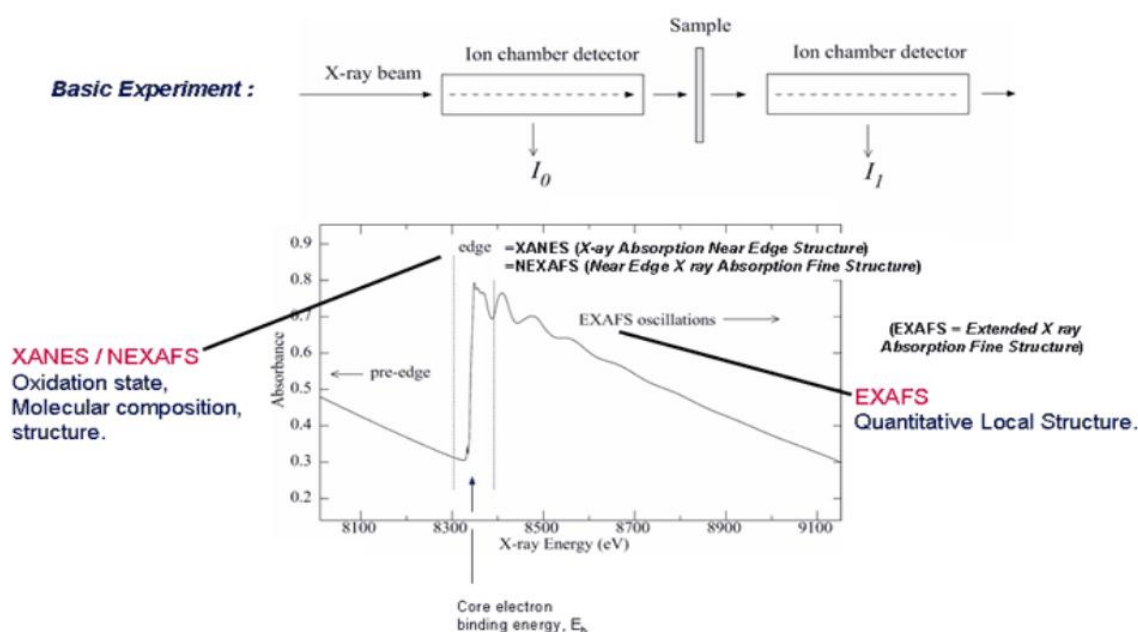


Figure 8. The various regions of the X-ray absorption spectrum (XANES – X-ray absorption near-edge structure, EXAFS – Extended X-ray absorption fine structure).

The part of the spectrum before the absorption edge is the pre-edge region. Information on the bonding character, the oxidation state and the coordination geometry of the element studied can be extracted from this part of the spectrum. Then, the absorption edge and its immediate surrounding follow – this is the XANES region. Both XANES and NEXAFS are acceptable terms for this part of the spectrum. The difference in usage is the energy range beyond the absorption edge. NEXAFS is synonymous with XANES, but NEXAFS by convention is usually reserved for soft X-ray spectroscopy ~photon energy less than 1000 electron volts. NEXAFS is generally used when applied to surface and molecular science, while XANES is used in most other fields. In the XANES region, starting about 5 eV beyond the absorption threshold, because of the low kinetic energy range (5–150 eV) the photoelectron backscattering amplitude by neighbouring atoms is very large, thus multiple scattering events become predominant in the XANES spectra. In the XANES region, the

electron transfers occur to unoccupied bonding orbitals in most cases, and with much less probability to the continuum. Changes in this region may serve as a fingerprint for the materials. This region is the most sensitive to the changes in the geometry around the absorber atom or ion, *i.e.*, very significant spectral changes may be observed. They are mainly due to the scattering of photoelectrons with low kinetic energies. Although in XANES the atoms/ions in the first coordination sphere predominate, other strongly bound scatterers have important effects as well. The last part is the EXAFS (Extended X-ray Absorption Fine Structure) region, from this region structural parameters like coordination number, bond lengths, *etc.* can be extracted.¹¹⁵

During a NEXAFS measurement the sample is irradiated with monochromatic X-rays. The energy of the X-rays is varied around the absorption edge. The predominant process in the soft X-ray energy range (<2000 eV) is (by orders of magnitude) photoabsorption. Opposite to the related X-ray photoemission spectroscopy (XPS or ESCA) technique, where the photon energy is fixed and the electron intensity is measured as a function of electron kinetic energy, in NEXAFS the X-ray energy is scanned and the absorbed X-ray intensity is measured. NEXAFS spectra can be recorded in different ways, the most common methods are transmission and electron yield measurements. The transmission technique requires thin foils while the electron yield technique, often called total electron yield (TEY) detection, can be used for conventional samples. The absorbed X-ray intensity is not measured directly in TEY measurements, but rather the photoelectrons that are created by the absorbed X-rays. X-rays are absorbed through excitations of core electrons to empty states above the vacuum or Fermi level. The created holes are then filled by Auger decay (dominant in the soft X-ray region over X-ray fluorescence). The intensity of the emitted primary Auger electrons is a direct measure of the X-ray absorption process and is used in so called Auger electron yield (AEY) measurements, which are highly surface sensitive, similarly to XPS. As they leave the sample, the primary Auger electrons create scattered secondary electrons, which predominate in the total electron yield (TEY) intensity. The TEY cascade involves several scattering events and originates from an average depth, the electron sampling depth L . Electrons created deeper in the sample lose too much energy to overcome the work function of the sample and, therefore do not contribute to the TEY. The sampling depth L in TEY measurements is typically a few nanometers, while it is often less than 1 nm for AEY measurements. In addition, electron detection provides the higher surface sensitivity and in the majority of studies published in the literature this detection scheme has been employed. The reason for the higher surface sensitivity is the relatively low kinetic energy of the electrons and the corresponding mean

free path in matter, which is typically less than 1 nm for energies between 250 eV and 600 eV. Although the X-ray photons penetrate many microns deep into the sample, the electrons generated at that depth do not emerge from the sample. The inelastic scattering process leads to an electron cascade, of which only those electrons with sufficient energy to overcome the work function of the material will escape the surface. The resulting effective escape depth – and therefore the information depth of electron yield NEXAFS – has been estimated to be in the range of 5 nm for metals and semiconductors, and slightly larger for insulators due to the reduced electron–electron scattering mechanism. The surface sensitivity can be further enhanced by applying a retarding voltage before the electrons enter the channeltron. By suppressing lower kinetic energy electrons, only those electrons that emerge from the outermost surface region (≈ 3 nm) are detected. For the investigation of adsorbates on surfaces, this so-called partial electron yield (PEY) detection has a better signal-to-background ratio than total electron yield (TEY) detection, where all electrons that emerge from the surface are detected. A further option is Auger electron yield (AEY) detection, where only elastically scattered Auger electrons are recorded. The AEY mode requires an electron energy analyser but provides the best surface sensitivity of the three detection techniques.¹¹⁶

NEXAFS is element specific because the X-ray absorption edges of different elements have different energies, and it is also very sensitive to the bonding environment of the absorbing atom. Information concerning the orientation of the molecule can be inferred from using polarised X-ray irradiation.

Actually, the I511-3 beamline is dedicated to RIXS (Resonant Inelastic X-ray Scattering) measurements, the prerequisite of which is registering the X-ray absorption spectra. Here, I am going to give the parameters of this part, even though our longer term aim is to exploit the full potential of the experimental station. (The RIXS spectrum is measuring X-ray emission at the absorption edges and can provide more detailed structural information than the absorption spectrum alone.)

The X-ray absorption spectra of the pristine $\text{Ca}_3\text{Fe-LDH}$ as well as the L-proline intercalated $\text{Ca}_3\text{Fe-LDH}$ samples were registered around the Ca1s , Fe2p , O1s and N1s absorption edges. The samples were inserted a high-vacuum chamber (the pressure was lower than 3.4×10^{-8} mbar), and the spectra were recorded at 0.05 eV steps around the absorption edges. Measurements were performed in the total fluorescence yield (TFY) mode and at various spots of the samples to avoid radiation damage.

4.7.7. UV-Vis spectroscopy

The quantities of the intercalated anions (in the case of indole-2-carboxylate) were measured by UV-Vis spectroscopy. After the acidic degradation of the layers, the indole-2-carboxylic acid concentration was determined at two different wavelengths (218 nm and 292 nm) in a Hewlett Packard 8452A diode array spectrophotometer. The extent of the intercalation is determined from the ratio of indole-2-carboxylate and Fe(III).

4.7.8. FT-IR spectroscopy

The Fourier-transform infrared (FTIR) spectra of the pristine, the organic anion-intercalated LDH and the functionalised silica gel or resin samples were recorded on a BIORAD FTS-65A/896 spectrometer equipped with a DTGS detector in diffuse reflectance. Spectral resolution was 4 cm^{-1} and 256 scans were used for a spectrum. The spectra were baseline corrected and smoothed using the WIN-IR software package. The samples were finely ground and combined with KBr (without pressing into pellets).

4.7.9. Molecular modelling

The sizes of the various intercalated carboxylate ions were determined after performing full geometry optimisation with the PM3 semiempirical quantum chemical code included in the Hyperchem 8.0 molecular modelling package.

4.7.10. Gas chromatography

The epoxidation of 2-cyclohexen-1-one was followed by gas chromatography with the aid of a Hewlett-Packard 5890 Series II: instrument (50 m long HP-1 column, flame ionisation detector) using the internal standard technique.

The chemical compositions of the reaction mixtures after the intermolecular cross-aldol dimerisation-condensation of acetone were determined with an YL6100GC-6000 series gas chromatograph (30 m long Cyclosil B column, inner diameter: 0.25 mm) working in the isothermal mode, at 383 K. Product identification and quantitative analysis were done with mass selective and flame ionisation detectors, respectively.

5. RESULTS AND DISCUSSION

5.1. Preparation and characterisation of Ca(II)Fe(III)- and Mg(II)Fe(III) layered double hydroxides

As it has been mentioned earlier, there are two main structural varieties in the family of layered double hydroxides. One is the group of hydrotalcites resembling the structure of brucite [layered $\text{Mg}(\text{OH})_2$]. In this group the layers contain octahedrally coordinated two- and trivalent metal ions, the edge sharing octahedra are connected by the hydroxide ions. They are located at edges of the layers. The other one is the group of hydrocalumites. The divalent ion is the calcium ion here, and it is heptacoordinated, thus, the layer consists of edge-sharing heptacoordinated calcium hydroxide decahedrons and hexa-coordinated trivalent metal hydroxide octahedrons. In this section I concentrate on describing the optimum experimental conditions for the synthesis of pristine Ca(II)Fe(III)- and Mg(II)Fe(III)-LDHs, representatives of hydrocalumite and hydrotalcite structural types, respectively.

Mg(II)Fe(III)- and Ca(II)Fe(III)-LDHs are already known from the literature,^{89,117,118} since we aimed at using them in intercalation studies, we needed more detailed information about their structural characteristics and the optimal synthetic conditions.

The preparation protocols were optimised through varying the NaOH concentrations, the ratio of the di- and trivalent ions, performing the synthesis in air or excluding the airborne CO_2 by blanketing the reaction mixture with N_2 .

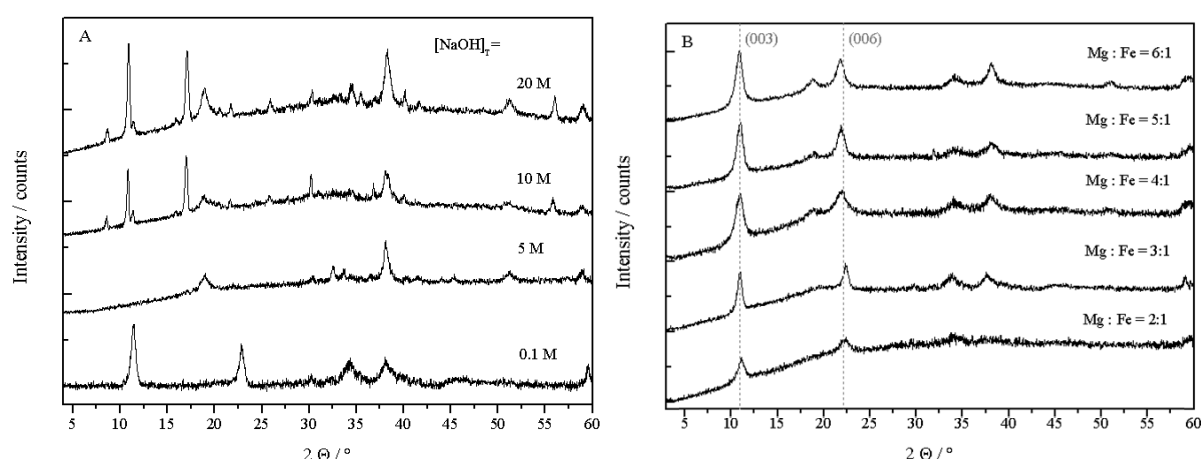


Figure 9. XRD patterns of the freshly prepared and air-dried $\text{Mg}(\text{II})_3\text{Fe}(\text{III})$ -LDH with varying $[\text{NaOH}]_T$ (A) and varying Mg/Fe ratio (B – The final pH value was 9.5 in the synthesis solution).

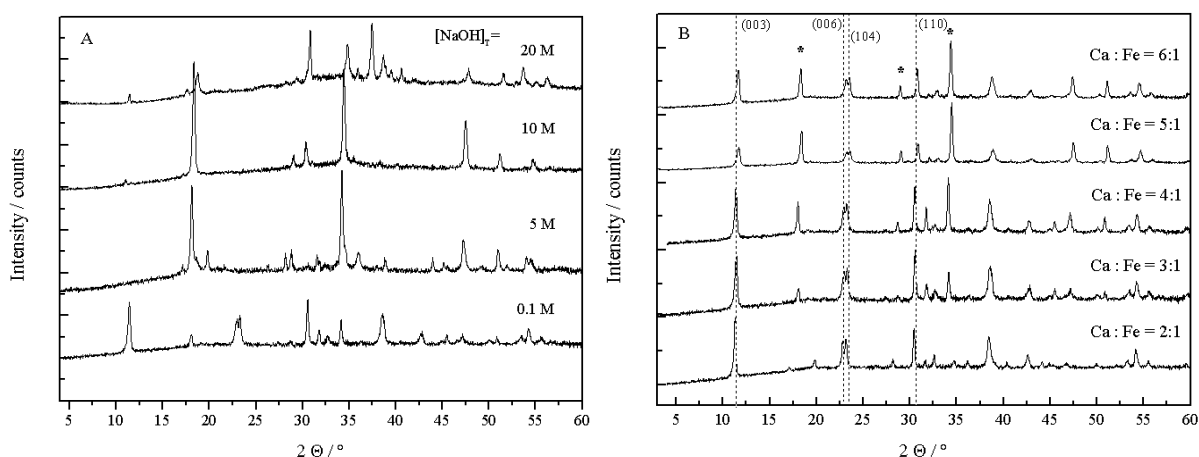


Figure 10. XRD patterns of the freshly prepared and air-dried $\text{Ca(II)}_3\text{Fe(III)-LDH}$ with varying $[\text{NaOH}]_T$ (A) and varying Ca/Fe ratio (B – The final pH value was 13 in the synthesis solution). Reflections associated with Ca(OH)_2 side product are indicated with *.

The diffractogram consists of basal and non basal reflections. The basal reflections ($00l$) represent the thickness of an l number of layers, each consisting of one octahedral metal layer and one interlayer. The typical reflections (003, 006) appearing on the diffractograms and most of the interlayer distances (calculated from the positions of the first reflections) in Table 1, prove that our syntheses were successful. Another important reflection is the (110), which represents the distance between two metal cations in the octahedral layer. The a -parameter of the crystal equals two times the d-spacing of the (110) reflection.¹¹⁹ The intensities of the non basal reflections are used to distinguish between the various polytypes.

As Figure 9. A) and Figure 10. A) attest the syntheses were not successful under highly alkaline (5 M, 10 M NaOH) or hyperalkaline (20 M NaOH) conditions either because layered double hydroxides were not formed or because the ratio of secondary products was too high. However, when the final NaOH concentration was set to 0.1 M, the majority of the sole products were layered double hydroxides. In methods A and B the final NaOH concentrations were set to $3.16 \cdot 10^{-5}$ M for $\text{Mg}_n\text{Fe-LDH}$ and 0.1 M for $\text{Ca}_n\text{Fe-LDH}$, in methods C, and D they were 1.875 M and 2.55 M, respectively. In method B N_2 -blanketing was applied.

XRD measurements confirmed the formation of LDH structures in Methods A, B and C. XRD patterns of the samples with different Mg(II)/Fe(III) ratio exhibited broad reflections corresponding to hexagonal LDH phase. Considerable (*ca.* 10 %) increase was found in the $d(003)$ basal spacing values (from 0.798 nm to 0.823 nm) as the Mg(II)/Fe(III) ratio was increased from 2 to 6.

The XRD traces revealed that $\text{Ca}_2\text{Fe-LDH}$ was the only one that was phase pure, coinciding with the observation of Rousselot *et al.*²¹ Here, all the reflections typical of a

layered double hydroxide could be found and there were no other reflections. For the samples with higher Ca(II)/Fe(III) ratios new reflections showed up, which could clearly be assigned to a Ca(OH)_2 phase. There was some increase in the d(003) basal spacing values with increasing n (it is though it is at the limit of detectability) verifying that LDH phase was always present in the samples (*Table 1*). The relative quantity of the Ca(OH)_2 phase could also be estimated (*Figure 11*). On increasing Ca(II) to Fe(III) ratios from 2 to 6, the quantity of Ca(OH)_2 almost linearly increased from 0% to ~60%.

Table 1. Interlayer distance (d/nm) for Mg(II)Fe(III)-LDHs and Ca(II)Fe(III)-LDHs having various di- to trivalent metal ratios prepared following different synthesis protocols.

Method	Mg(II) : Fe(III) molar ratio				
	2:1	3:1	4:1	5:1	6:1
	Interlayer distance, d/nm				
A	0.796	0.798	0.809	0.806	0.812
B	0.798	0.801	0.799	0.823	0.806
C	0.758	0.771	0.785	0.793	0.788
D	0.793	0.478	0.775	0.441	0.469

Method	Ca(II) : Fe(III) molar ratio				
	2:1	3:1	4:1	5:1	6:1
	Interlayer distance, d/nm				
A	0.789	0.778	0.763	0.759	0.769
B	0.782	0.774	0.775	0.754	0.761
C	0.773	0.775	0.775	0.773	0.777
D	0.489	0.489	0.490	0.491	0.481

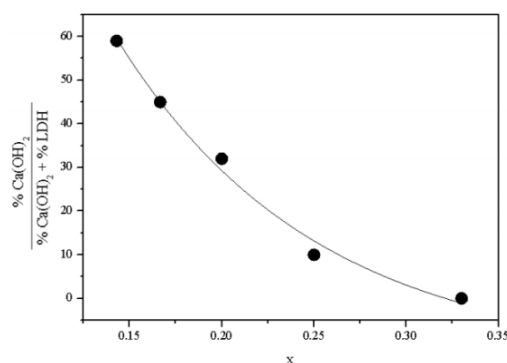


Figure 11. The relative quantity of the Ca(OH)_2 phase in the function of the molar fraction (x) of Fe(III) in the $\text{Ca}_n\text{Fe-LDH}$ samples (where n is the Ca(II)/Fe(III) ratio in the synthesis mixture).

As it is seen, the Ca(OH)_2 content almost linearly increased with increasing Ca(II)/Fe(III) ratio, *i.e.*, as the relative Ca(II) content increased, substantially smaller amount of Ca was incorporated into the layers of the LDH compared to the intended composition. However, the basal spacing increased as the Ca(II) content increased, which may be taken as a sign of the increasing number of Ca(II) ions in the environment of Fe(III) ions.

Data reveal that 0.1 M concentration for the NaOH solution is adequate for the successful synthesis of both hydrotalcite and hydrocalumite LDH types and using N_2 blanket is advantageous if one does not want the strongly adhering CO_3^{2-} ions to be present among the LDH layers. The evaluation of the diffractograms with the aid of the EXRAY program and comparing the results to ASTM standard data files reveals that the reflections of $\text{Ca(II)}_n\text{Fe(III)-LDHs}$ can be indexed for a hexagonal lattice with R3m rhombohedral symmetry (Hexagonal Scalenohedral class), which is commonly used for description of LDH structures; from thus the lattice parameters could be determined (*Table 2*).

Table 2. Lattice parameters of $\text{Ca}_n\text{Fe-LDHs}$.

Sample (from <i>Method B</i>)	$d(003)$ / nm	a / nm	c / nm	D (thickness) / nm
$\text{Ca}_2\text{Fe-LDH}$	0.782	0.583	2.302	35.37
$\text{Ca}_3\text{Fe-LDH}$	0.774	0.583	2.306	35.61
$\text{Ca}_4\text{Fe-LDH}$	0.775	0.586	2.329	36.66
$\text{Ca}_5\text{Fe-LDH}$	0.754	0.579	2.270	34.64
$\text{Ca}_6\text{Fe-LDH}$	0.761	0.581	2.277	34.36

The average value of D was calculated from FWHM of peak (003) and (006) using the Scherrer equation:

$$D = \frac{B\lambda}{\beta \cos \theta}$$

(where B is the shape factor, λ is the X-ray wavelength, β is the line broadening at half of the maximum intensity (FWHM) in radians, and θ is the Bragg angle). The observed lattice parameters (a and c) are similar to that reported elsewhere.¹²⁰ $\text{Ca}_n\text{Fe-LDH}$ has lattice parameter a of ~ 0.58 nm due to the seven-coordination structure of Ca(II) .¹²¹ The FWHM of (hk0) was determined to be higher in MgFe- than in CaFe-LDHs showing the better crystallinity of CaFe-LDHs .

^{57}Fe Mössbauer spectra recorded at 295 K and 78 K are displayed in *Figure 12* and relevant data are summarised in *Table 3* for $\text{Mg}_n\text{Fe-LDH}$ and in *Figure 13* and *Table 4* for

Ca_nFe-LDH. The evaluation of the Mössbauer spectra obtained at 295 K was optimal with fitting an asymmetric doublet. It should be pointed out at once that this asymmetry is probably not related to texture effects as one might think. The asymmetry may be attributed to Fe³⁺ positional disorder within the Fe(OH)₆ octahedra. This is expected since the iron centres are surrounded by Fe³⁺ and M(II) at random, and these randomly distributed neighbouring octahedra exert perturbations on the Fe³⁺ centres with varying intensities.²³

The ⁵⁷Fe Mössbauer parameters reflect high-spin Fe(III) microenvironments for all cases. ⁵⁷Fe Mössbauer measurements were repeated on a series of freshly prepared samples cooled immediately to 78 K after their preparation to avoid structural changes due to the possible reaction with aerial CO₂. Spectra and parameters obtained were reproducible for every sample. At 295 K the Mössbauer parameters were in excellent correspondence with those measured at 78 K, except the isomer shifts, which displayed some changes due to second order Doppler shift.

Table 3. ⁵⁷Fe Mössbauer parameters obtained at 78 K and 295 K for Mg_nFe-LDHs.

		Mg(II) : Fe(III) molar ratio				
		2:1	3:1	4:1	5:1	6:1
78 K	δ / mm/s	0.46 ± 0.004	0.46 ± 0.003	0.46 ± 0.005	0.46 ± 0.004	0.46 ± 0.005
	Δ / mm/s	0.63 ± 0.01	0.57 ± 0.01	0.54 ± 0.01	0.52 ± 0.01	0.52 ± 0.01
	W / mm/s	0.53 ± 0.01	0.47 ± 0.01	0.46 ± 0.01	0.46 ± 0.01	0.48 ± 0.015
295 K	δ / mm/s	0.36 ± 0.000	0.37 ± 0.003	0.36 ± 0.002	0.37 ± 0.002	0.37 ± 0.008
	Δ / mm/s	0.62 ± 0.001	0.54 ± 0.003	0.51 ± 0.002	0.51 ± 0.003	0.52 ± 0.009
	W / mm/s	0.63 ± 0.002	0.76 ± 0.007	0.74 ± 0.004	0.68 ± 0.005	0.65 ± 0.017

No change was observed in the isomer shift with the variation of Mg(II)/Fe(III) ratio, reflecting no change in the electronic density at the site of the iron nucleus in these LDHs. This is in agreement with the ionic character of these compounds. However, it has been found that the quadrupole splitting significantly decreased with increasing Mg/Fe ratio indicating that the electric field gradient at the iron site increased on increasing iron content. This is consistent with the variations in the spatial charge distribution around the iron. At low iron content, in Mg₆Fe-LDH, iron is situated in a layer where there are mainly Mg(II) ions in its second coordination sphere, which can supply a more symmetric charge distribution, consequently, a smaller electric field gradient and quadrupole splitting. In Mg₂Fe-LDH, some

Mg atoms in the second coordination sphere must be replaced by Fe(III) atoms increasing the electric field gradient and the quadrupole splitting. The results revealed that different microenvironments of iron were incorporated into Mg site in Mg_nFe -LDH structures at different Mg(II)/Fe(III) ratios.

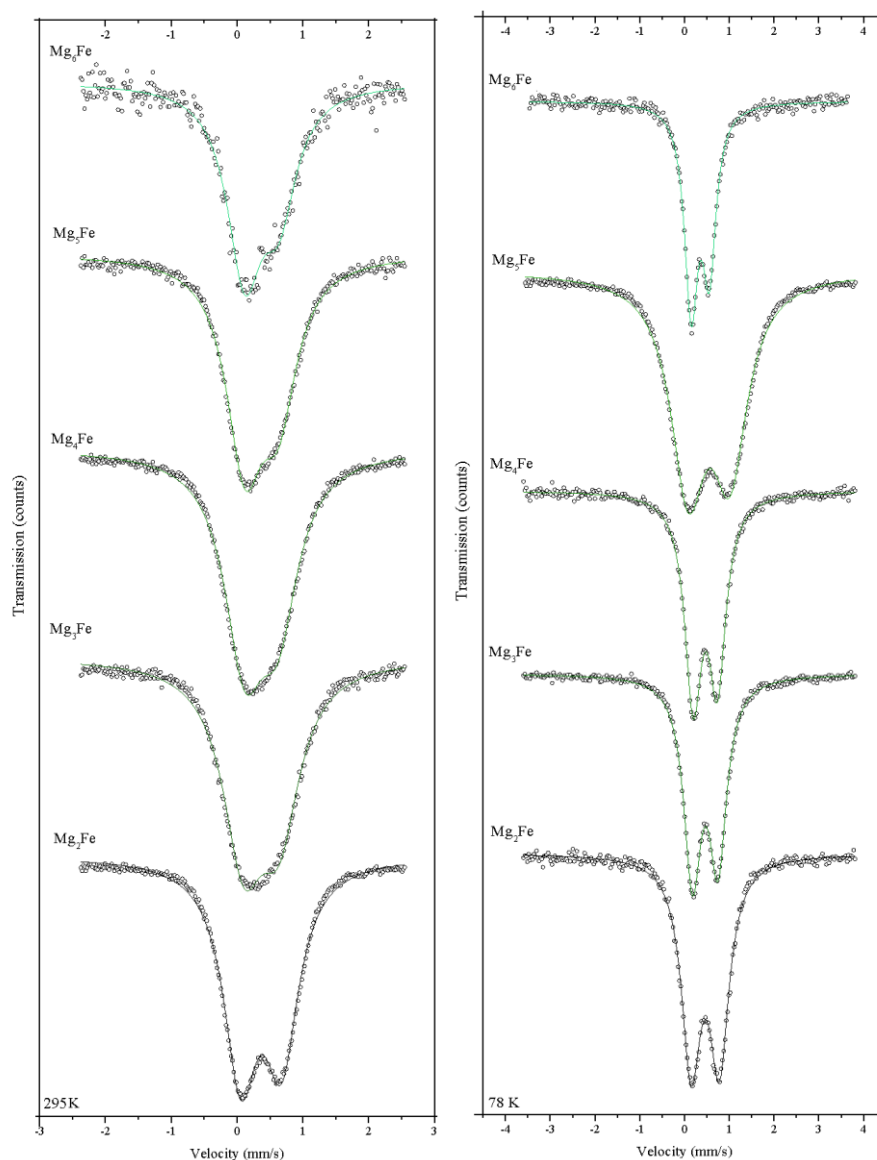


Figure 12. The ^{57}Fe Mössbauer spectra of Mg_nFe -LDH at 78 K (left) and 295 K (right).

^{57}Fe Mössbauer measurements revealed significant differences only in the values of quadrupole splitting between Ca_2Fe -LDH and the other Ca-containing samples (Table 4). It may indicate a change in the charge distribution asymmetry between Ca_2Fe -LDH and the other samples, which is also the sign of the change in the amount of Ca(II) ions around the Fe(III) ions next to their immediate surroundings. The same isomer shift for all substances shows that the electron field density measured at the iron nucleus – which is characteristic of the chemical bond – was identical for every sample.

Table 4. ^{57}Fe Mössbauer parameters obtained at 78 K and 295 K.

		Ca(II) : Fe(III) molar ratio				
		2:1	3:1	4:1	5:1	6:1
78 K	δ / mm/s	0.46 ± 0.001	0.47 ± 0.002	0.47 ± 0.001	0.47 ± 0.011	0.47 ± 0.003
	Δ / mm/s	0.52 ± 0.001	0.45 ± 0.003	0.46 ± 0.001	0.45 ± 0.01	0.45 ± 0.004
	W / mm/s	0.49 ± 0.003	0.43 ± 0.005	0.41 ± 0.003	0.41 ± 0.01	0.39 ± 0.008
295 K	δ / mm/s	0.37 ± 0.003	0.37 ± 0.002	0.37 ± 0.003	0.36 ± 0.005	0.37 ± 0.003
	Δ / mm/s	0.49 ± 0.004	0.41 ± 0.002	0.41 ± 0.004	0.40 ± 0.005	0.40 ± 0.004
	W / mm/s	0.60 ± 0.007	0.54 ± 0.004	0.61 ± 0.007	0.64 ± 0.010	0.56 ± 0.007

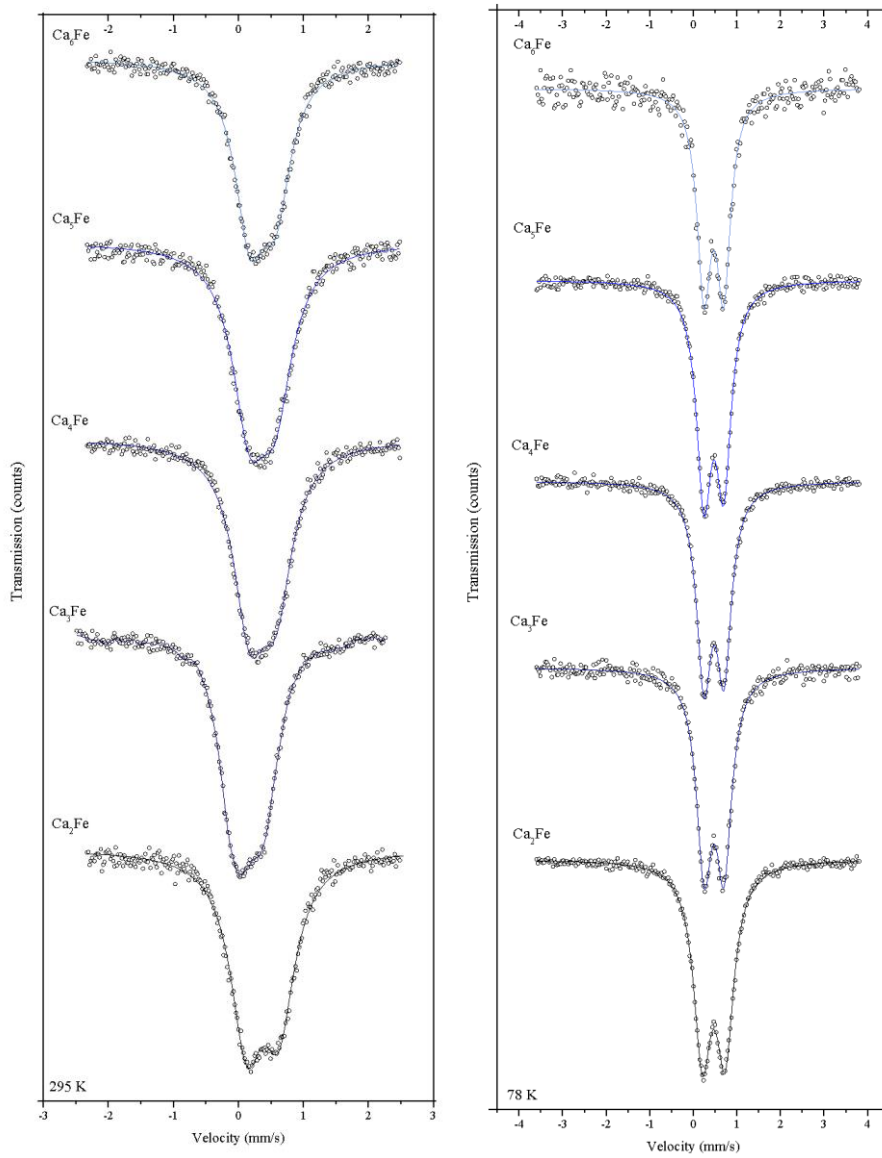


Figure 13. The ^{57}Fe Mössbauer spectra of $\text{Ca}_n\text{Fe-LDH}$ at 78 K (left) and 295 K (right).

It has been observed that letting the $\text{Ca}_2\text{Fe-LDH}$ stand in air for an extended period of time (~ 3 months), the quadrupole splitting has changed from 0.49 mm/s to 0.69 mm/s at 298 K. Since the Mössbauer parameters of a freshly prepared sample were the same as of the original one before ageing, and those of the other samples did not vary with ageing, it can be stated that phase-pure $\text{Ca}_2\text{Fe-LDH}$ decomposed on ageing and CaCO_3 became the predominant crystalline phase. This is verified with the X-ray diffractogram of the aged sample (*Figure 14*).

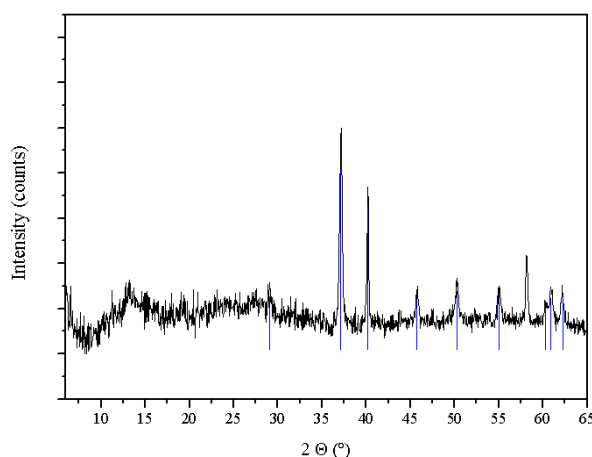


Figure 14. The X-ray diffractogram of $\text{Ca}_2\text{Fe-LDH}$ after ageing in air for ~ 3 months – CaCO_3 is the predominant crystalline phase (reflections denoted by vertical lines).

It seems to be clear that the presence of Ca(OH)_2 , even in small amount, inhibits the decomposition of the LDH phase, and therefore, exerts a stabilising effect. Although the M(II):M(III) ratio is 2 in hydrocalumites – M(OH)_2 is also formed in all other compositions –, this ideal compositions of CaFe-LDH suffers from some instability. The 3:1 composition is proved to be ideal for further works of longer duration, since it is stable in air and contains Ca(OH)_2 of only $\sim 10\%$.

For more detailed investigations, described in the followings, the $\text{Mg}_4\text{Fe-LDH}$ and the $\text{Ca}_3\text{Fe-LDH}$ samples were chosen, since they nearly completely phase pure and they do not suffer such instability than lower M(II)/Fe(III) ratios. (In the sections where the intercalation work is described and discussed they will be mentioned as CaFe- and MgFe-LDHs .)

X-ray absorption spectra of the pristine $\text{Ca}_3\text{Fe-LDH}$ sample registered around the $\text{Ca}2p$, $\text{Fe}2p$ and $\text{O}1s$ edges are seen in *Figure 15*. I am only going to give their qualitative description, and they will be used as references for those of the L-proline– CaFe-LDH sample.

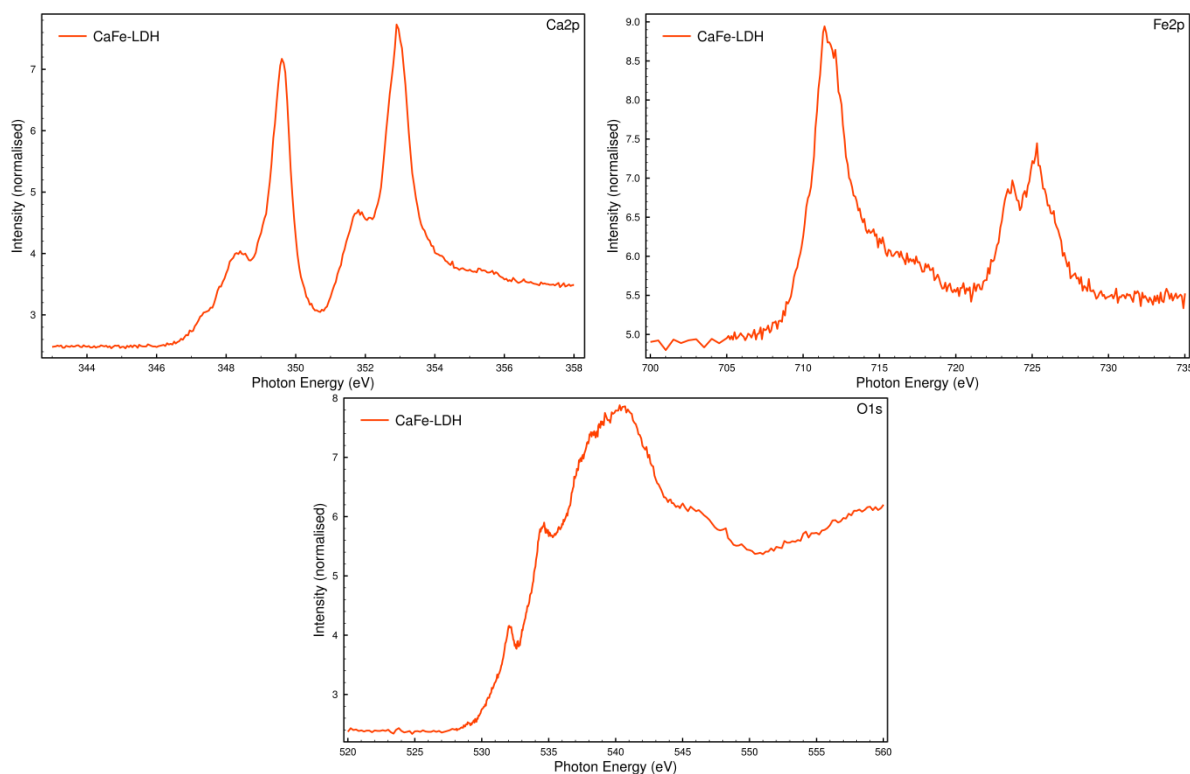


Figure 15. X-ray absorption spectra of the $\text{Ca}_3\text{Fe-LDH}$ sample performed around the $\text{Ca}2p$, $\text{Fe}2p$ and $\text{O}1s$ absorption edges.

Both the Ca and Fe X-ray absorption spectra contain two intense peaks, since the $2p$ and the $2p_{1/2}$ energies are close to each other for both elements. The less intense peaks probably indicate separate phases and/or imperfections in the crystal structure. We know from XRD measurements that $\text{Ca}(\text{OH})_2$ is present as a minor but important stabilising component beside the LDH. Since there is no sign a separate Fe-containing non-LDH phase, the splitting in the peak at higher energy in the Fe X-ray absorption spectrum may be due to imperfections, probably vacancies in the LDH crystal structure. The $\text{O}1s$ X-ray absorption spectrum has two pre-edge features indicating that oxygen is present in various environments. Beside the octahedral location in the LDH structure, the geometric environment in the $\text{Ca}(\text{OH})_2$ phase is probably different, just as at the imperfections of the LDH crystal lattice.

The results of thermal measurements are consistent with those characteristic of MgFe-LDH compounds.²³ The DTG curve for Mg_nFe sample is shown in Figure 16. Two endothermic peaks located between 100 and 170 °C and at 320 °C are observed. The first thermal event is attributed to the loss of physisorbed and interlamellar water (without the collapse of the layered structure) along with a grafting process of the interlamellar anion. The second thermal event (at 320 °C) is related to the collapse of the lamellar structure where both

hydroxyl groups and interlamellar anions are released. The results are qualitatively consistent with those observed for other hydrotalcite systems.¹²²

As for the $\text{Ca}_3\text{Fe-LDH}$, until the collapse of the layered structure, water loss occurred in three major steps: first, desorption of physisorbed water (100–150 °C), then removal of interlayer water (175–350 °C) and finally, the loss of structural water (400–475 °C – it is in the form of structural OH groups) leading to the deterioration of the layered structure. The temperature ranges differed for the two compounds.

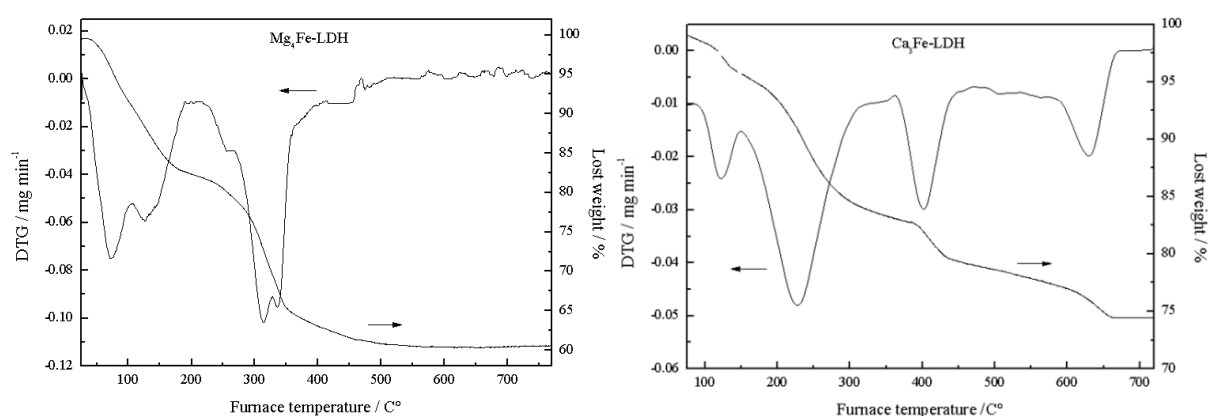


Figure 16. TG/DTG curves for Mg_4Fe and Ca_3Fe LDHs.

The FT-IR spectra (Figure 17) indicate the presence of isolated $(\text{Ca(II)}_3\text{Fe(III)})\text{-LDH}$: 3640 cm^{-1} , $\text{Mg(II)}_4\text{Fe(III)}\text{-LDH}$: 3731 cm^{-1}) as well as hydrogen-bonded OH^- groups in both samples (the broad bands above 3000 cm^{-1}). This hydrogen-bonded network is among OH^- groups and water molecules adsorbed on the outer surface as well as present in the interlayer spacing. This band is much broader for $\text{Mg(II)}_4\text{Fe(III)}\text{-LDH}$, indicating more extended hydrogen-bonded network.

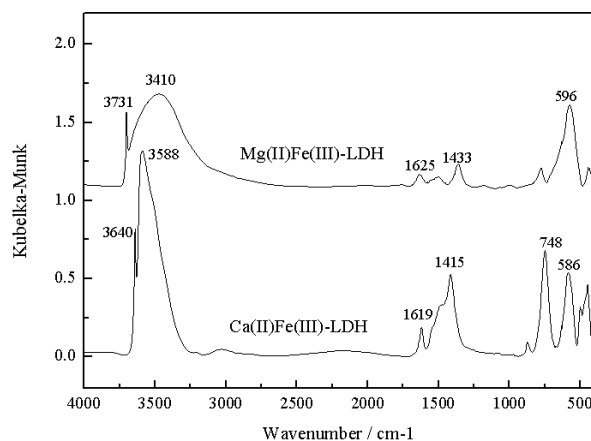


Figure 17. FTIR spectra of the Ca_3Fe - and the Mg_4Fe -LDH.

Bands near 1620 cm^{-1} ($\text{Mg}_4\text{Fe-LDH}$: 1625 cm^{-1} , $\text{Ca}_3\text{Fe-LDH}$: 1619 cm^{-1}) are due to the deformation vibrations of the interlayer water molecules. Although not as widespread but equally important, FT-IR can describe the LDH lattice vibrations with an excellent degree of validity. Bands under 1000 cm^{-1} may be assigned to the O-metal ion-O units of the layers. These vibrations are dependent on the type of metals in the LDH, so different metals will lead to different vibrational mode¹²³ assignments. Since chloride salts and NaOH were used in the synthesis, Cl^- and OH^- ions were the main interlayer anions. It should be noted that the band characteristic to the carbonate ion ($\sim 1360\text{ cm}^{-1}$) is not seen in the spectra, therefore it is present in insignificant quantities among the layers.

SEM images also indicated the layered structure for both chosen samples (*Figure 18* for $\text{Mg}_4\text{Fe-LDH}$, *Figure 19* for $\text{Ca}_3\text{Fe-LDH}$). This is fortunate, since arrangement at the atomic level is not always reflected in the morphology of the materials. The basic shape of an LDH crystal is a hexagonal platelet. These large amounts of tiny crystals hardly grow out; instead they agglomerate in regions of less turbulence, resulting in a broad size distribution of agglomerated particles. In the agglomerated particles, the platelets are piled on top of each other. The di- and trivalent metal ions are largely evenly distributed in the samples, as it is seen in the SEM-EDX elemental maps.

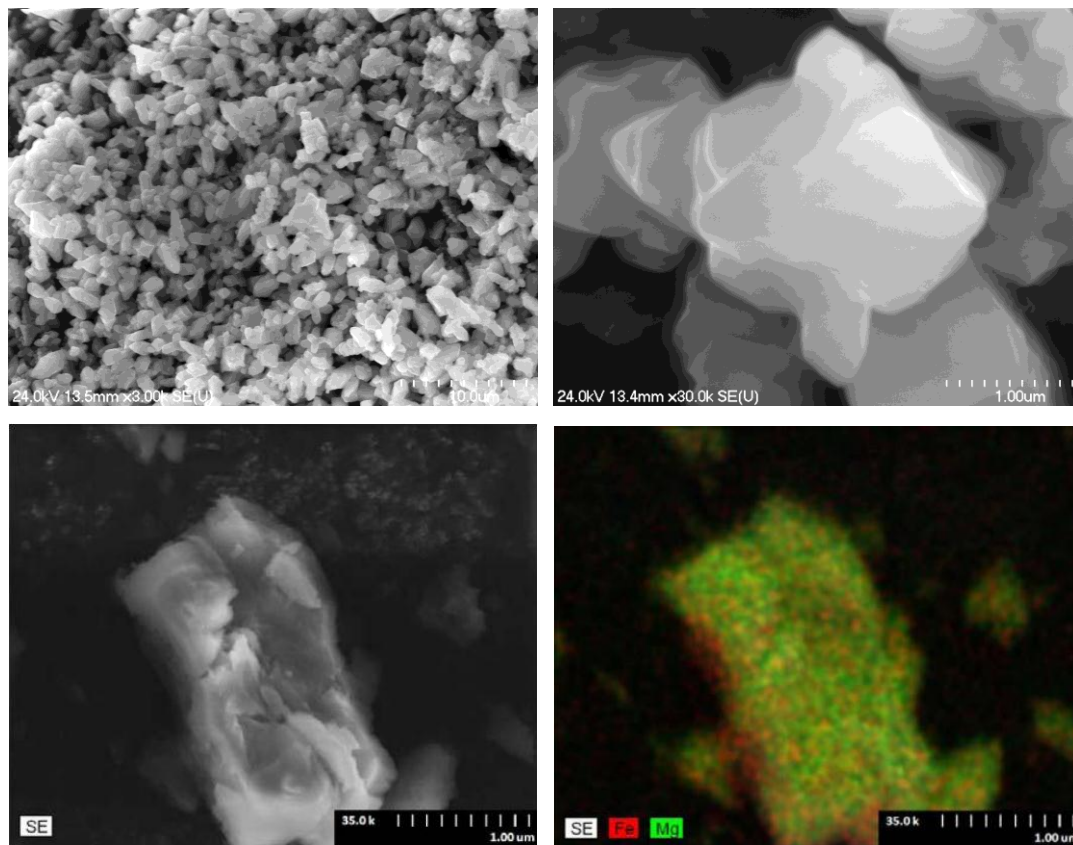


Figure 18. SEM images of $\text{Mg(II)}_4\text{Fe(III)-LDH}$ at various magnifications and elemental map at magnification of 35,000.

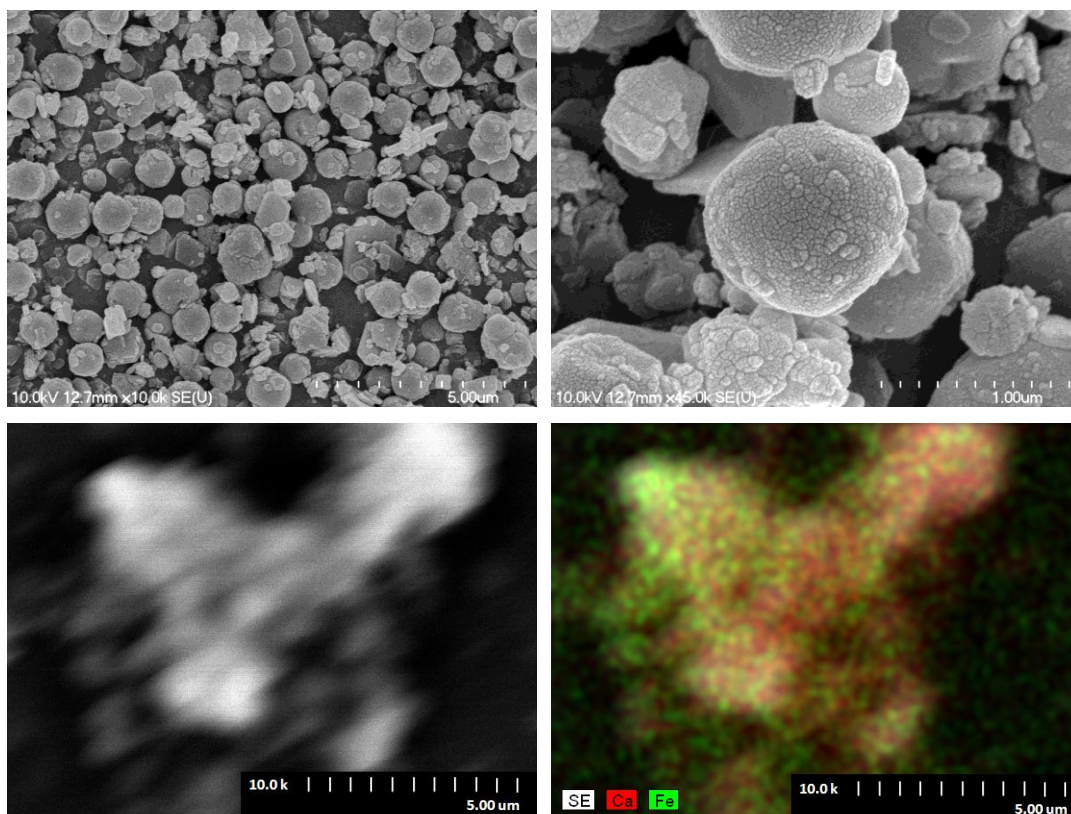


Figure 19. SEM images of $\text{Ca(II)}_3\text{Fe(III)-LDH}$ at various magnifications and elemental map at magnification of 10,000.

As stated earlier, $\text{Ca}_3\text{Fe-LDH}$ has a rhombohedral crystal space group. When viewed by SEM, the LDH crystals appear as (hexagonally shaped) platelets, but the actual hexagonal shape is more clearly seen by the TEM image (Figure 20). The hexagonal platelets are the most common image for LDH with simple anions (halides, nitrate and carbonate), even if the LDH have a rhombohedral crystal polytype. This is not a contradiction, because the rhombohedral polytype refers to the layer stacking sequence and the hexagonal platelets refer to overall crystal growth. Note, that LDHs have been observed to have quite different morphologies with certain organic anions.¹²⁴

As can be seen, the pristine $\text{Ca}_3\text{Fe-LDH}$ particles are of typical plate-like shape with the lateral size of 150–300 nm, but the sample had a relatively broad size distribution because of crystal aggregation.

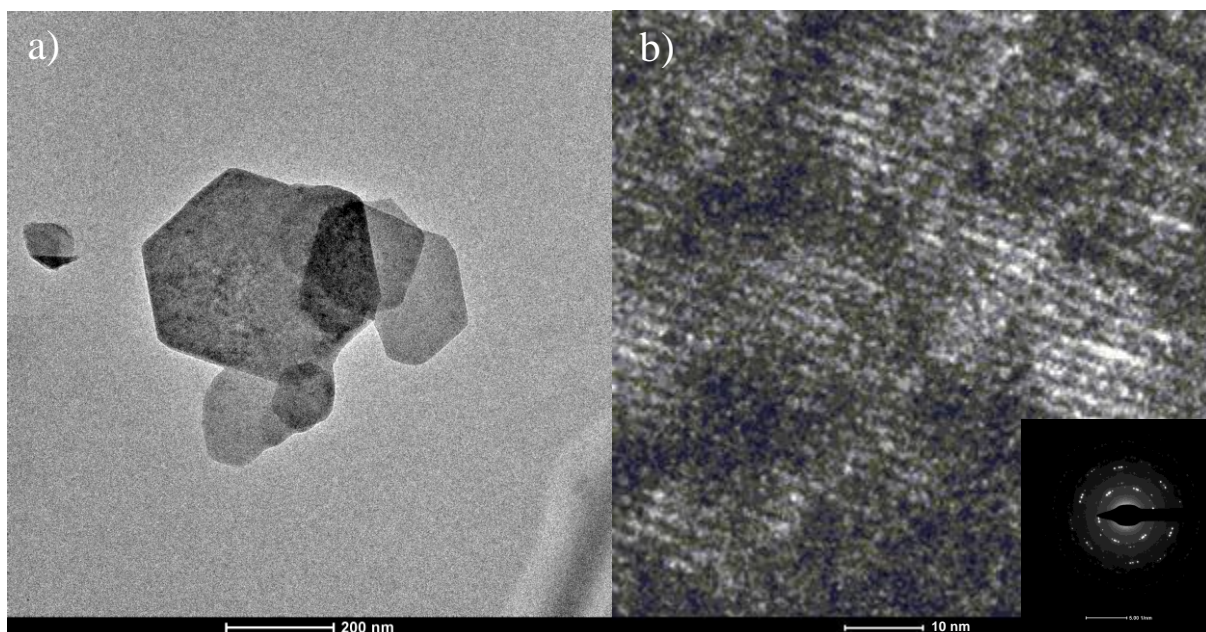


Figure 20. Bright field (a) and dark-field (b) TEM images of $\text{Ca}_3\text{Fe-LDH}$.

The distance of two layers in the $\text{Ca}_3\text{Fe-LDH}$ sample was estimated from a transmission electron microscopic (TEM) dark-field image (Figure 20. b), giving a value of approximately 0.58 nm. If one subtracts this from the basal spacing obtained from powder XRD, the layer thickness value (0.19 nm) is in good agreement with the 0.178 nm, determined by others from high-precision XRD data.²¹

5.2. Intercalation into the Ca₃Fe-LDH

It has been found that the ideal LDH to prepare intercalated organic-inorganic composites is the Ca₃Fe-LDH (denoted as CaFe-LDH in the followings), which is not air sensitive, stable in aqueous solution, and has reasonably large primary particle size.

The carboxylate anions were intercalated into CaFe-LDH with the dehydration-rehydration method, utilising the memory effect of the layered double hydroxides.

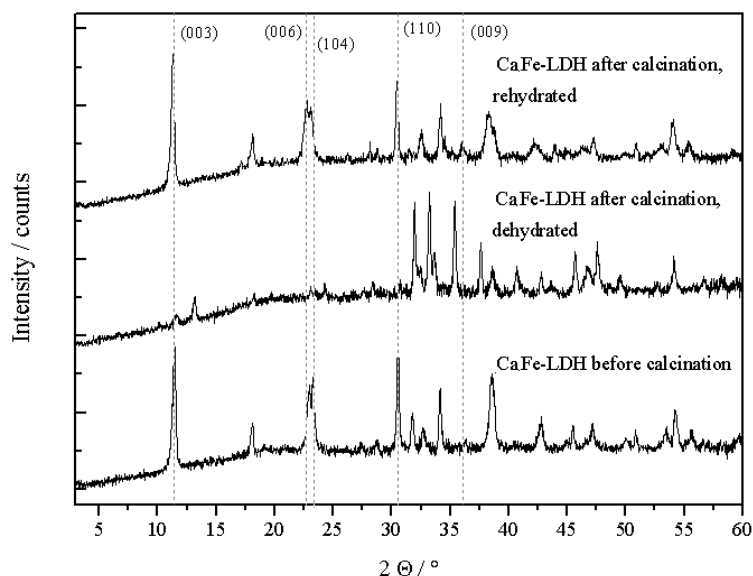


Figure 21. Dehydration (at 500 °C, N₂) and rehydration (in ethanol/water solution) of the CaFe-LDH.

First, it was verified that upon these conditions the rehydration of the "layered double oxide" occurred and the original structure restored indeed (Figure 21).

In the course of intercalation the heterocyclic compounds were suspended in alkaline ethanol/water or acetone/water solvent mixtures. Upon rehydration, ion exchange occurred as well. Powder XRD measurements were performed on the pristine LDH and the sodium salt of the carboxylic acids, as well as the intercalated samples obtained from both solvent mixtures. Carbon dioxide was carefully excluded from the reaction mixture, to avoid intercalation of carbonate ion in the positively charged layer, since in this case further ion exchange (*i.e.*, substitution of the carbonate ion) would have been tremendously difficult.

Obviously, one has to make sure that the intercalation was successful, therefore characterisation steps followed to prove the presence of the organic anions between the layers of the LDH. Powder XRD measurements were performed first on the pristine as well as the intercalated samples. The diffractograms obtained (Figure 22) were typical of LDHs, but for ease of comparison and perspicuity, only the first reflection are presented ($2\theta = 3\text{--}14^\circ$).

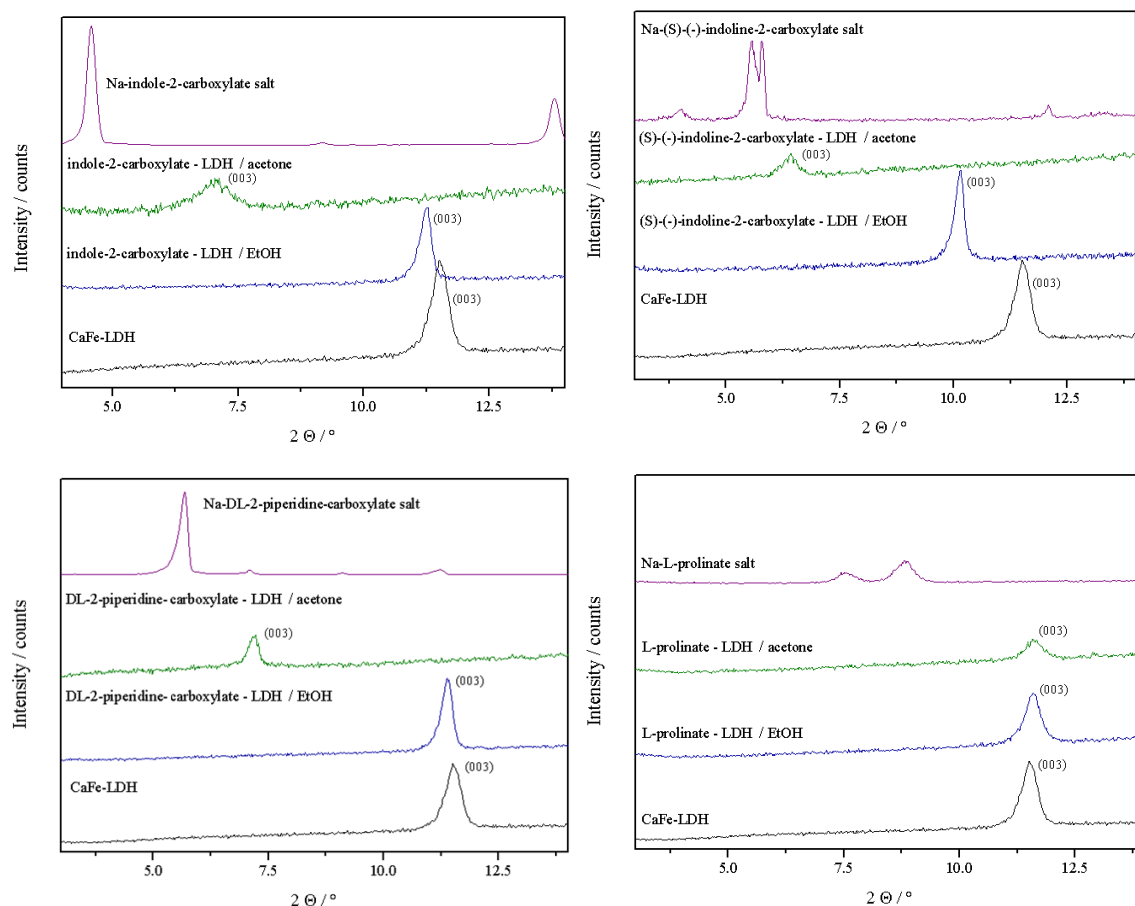


Figure 22. XRD traces of the pristine CaFe-LDH, the intercalated LDH prepared from alkaline ethanol/water and acetone/water mixtures and the Na-salts of the carboxylate anions.

Basal spacings were calculated from the (003) reflection. The measured interlayer spacings contain one layer of the host material, which may be approximated as 0.178 nm, according to Rousselot *et al.*²¹ Thus, the distance of the layers is shown in Table 5 along with the dimensions of the anions, optimised by the PM3 semiempirical code. Since the sizes of the D and L isomers are different, the dimensions of both were calculated.

Table 5. The $d_{(003)}$ values for the intercalated LDHs.

N-containing heterocycles	EtOH/H ₂ O (nm)	Acetone/H ₂ O (nm)	Dimensions of the anions* (nm)	Interlayer distance EtOH/H ₂ O (nm)**	Interlayer distance Acetone/H ₂ O (nm)**
indole-2-carboxylate	0.79	1.24	0.50 0.30 0.78	0.61	1.06
(S)-(-)-indoline-2-carboxylate	0.79	1.22	0.50 0.30 0.78	0.61	1.04
			0.50 0.27 0.76		
DL-2-piperidine-carboxylate	0.78	1.24	0.43 0.33 0.57	0.60	1.06
			0.43 0.30 0.63		
L-prolinate	0.79	0.76	0.39 0.28 0.52	0.61	0.58
			0.39 0.35 0.53		

* The edges of a cuboid in which the anion precisely fit, optimized by the PM3 semiempirical method

** calculated as the experimentally observed $d_{(003)}$ reduced by the layer thickness of $\text{Ca}_3\text{Fe-LDH}$ (0.178 nm)²¹

The interlayer distances were found to be significantly different in the intercalated LDHs prepared in different solvents. If the rehydration took place in alkaline acetone/water, XRD measurements indicated extremely increased interlayer distances in all cases except for the intercalated L-prolinate – sure sign of successful intercalation. In contrast if alkaline ethanol/water mixture was applied during syntheses the interlayer distances did not change significantly. Two possible explanations may account for these experimental results. Either there was no intercalation or the dimensions of the anions allow an arrangement in the gallery space of LDH that does not cause appreciable change in the basal distance. This issue and the possible arrangement of the organic molecules in the gallery space of LDHs will be discussed in the followings.

Determination of the amount of the intercalated indole-2-carboxylate between the layers was also attempted. Theoretically, the amount of the interlayer anions is equal to the Fe^{3+} – content of the layer. By ICP-OES measurements the iron-content of our pristine LDH was $6.859 \cdot 10^{-4}$ mol/g. This is the maximum quantity of the carboxylate anions that can be intercalated. UV-VIS spectroscopy was applied to find out the actual intercalated amount. Only the indole-2-carboxylic acid has appreciable absorbance in the range of 200–800 nm ($\lambda = 218$ nm and 292 nm), therefore similar measurements could not be applied for the other intercalated ions.

Table 6. The indole-2-carboxylate content of the LDHs.

	indole-2-carboxylate-LDH EtOH/H ₂ O	indole-2-carboxylate-LDH acetone/H ₂ O
indole-2-carboxylate intercalated to the LDH (mol/g)	$1.88 \cdot 10^{-4} - 2.20 \cdot 10^{-4}$	$2.38 \cdot 10^{-4} - 2.75 \cdot 10^{-4}$
$(n_{\text{indole}}/n_{\text{Fe}}) \cdot 100$	27–32 %	34–40 %

According to the UV-Vis measurements, the intercalation of indole-2-carboxylate in both in ethanol/water and in acetone/water was successful (*Table 6*), although slightly lower amount of organic anion was incorporated between the layers when aqueous ethanol was the solvent. A possible explanation can be that an aqueous medium favours the exchange with inorganic anions, whilst an organic solvent does it with organic anions.⁴⁷

In order to confirm that the intercalation was successful, the samples were further studied by scanning electron microscopy followed by elemental mapping and EDX measurements. SEM micrographs of the samples were taken at various magnifications.

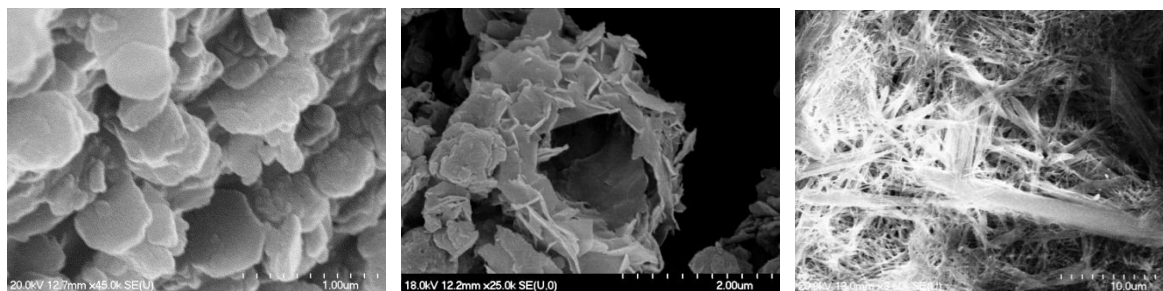


Figure 23. SEM images of (a) the indole-2-carboxylate-LDH prepared in EtOH/H₂O, (b) the indole-2-carboxylate-LDH prepared in acetone/H₂O, (c) the sodium salt of the indole-2-carboxylic acid.

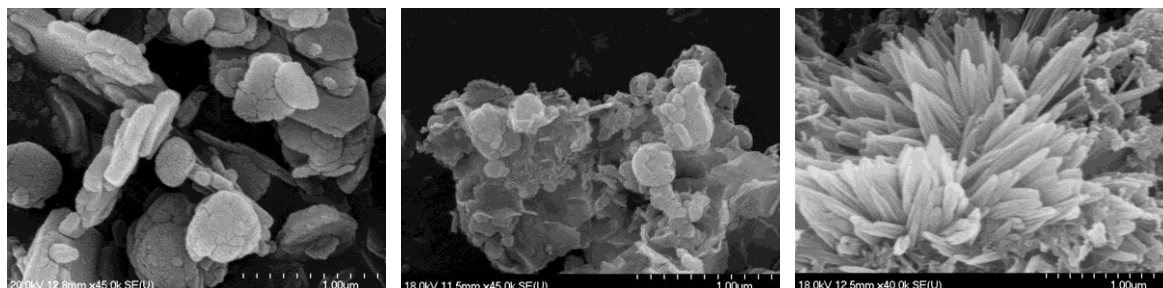


Figure 24. SEM images of (a) the (S)-(-)-indoline-2-carboxylate-LDH prepared in EtOH/H₂O, (b) the (S)-(-)-indoline-2-carboxylate-LDH prepared in acetone/H₂O, (c) the sodium salt of the (S)-(-)-indoline-2-carboxylic acid.

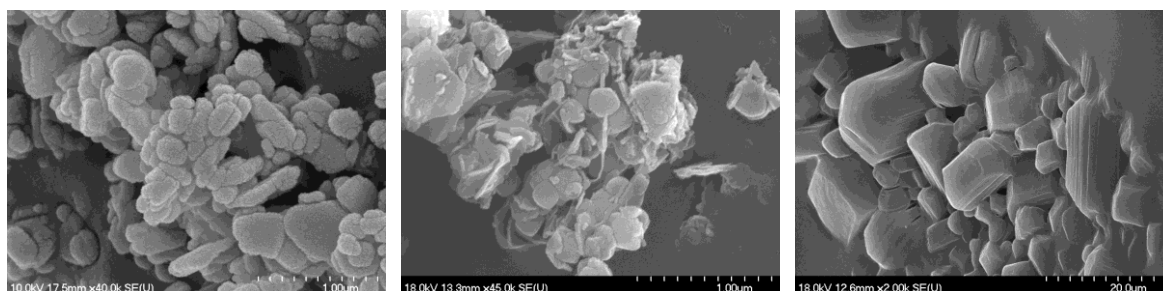


Figure 25. SEM images of (a) the DL-2-piperidine-carboxylate-LDH prepared in EtOH/H₂O, (b) the DL-2-piperidine-carboxylate-LDH prepared in acetone/H₂O, (c) the sodium salt of the DL-2-piperidine-carboxylic acid.

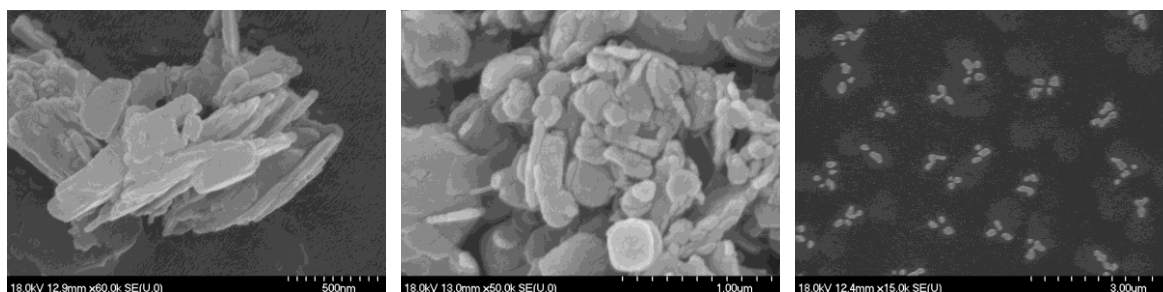


Figure 26. SEM images of (a) the L-prolinate-LDH prepared in EtOH/H₂O, (b) the L-prolinate-LDH prepared in acetone/H₂O, (c) the sodium salt of the L-proline.

The lamellar structures of the samples are clearly seen even at the lowest magnification. At the highest magnification one can see some minor differences in the morphologies of the

samples obtained from the different solvents. The images reveal that the carboxylate ions are within the layers, since the significantly different crystals forms of the carboxylate salts are not seen on the outer surfaces of the lamellae of the hybrid materials even at relatively high magnifications.

The SEM–EDX combination allowed us to prepare the elemental map of the intercalated material. They are seen in *Figure 27. a) – h)* on the SEM images of the hybrids.

Figure 27.a-h) Elemental maps made on the SEM images of the samples.

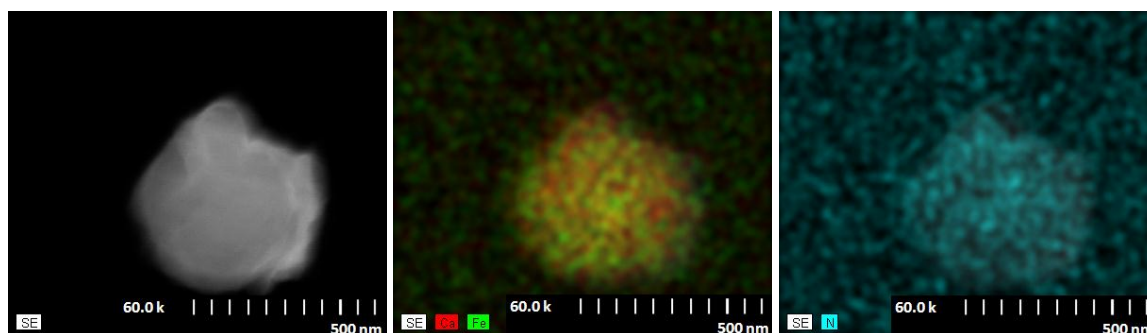


Figure 27.a) indole-2-carboxylate-LDH prepared in EtOH/H₂O (magnification at 60,000).

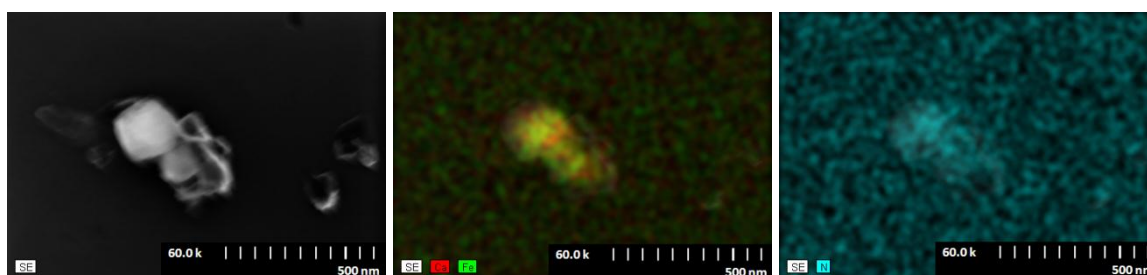


Figure 27.b) indole-2-carboxylate-LDH prepared in EtOH/H₂O (magnification at 60,000).

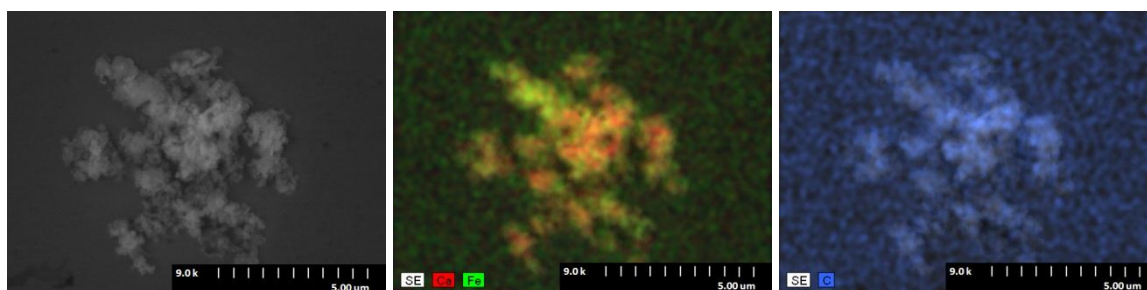


Figure 27.c) (S)-(-)-indoline-2-carboxylate-LDH prepared in EtOH/H₂O (magnification at 9,000).

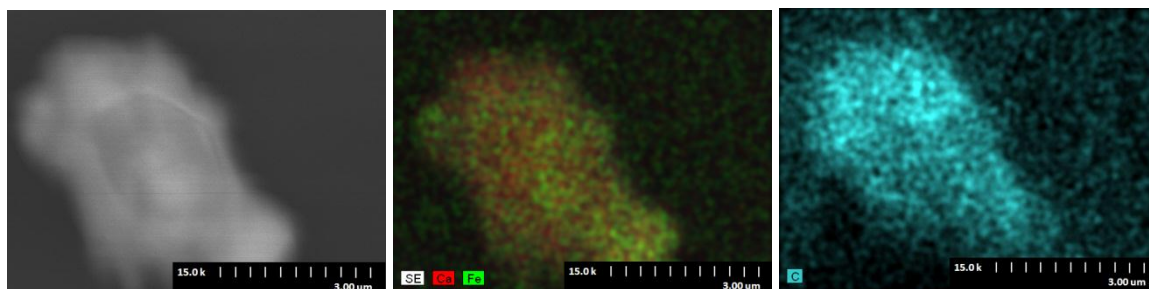


Figure 27.d) (S)-(-)-indoline-2-carboxylate-LDH prepared in acetone/H₂O (magnification at 15,000).

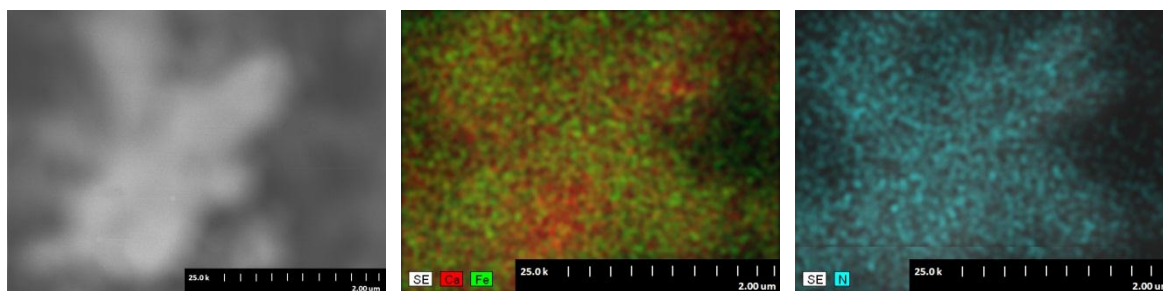


Figure 27.e) DL-2-piperidine-carboxylate-LDH prepared in EtOH/H₂O (magnification at 25,000).

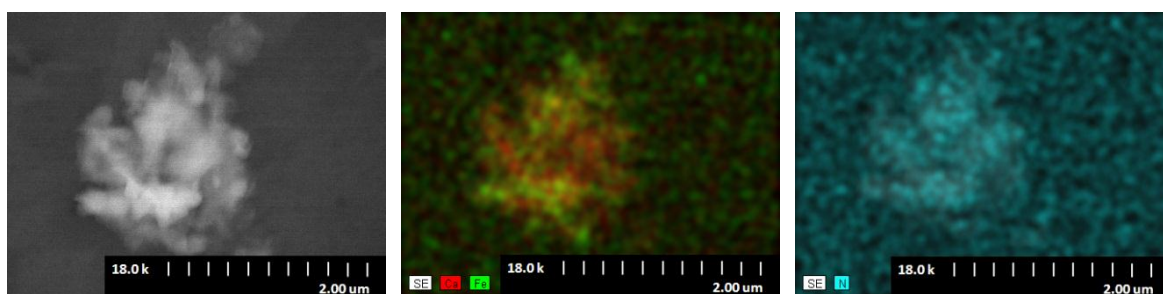


Figure 27.f) DL-2-piperidine-carboxylate-LDH prepared in acetone/H₂O (magnification at 18,000).

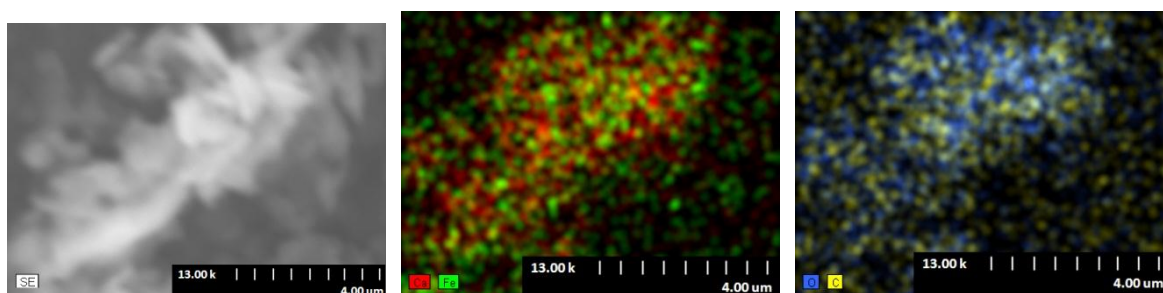


Figure 27.g) L-prolinate-LDH prepared in EtOH/H₂O (magnification at 13,000).

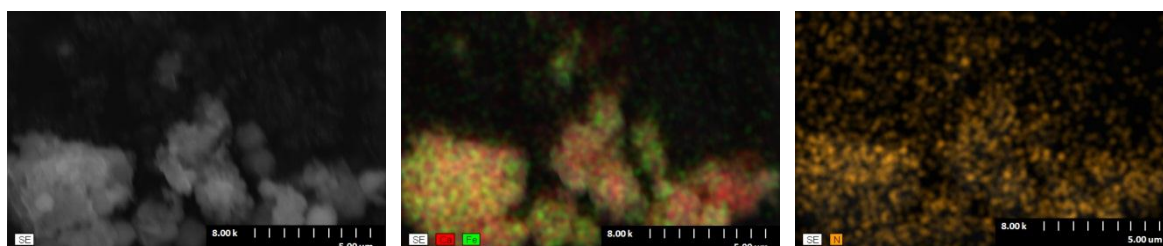


Figure 27.h) L-prolinate-LDH prepared in acetone/H₂O (magnification at 8,000).

The Ca–Fe maps verify that we have double hydroxides in our hands indeed, not only because the metals (ions) are evenly distributed in the sample, but also because there is no Fe or Ca accumulation, *i.e.* individual segregated oxides are not formed. The C–O, the C and the N maps indicate that the respective organic materials are also evenly distributed in the samples, *i.e.* the SEM images and this map – supplemented with the fact that we could not find any sign of Na which would refer to the presence of sodium salts – together convincingly show that the intercalation, and not adsorption on the outer surface of the LDH took place.

Thermal properties of the neat LDH and those of the intercalated samples were also compared and the major findings are shown on the example of the indole-2-carboxylate–LDH. (Figure 28–Figure 29).

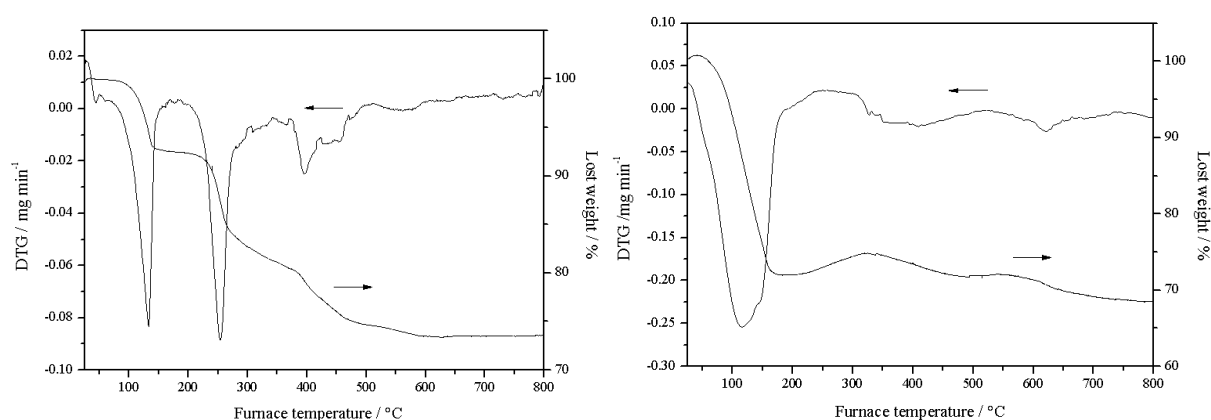


Figure 28. TG and DTG analysis of the original LDH and the indole-2-carboxylate–sodium salt.

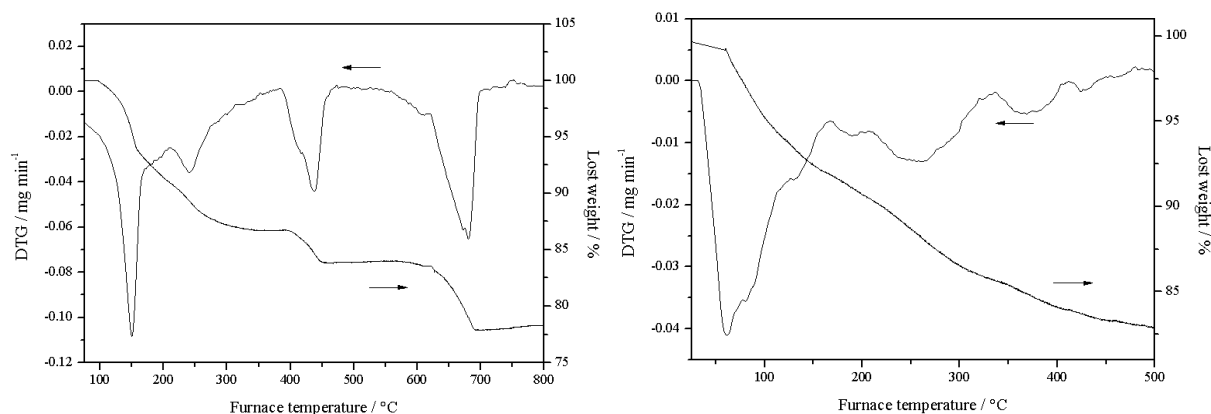


Figure 29. TG and DTG analysis of the indole-2-carboxylate–LDH prepared in EtOH/H₂O and the indole-2-carboxylate–LDH prepared in acetone/H₂O.

The LDH without the organic compound displayed the expected behaviour typical of LDHs. First, the physisorbed water is desorbed in a relatively narrow temperature range (383–423 K), after that, the interlayer water is gradually removed in a wide temperature range (423–613 K), then the structural water leaves in a relatively narrow temperature range (643–723 K) and the layered structure collapses. The intercalated structure behaves

differently in the sense that now we do not see the slowly leaving interlayer water. Instead, within 100 degrees (623–723 K) the organic material and possibly the structural water leave and the layered structure collapses. In both examined cases weight losses happened at slightly lower temperatures if acetone was used during synthesis.

The IR spectra of the samples (organic salts, and the intercalated CaFe-LDH) were also taken and compared. The main goals were to see if there were organic molecules in the sample on one hand and if the carboxylate anions remained intact on the other hand, *i.e.*, no undesired chemical reactions (*e.g.* degradation) took place during preparation.

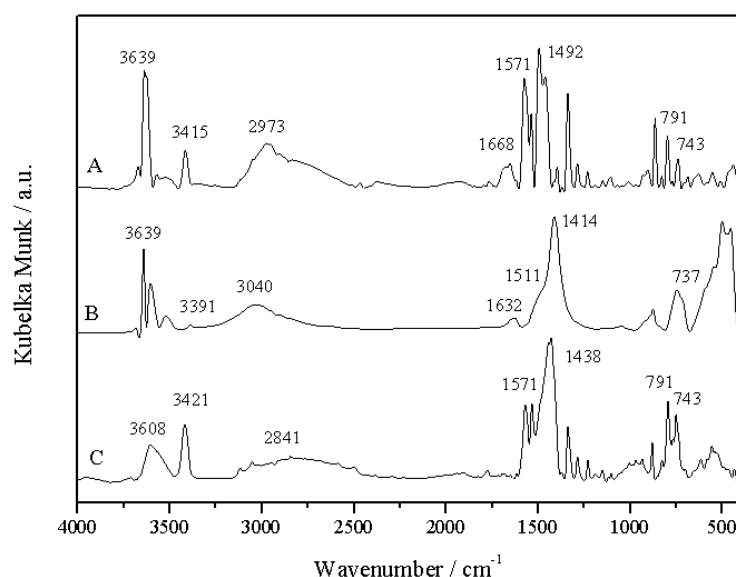


Figure 30. The difference IR spectra of the indole-2-carboxylate–LDH prepared in acetone/H₂O (A), the indole-2-carboxylate–LDH prepared in EtOH/H₂O (B) (the spectrum of the LDH was subtracted) and the IR spectrum of the sodium salt of indol-2-carboxylate (C).

The difference spectra and those of the corresponding spectra of the indole-2-carboxylate ions show close resemblance, therefore, it can be stated that the LDH samples contained the organic ions and they were intact. The band due to the N–H stretching vibration (3400–3250 cm^{−1}) is approximately equal in intensity in the spectra of the sodium salt and the organic-inorganic composite. However, for the intercalated anion, the peak shifted to higher energies and became less elongated demonstrating the success of intercalation. It can be seen in the vibrations of the carboxylate group (~1550 cm^{−1}) that the peaks are displaced and their intensities decrease also suggesting that the organic anion interacts with the layered double hydroxide.

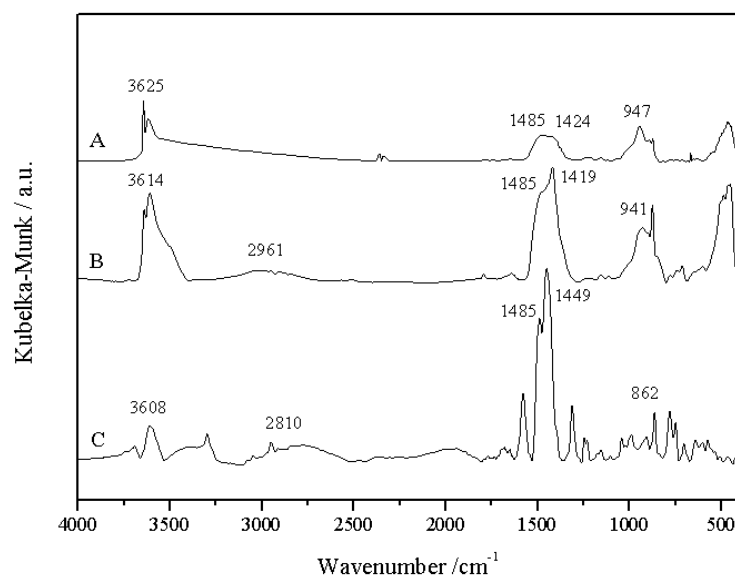


Figure 31. The difference IR spectra of the dihydroindole-2-carboxylate-LDH prepared in acetone/H₂O (A), the dihydroindole-2-carboxylate-LDH prepared in EtOH/H₂O (B) (the spectrum of the LDH was subtracted), and the sodium salt of dihydroindol-2-carboxylate (C).

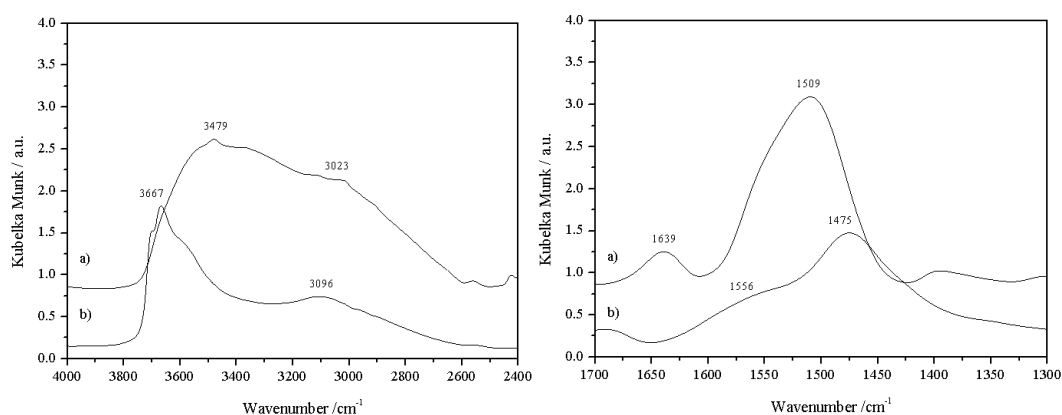


Figure 32. The IR spectra of the sodium salt of dihydroindol-2-carboxylate (a) and dihydroindole-2-carboxylate-LDH prepared in acetone/H₂O (b) (the spectrum of the LDH was subtracted) focusing on the characteristics bands.

The same conclusions may be drawn regarding the composites containing dihydroindol-2-carboxylate: the amine band vibrations are approximately the same for the sodium salt and for the intercalated compound. The vibration bands around 3100-3000 cm⁻¹ in all cases are probably due to the -CH group in the framework of the anion. In Figure 32, the characteristic band are enlarged: the vibrations due to the N-H stretching and of the carboxylate group are depicted, thus one can clearly see the similarity.

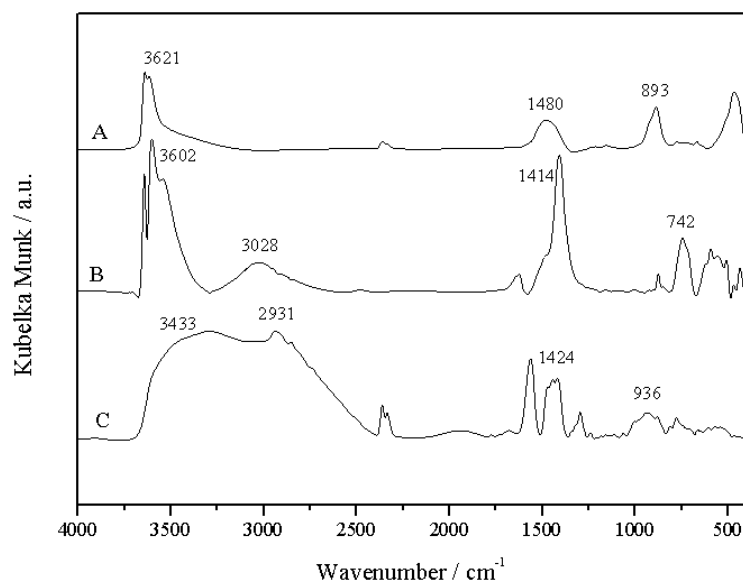


Figure 33. IR spectra of the DL-pipecolate-LDH prepared in acetone/H₂O (A), the DL-pipecolate-LDH prepared in EtOH/H₂O (B) and the sodium salt of DL-pipecolate (C).

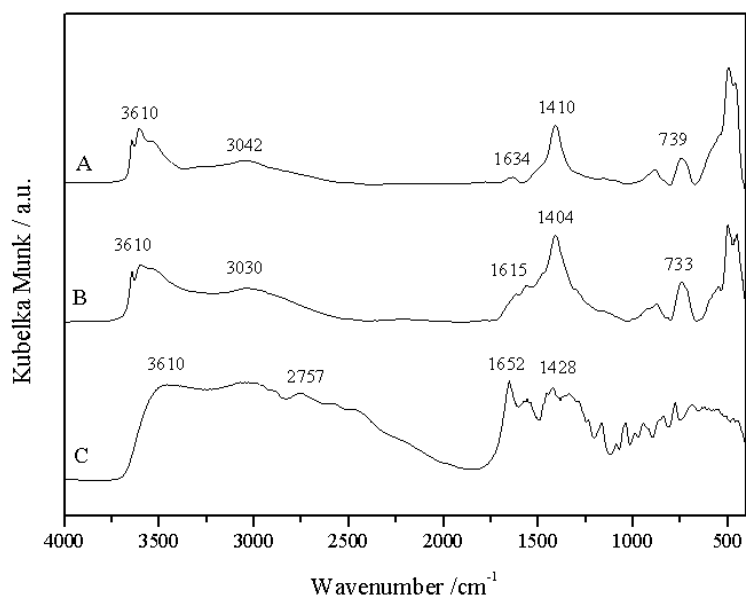


Figure 34. IR spectra of the L-proline-LDH prepared in acetone/H₂O (A), the L-proline-LDH prepared in EtOH/H₂O (B), and the sodium salt of L-proline (C).

In Figure 34, the strong, wide bands at higher wavenumbers are most probably due to the amino groups. In the difference spectra of the intercalated LDH they are much sharper and less intense. There are significantly more absorption bands in the spectra of the pristine L-proline, compared to the intercalated anion. Nevertheless, the spectra of L-proline-LDH prepared in both solvents contain the peak around 1400 cm^{-1} , which is presumably the vibration of the carbonyl in the carboxylate group. The difference spectra clearly show that

the carboxylate anions are present in the composite and their bands are shifted compared to the sodium salt, *i.e.*, the anion interacted with the layers of the LDH.

X-ray absorption spectra of the pristine CaFe-LDH and the L-prolinate–CaFe-LDH samples are depicted in *Figure 35*.

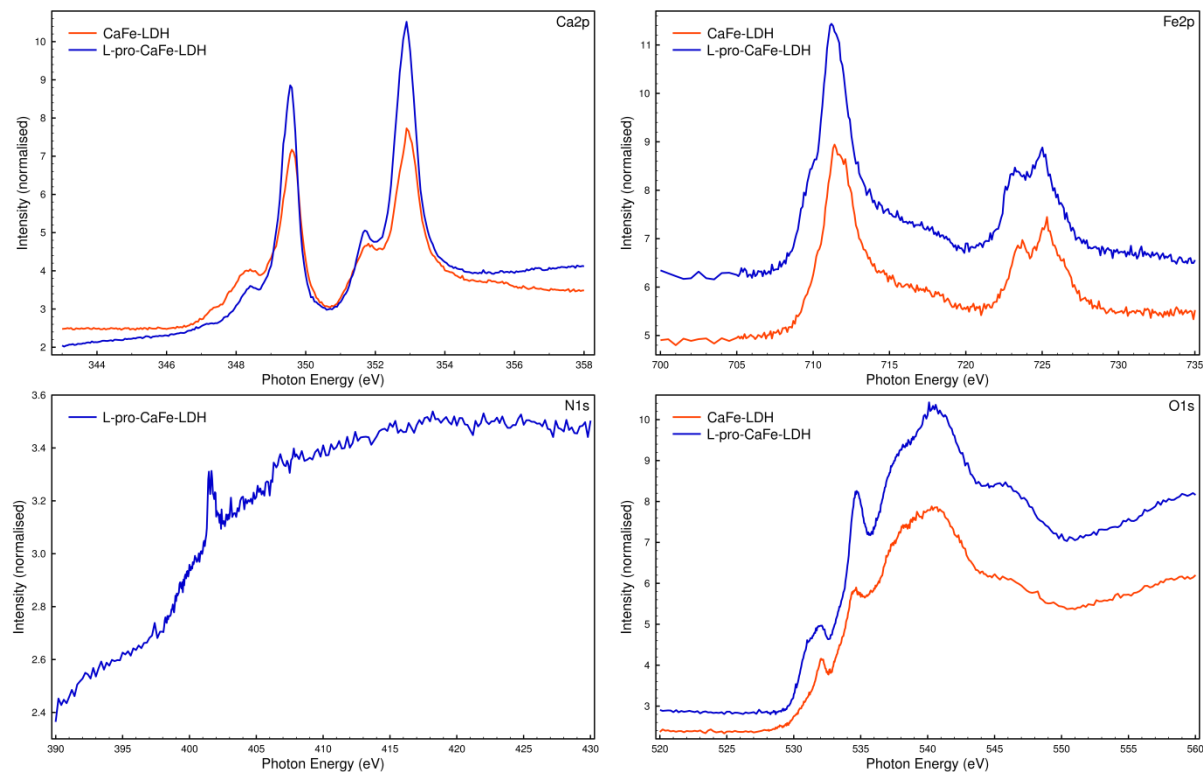


Figure 35. X-ray absorption spectra of the L-prolinate–CaFe sample performed around the Ca2p, Fe2p, N1s and O1s absorption edges.

It is to be observed that the intercalated prolinate does not perturb the structure of the sample neither that of the LDH nor the $\text{Ca}(\text{OH})_2$. One may think that it is not even intercalated, however, the N1s X-ray absorption spectra clearly verifies its presence. Moreover, the shoulder at 531 eV and the intensified peak around 547 eV the $\sigma \rightarrow \pi^*$ and $\pi \rightarrow \sigma^*$ transitions of its carboxylate bond.¹²⁵

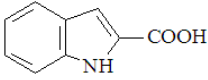
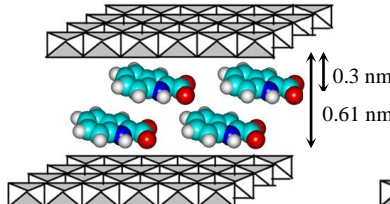
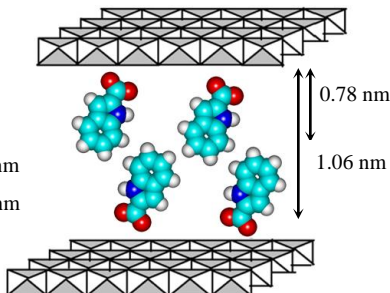
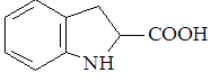
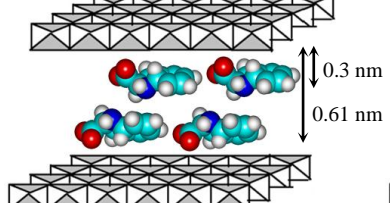
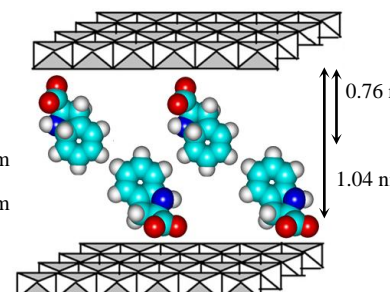
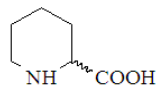
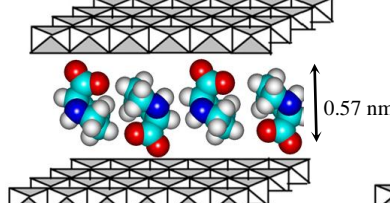
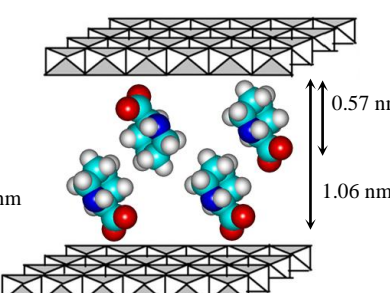
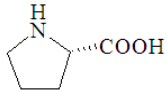
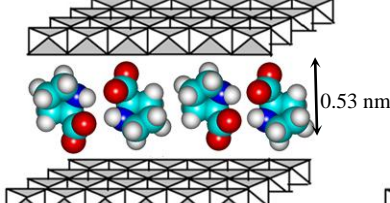
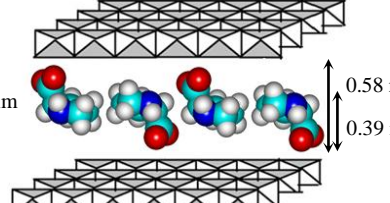
In conclusion, it can be said with great certainty that the intercalation was successful in all cases, but the application of different solvent mixtures during the synthesis affected tremendously the arrangement of the anions between the layers, and thus, the basal distances of the LDHs.

After verifying that the organic anions were intercalated indeed, whichever solvent mixture was used, through the combination of the interlayer distance values and the dimension data of the organic anions a schematic representation of the possible arrangement of the anions between the layers may be given (*Table 7*). It can be envisaged that when

aqueous acetone was used during preparation, both the indole-2-carboxylate and the dihydroindole-2-carboxylate fit between the layers if they are located perpendicularly. Upon using aqueous ethanol the anions can be accommodated in two layers of horizontal orientation. By the calculated parameters it is also possible that one layer of anions are intercalated in a vertical fashion, however, since the UV-Vis results indicated that the amount of both incorporated anions were nearly the same, the bilayer arrangement seems plausible even when the ethanolic mixture was applied in the synthesis. Nevertheless, the dimension data for the DL-2-piperidine-carboxylate and the L-prolinate anion allow the perpendicular orientation to the layers.

This phenomenon is not entirely unprecedented, although it was not observed for the effects of solvents yet. For fatty acids there are three possible assemblies: monolayer, bilayer and partial overlap packing. The various arrangements were induced by the amount of accessible anion or the pH.^{126,127}

Table 7. A schematic representation of the possible arrangement for the intercalated anions of the compounds between the layers of CaFe-LDH in both solvents used for the syntheses.

Intercalated organic compound	Structural formula	Schematic representation of a possible arrangement	
		ethanol/water	acetone/water
indole-2-carboxylic acid			
dihydroindole-2-carboxylic acid			
DL-2-piperidine-carboxylic acid			
L-proline			

5.3. The application of pristine CaFe-LDH as a catalyst in an epoxidation reaction

Among other applications layered double hydroxides are very often used in catalysis, mostly in base-catalyzed reactions.⁷¹ Usually, they are employed as catalyst precursors. After calcination, the layered structure collapses and the catalytic activity of the resulting mixed oxide often increases, because of the presence of many defects in its structure.¹²⁸ To extend the scope of catalytic applications it was decided to search for reaction that is catalysed by the pristine, uncalcined LDH. Preferably, the reaction should be synthetically useful as well. After surveying the literature, I ended up with the epoxidation of electron-deficient carbon-carbon double bonds of α,β -unsaturated ketones using hydrogen peroxide as oxidant. An earlier study with the most commonly used MgAl-LDH revealed that the reaction was feasible.¹²⁸

The unsaturated ketone was 2-cyclohexene-1-one, the oxidant was 30 wt% H_2O_2 and the reaction was performed in methanol at 298 K under vigorous stirring. A range of LDHs (CaFe-LDH, MgFe-LDH, CaAl-LDH) were used in uncalcined forms, and for comparison the reaction was performed over TiO_2 (P25), calcined CaFe-LDH as well as without catalyst. The epoxidation of 2-cyclohexene-1-one takes place according to the following equation:

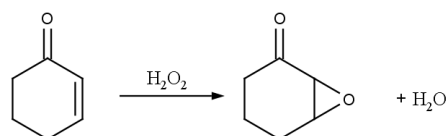


Table 8. Conversion data of the epoxidation reaction over various LDHs and other catalysts in methanol as solvent.

Catalyst	Conversion (%) after 120 min
without catalyst	<1
TiO_2 (P25)	8
calcined $\text{Ca}_3\text{Fe-LDH}$	10
$\text{Mg}_2\text{Al-LDH}$	19
$\text{Mg}_2\text{Fe-LDH}$	15
$\text{Ca}_2\text{Al-LDH}$	27
$\text{Ca}_2\text{Fe-LDH}$	47
$\text{Ca}_3\text{Fe-LDH}$	36
$\text{Ca}_4\text{Fe-LDH}$	29

In the first set of experiments, all reactions have been going on for 2 h and the degree of conversion was determined. The results are summarised in Table 8. The reproducibility of the data was within $\pm 1\%$. Each LDH-type was more active than the calcined CaFe-LDH proving that the layered structure was advantageous for the epoxidation of 2-cyclohexen-1-one. It is worth to notice that the hydrocalumite-type LDHs resulted better conversions in the studied

cases than the hydrotalcite-like layered materials. Varying the Ca(II) : Fe(III) ratio had some minor effect on the activity rendering: Ca₂Fe-LDH is the most active, affording 47% yields of the 2,3-epoxycyclohexanone. It is known that perfect hydrocalumite structure only forms at this composition, pointing again at the observation that the layered structure suits best to this reaction. However, as was discussed before, as far as stability is concerned the Ca(II) : Fe(III) = 3 : 1 ratio is the best, and since the activity was just slightly lower than with Ca₂Fe-LDH, the Ca₃Fe-LDH was used for temperature-, time- and solvent dependence studies.

The effect of reaction temperature on the efficiency of hydrogen peroxide utilisation was also examined. Here methanol was the solvent and the results are summarised in *Table 9*.

Table 9. Conversion data of the epoxidation reaction over uncalcined Ca₃Fe-LDH using methanol as solvent.

Temperature	Conversion (%) after 120 min
15 °C	27
25 °C	36
40 °C	39
55 °C	26
70 °C	29

Reaction time	Conversion (%)
5 min	2
30 min	11
1 h	22
2h	36
4 h	48
6 h	56
24 h	63

Catalyst	Conversion (%) after 120 min
Ca ₃ Fe-LDH (freshly prepared)	36
Reuse I	36
Reuse II	36

The highest efficiency in hydrogen peroxide utilization was observed when the reaction was performed at mild temperatures. The increase of reaction temperature over 40 °C resulted in a slight decrease in efficiency. Epoxidation at 40 °C was the most suitable from the standpoints of hydrogen peroxide efficiency and the reaction rate, in good agreement with the observations of Yamaguchi *et al.*¹²⁸

In order to achieve the maximum conversion, a time-dependence study was performed. The results are summarised in *Table 9*. The epoxidation of 2-cyclohexen-1-one carried out with the as-prepared Ca₃Fe-LDH catalyst in methanol solvent at 25 °C leads to 36% conversion in 2 h and 63% in 24 h with 2,3-epoxycyclohexanone as the only product (*Figure 36*). The time dependence data were fitted based on

first order kinetics. As a result, the experiments strictly follow the first order kinetics with $k=0.0068\pm0.0003\text{ min}^{-1}$. It may point out that there is no catalyst degradation, but this fact was also checked explicitly. The further increase of the conversion may be due to other

effects, *e.g.* the conscious choice of solvent. The use of a solid LDH makes the workup procedure very simple. The catalyst could easily be separated from the reaction mixture by a simple filtration. The recovered catalyst was then reused in the same reaction (*Table 9*). The oxidation using the spent catalyst gave the epoxyketone with the same conversion (under the same conditions) as those of the first run. The conversion was not decreased even after the catalyst was recycled twice.

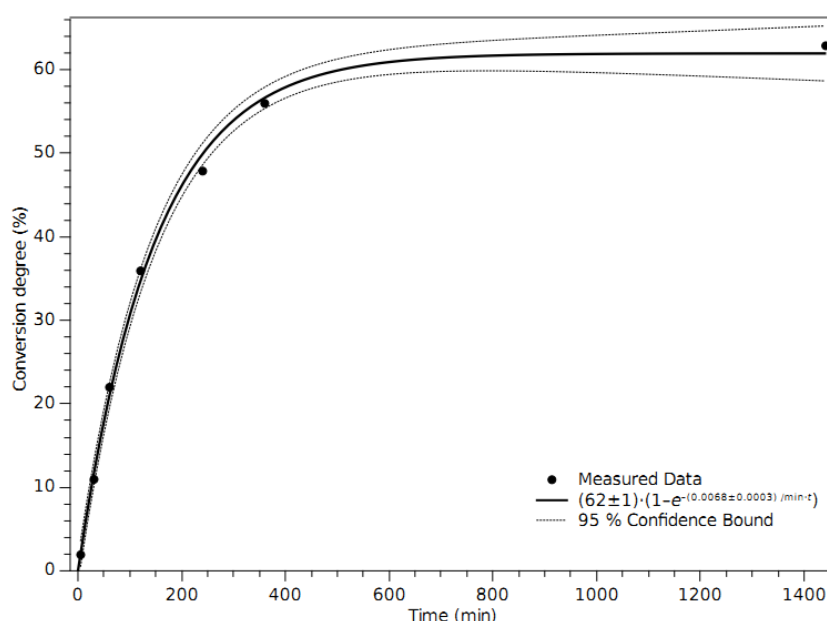


Figure 36. Catalytic activity of the $\text{Ca}_3\text{Fe-LDH}$ in the epoxidation of 2-cyclohexen-1-one in methanol solvent at 25 °C.

Table 10. Conversion data for the epoxidation reaction after 2 hour over uncalcined $\text{Ca}_3\text{Fe-LDH}$ using various solvents.

Solvent	Conversion (%)
2-methyl-2-propanol	<1
ethanol	27
methanol	36
acetone	18
1,4-dioxane	12
formamide	58
cyclohexene	42
n-hexane	49

Altering the solvent had occasionally dramatic effect on the conversion and thus the reactivity of the catalyst. The highest conversion was observed in formamide; n-hexane and cyclohexene were better solvents than methanol. In turn methanol proved to be a better solvent for this reaction than ethanol. The rest of the solvents, 2-methyl-2-propanol, acetone and 1,4-dioxane performed poorly in this reaction (*Table*

10). The excellent activity in the presence of formamide is most likely to be due to the delamination of the layers¹²⁹ making the basic sites significantly more accessible. If the solvent is alcohol, lengthening the carbon-chain results in a dramatic decline in conversion.

The explanation of the poor conversion rate in 1,4-dioxane may lie in the effect of the solvent on the layered double hydroxide. It is similar to that of heat-treatment, in the sense that both destroy the structure, as *Figure 37* attests.

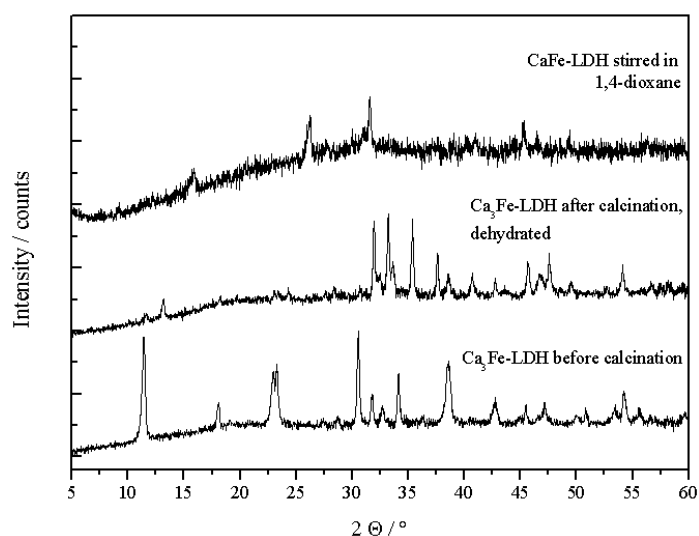


Figure 37. The effect of heat-treatment (500°C) and treatment with 1,4-dioxane on $\text{Ca}_3\text{Fe-LDH}$.

The catalytic properties of intercalated derivatives (indole-2-carboxylate- CaFe-LDH and L-prolinate- $\text{Ca}_3\text{Fe-LDH}$) were also examined. It is apparent from *Table 11* that the quality of the intercalated anion did not affect the conversion of 2-cyclohexen-1-one. Rather, the solvent mixture in which the intercalated LDHs were synthesised had some effects on the conversions. In both cases they increased when the ethanol/water/NaOH mixture were used. It may be due to the solvent residue in the composite materials rather than the arrangement of the anions since, *e.g.*, for L-prolinate-LDH the basal spacing was similar irrespective to the solvent mixture applied in the syntheses.

Table 11. Conversion data of the epoxidation reaction after 2 hour over various intercalated LDHs prepared in different solvents and the dodecylbenzenesulphonate-treated (DBS-treated) LDHs.

Catalyst	Conversion (%)
L-prolinate-LDH EtOH/H ₂ O	55
L-prolinate-LDH acetone/H ₂ O	37
indole-2-carboxylate-LDH EtOH/H ₂ O	47
indole-2-carboxylate-LDH acetone/H ₂ O	37
DBS-LDH	35
DBS + LDH (separate)	27

This fact could be confirmed by the data obtained from reactions with the dodecylbenzenesulphonate (DBS) intercalated $\text{Ca}_3\text{Fe-LDHs}$. DBS is an anionic surfactant which inhibits the epoxidation of the unsaturated ketones.¹²⁸ It is consistent with the fact, on adding the $\text{Ca}_3\text{Fe-LDH}$ and the DBS to the reaction mixture separately, the conversion of 2-cyclohexen-1-one decreased. However, when the dodecylbenzenesulphonate was incorporated into the layers by the dehydration-rehydration method (ethanol/water solvent mixture was used), the surfactant had no effect on the conversion.

5.4. Preparation of immobilised organocatalysts and their application in cross-aldol dimerisation

In the organocatalytic transformations, the organocatalysts are in the same phase as the reactants and the products in most cases. However, if they are attached to a solid or quasi-solid support, the work-up procedure is made easier on one hand, and the catalyst can be recycled making the reactions more benign to the environment on the other. No wonder that the second generation organocatalysts are organic molecules immobilised on various supports. There are many possibilities of immobilisation (covalent grafting, non-covalent attachment [ion exchange, hydrogen bonding interactions], biphasic catalysis [organocatalyst bonded to ionic liquids]) and the support can be of many kinds (functionalised/modified resins, silica gel or silicates, cyclodextrins, *etc.*). It was not surprising that proline was also immobilised^{130,131} using polyethylene-glycol (PEG), polystyrene, various forms of silica gel and silicates, alumina, magnetite, dendrimers, ionic liquids, *etc.*^{132,133} These catalysts were tested in aldol dimerisation as well, in some cases in types providing enantiomers. Both the activities and enantioselectivities of aldol dimerisation largely depended on the reaction conditions as well as the supports and the modes of immobilisation.

In the followings, the behaviour of various functionalised materials are examined in this reaction. First, chloropropylated silica gel was chosen as support and N- or C-protected L-proline was covalently grafted on it. For immobilisation either Boc-protected L-proline (Boc-Pro-OH) or C-protected L-proline (H-Pro-OCH₃) were used (*Figure 26 a*) and *b*)) and after covalent grafting (esterification or N-alkylation were the two reactions), the immobilised amino acids were deprotected. The materials were used in the aldol dimerisation reaction in these forms. For comparison the catalytic activity of the commercially available L-prolinol anchored on polystyrene (*Figure 26 c*)) was also investigated.

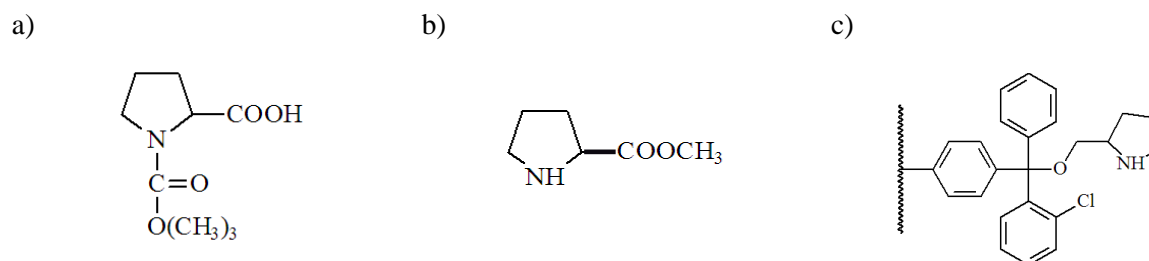


Figure 38. The covalently grafted a) N-protected L-proline (tert-butoxycarbonyl-L-proline); b) C-protected L-proline (L-proline methylester) and c) resin-anchored L-prolinol-2-chlorotrityl ether.

Layered double hydroxides were very sparingly applied as host for the intercalation of deprotonated proline.^{134,135} It is surprising, because they should be ideal hosts. Previously

enantiopure proline was only intercalated into MgAl-LDH. The intercalated structures were tested in aldol dimerisation–condensation of benzaldehyde and acetone. The catalysts were active and selective towards dimerisation. Both low (6%, Choudhary *et al.*¹³⁵) and high (94%, An *et al.*¹³⁴) enantioselectivity values were detected. In order to extend the scope of the studied organocatalyst immobilised in LDHs, beside proline, another N-containing saturated cyclic amino acid (pipecolinic acid) was used for intercalation. The host was also different, CaFe-LDH was applied.

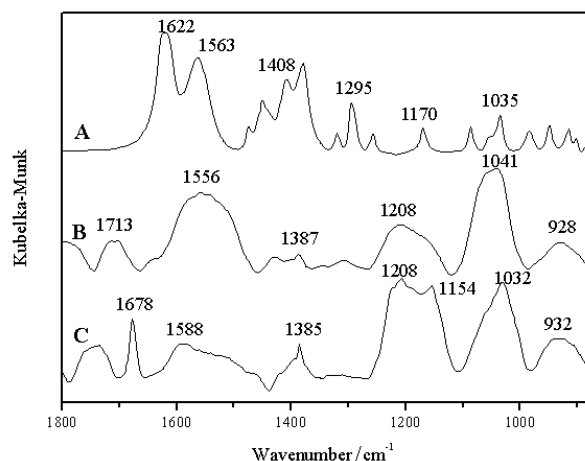


Figure 39. The FT-IR spectrum of (A) L-proline, (B) SG-Pro-OH (spectrum of SG is subtracted), (C) H-Pro-O-SG (spectrum of SG is subtracted).

From the detailed comparative analysis of the IR spectra of the amino acid and the composite materials, one could see if the amino acids attached were intact or not (Figure 39). To make comparison easier the spectrum of the support was subtracted from that of the composite and it was compared to that of the pristine proline in the most informative region. It is clear from trace A (see the bands between 1400–1600 cm^{-1}) that the pristine proline was in zwitterionic form.

When L-proline was immobilised *via* the N atom, the compound is present in protonated form – the carboxylate doublet disappeared and only the carbonyl vibration is seen at 1713 cm^{-1} . The wide, medium intensity band (1208 cm^{-1}) indicates aliphatic tertiary amine while the intense band around 1000 cm^{-1} refers the remaining aliphatic ring. These observations verify that the covalent immobilisation of L-proline through its nitrogen atom was successful.

In trace C, the wide band at 1032 cm^{-1} indicates that the ring is kept during covalent grafting and deprotection. The relatively intense bands at 1678 cm^{-1} and 1208 cm^{-1} are typical

for esters indicating that the attachment of the N-protected proline *via* an esterification reaction was successful.

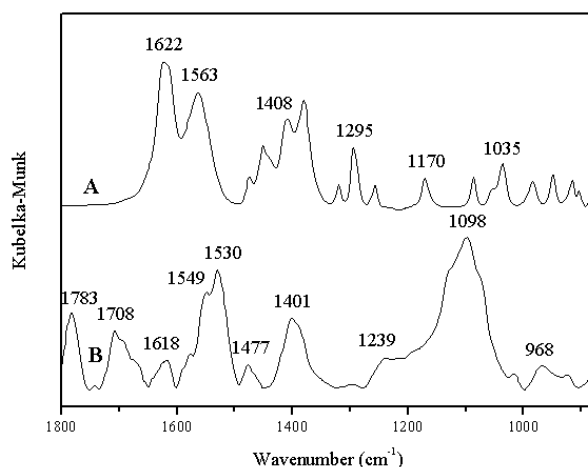


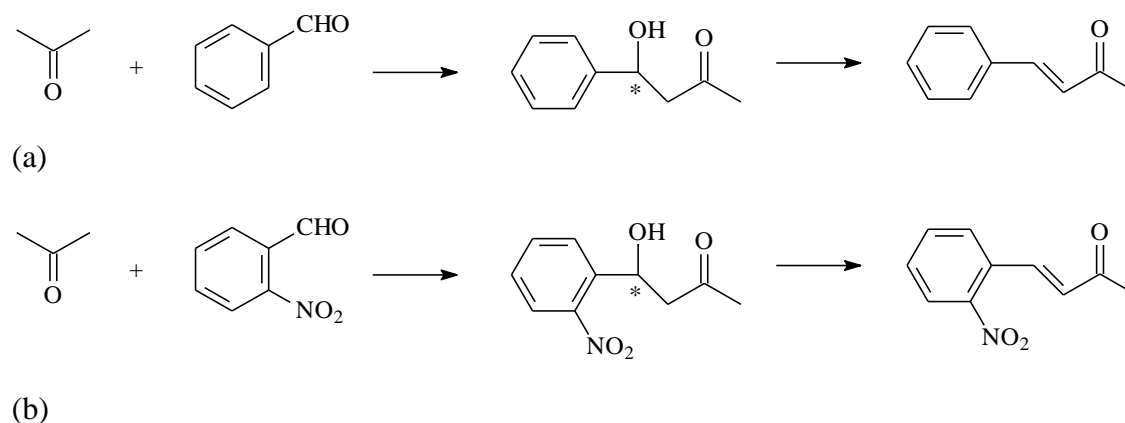
Figure 40. The FT-IR spectrum of (A) *L*-proline, (B) resin-anchored *L*-prolinol-2-chlorotrityl ether.

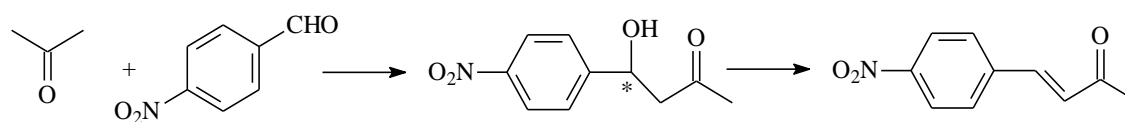
The resin-anchored *L*-prolinol-2-chlorotrityl ether was a commercial product with limited amount of characteristic data provided by the supplier. Since I intended to use its resin-anchored variety for similar purposes as the functionalised materials that I prepared, it seemed worthwhile to learn about its properties. The wide, intense and structured vibration at 1098 cm^{-1} includes ring deformation vibrations as well as vibration typical for the secondary nitrogen of the ring as shoulders (*Figure 40*).

The detailed characterisation of *L*-prolinate-LDH and DL-2-piperidine-carboxylate-LDH was described in earlier (Ch. 5.2., pp 46–59.). For the catalytic studies the samples prepared in EtOH/H₂O/NaOH mixture were used.

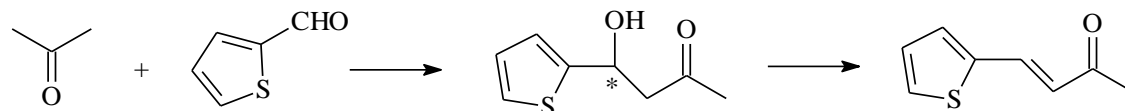
5.4.1. Composite materials as catalysts for aldol dimerisation reactions

The synthesised functionalised materials were tested in the following reactions (*Figure 41*)





(c)



(d)

Figure 41. Aldol dimerisation reactions and the accompanying condensations.

The test reactions were characterised by three sets of data: conversion, selectivity (rate of dimerisation *vs.* condensation) and enantioselective excess (by definition: $ee = [R] - [S] / [R] + [S]$, where R and S refer to the absolute configuration).

The purchased catalyst was thoroughly studied, because significantly larger quantities were available and thus it was possible to study the effect of solvents, and moreover the processing and analysis of the reaction mixture were easier.

Table 12. Conversion, selectivity and enantioselective excess (ee) data in the dimerisation-condensation reaction with covalently grafted L-proline as catalyst.

	acetone + benzaldehyde			acetone + 2-NO ₂ -benzaldehyde			acetone + 4-NO ₂ -benzaldehyde			acetone + 2-thiophene carbaldehyde		
	conv. %	sel. %	ee %	conv. %	sel. %	ee %	conv. %	sel. %	ee %	conv. %	sel. %	ee %
H-Pro-O-SG	20	90	12	0	0	0	82	85	0	0	0	0
Prolinol-resin												
(1)	94.5	62.5	20	95	90.5	-12	89	83.5	11	70	35	nd
(2)	37	32	1	84	92.5	3	18	55	5	0	0	0
(3)	71.5	51	18	93	94.5	0	81	79	3	34	44	nd
(4)	62	86	-9	90	95	-10	52	72	0	24	62*	nd

The composition of the mixture was as follows:

1 g H-Pro-O-SG, 15 g 2- or 4-nitro benzaldehyde, 20 cm³ 2- thiophene carbaldehyde, respectively, 24 h, 298 K

H-Pro-O-SG : acetone + aldehyde, 24 h, 298 K

Prolinol-resin : 0.3 g catalyst

(1): acetone + aldehyde, 24 h, 298 K

(2): DMSO + water + acetone + aldehyde, 24 h, 298 K

(3): DMSO + acetone + aldehyde, 24 h, 298 K

(4): water + acetone + aldehyde, 24 h, 298 K

* = dimer only + dehydrated product

nd = no data

According to the results detailed in *Table 12* one can make the following observations: if L-proline is grafted to the surface of the silica gel through its N-terminal, there is no aldol dimerisation. If L-proline is grafted to the surface of the silica gel through its C-terminal, the composite catalysed the dimerisation of acetone and benzaldehyde with moderate and 2-nitrobenzaldehyde with high conversion rates, and with high selectivities. Moderate enantioselectivity was achieved in the reaction with benzaldehyde. There was no transformation with any of the other reactants, but, perhaps, an optimisation of the reaction conditions would change this situation.

The resin-anchored L-prolinol-2-chlorotrityl ether was active with almost every reactant pair, with the exception of acetone-2-thiophene-carboxaldehyde in DMSO–water solvent mixture. Generally speaking, this solvent (mixture) proved to be the worst option among the solvents or solvent combinations tried. When a reaction occurs, the conversion and the selectivity of the dimerisation were good and, occasionally, both data were very high (this was the case in the acetone–2-nitrobenzaldehyde reactant pair, in particular). As far as enantioselectivity of the dimerisation is concerned, many nonzero *ee* values were obtained, but none of them is unusually high. It is worth to note that for two of reactant combinations (acetone–benzaldehyde and acetone–2-nitrobenzaldehyde) the choice of solvent influenced the direction of rotating the plane-polarised light of the product.

Unfortunately, the enantioseparation of the dimers from the reactant combination of acetone–2-thiophene-carbaldehyde was not successful, therefore no information could be gathered on the enantioselectivity of the dimerisation. It should be noted that in this reactant combination products with much higher molecular weights than thus of the dimers were found in almost all cases (except for the reaction in water). The resulting products have not been identified yet.

It was hoped that providing a sterically confined environment with the L-prolinate–CaFe-LDH catalyst system the selectivity of the dimerisation reaction would be significantly influenced.

The immobilised organocatalysts (L-prolinate–CaFe-LDH and DL-pipecolate–CaFe-LDH) were tested in the cross-aldol dimerisation–condensation of benzaldehyde and acetone. It was found that both catalysts were active and gave the dimer as well as the condensation product. Let me note that there was no reaction with the pristine LDH at room temperature. The reuse of the L-prolinate–CaFe–LDH catalyst was also attempted. The composition of the mixture was as follows: 1 cm³ of H₂O, 4 cm³ of acetone, 1 cm³ of benzaldehyde, 0.3 g of

catalyst. The mixture was vigorously stirred for 24 h at 298 K. Acetone served as the reactant as well as the solvent, water was used as proton source. The L-prolinate-CaFe-LDH catalyst was reused twice without any special reactivation except rinsing it with acetone. Results obtained are summarised in *Table 13*.

Table 13. Conversion, selectivity and enantioselective excess (ee) data in the dimerisation–condensation reaction of acetone and benzaldehyde catalysed by L-prolinate and DL-pipecolate immobilised between the layers of CaFe-LDH

Materials	Convers. (%)	Selectivity of dimerization (%)	Selectivity of condensation (%)	ee (%)
CaFe-LDH	0	0	0	0
L-prolinate–CaFe-LDH				
Freshly prepared	3	85	15	53
Reuse I	19	88	12	12
Reuse II	59	76	23	6
DL-pipecolate–CaFe-LDH	0.5	95	5	0

At room temperature, initially, the activity of the intercalated materials was low. Nevertheless, selectivity towards dimerisation was high and the *ee* value with L-prolinate–CaFe-LDH was appreciable. The catalyst could be recycled and then gradual activation and the gradual decrease in both dimerisation selectivity and enantioselectivity were observed. This observation is in complete coincidence with the observation that under basic conditions the carboxylate ions undergo enolisation.¹³⁶ Due to this reaction the chirality of the α -carbon atom is lost. Since LDHs are known to be basic materials they catalyse enolisation. The other catalyst DL-pipecolate–CaFe-LDH that is, had low activity in the cross-aldol dimerisation–condensation reaction, however its selectivity for condensation was very high. Since no chiral information was introduced into the system, racemate was formed.

6. CONCLUSIONS

Layered Double Hydroxides (LDH) form a unique group of clays that have an anionic exchange capability. Contrary to the large number of cation exchanger materials, the number of known anion-exchange frameworks is rather limited. LDHs are known as structures consisting of positively-charged mixed-metal hydroxide layers, between which balancing anions and water molecules are found.

During the experimental work leading to this dissertation, a variety of MgFe hydrotalcite-like and CaFe hydrocalumite-like compounds was synthesised using co-precipitation. The synthesised materials were extensively characterised by various methods like X-ray diffractometry (XRD), inductively coupled plasma-optical emission, IR, ^{57}Fe Mössbauer and near edge X-ray absorption fine structure spectroscopies, thermogravimetric analysis, transmission and scanning electron microscopies and scanning electron microscopy coupled with energy dispersive X-ray spectroscopy.

XRD patterns for the synthesised LDHs exhibited characteristic features indicative of an ordered layered material. The optimum synthesis conditions were identified both for CaFe- and MgFe-LDHs and it was confirmed that if the LDHs are intended to be used as hosts of intercalated anions, the syntheses should be performed under N_2 blanket and the NaOH concentration should not exceed 3 M. It has been found that on increasing Ca(II) to Fe(III) ratios from 2 to 6, the quantity of $\text{Ca}(\text{OH})_2$ almost linearly increases from 0% to ~60%. At the same time stabilities of the materials increased – the ideal hydrocalumite structure (Ca(II):Fe(III) = 2) is the least stable. ^{57}Fe Mössbauer measurements revealed that Fe(III) was in a high-spin, somewhat disordered octahedral environment in both CaFe- and MgAl-LDHs at every composition. The layer thickness, inevitable for assuming reasonable spatial arrangements was estimated from TEM dark-field image and was measured to be 0.19 nm, in good agreement with the 0.178 nm determined by others from high-precision XRD data.

The subsequent intercalation of various N-containing carboxylic acid anions was performed by the dehydration-rehydration method. The structures as well as the morphologies of the composite samples have been characterised by the instrumental techniques listed above complemented with UV-Vis spectroscopy and molecular modelling. Particular attention was paid to the influence of solvent mixture used during preparation; various solvent mixtures resulted in different interlayer distances and thus different arrangements of the anions between the layers. The intercalation chemistry of Ca_3Fe -LDH could be tremendously influenced by the choice of solvent mixture used. The dimensions of the intercalated anions

were estimated from those of the parallelepipeds used for the inclusion of the anions to be intercalated optimised by the PM3 semiempirical quantum chemical method. These dimensions gave clues for the reasonable prediction of the spatial arrangements of the anions in the interlamellar space. The ethanol : H₂O : NaOH and the acetone : H₂O : NaOH solvent mixtures allowed the intercalation of N-containing aromatic, partially as well as fully saturated N-containing heterocycles in single and multilayers, respectively, while preserving the layered structure in both cases.

There is an increasing interest to environmentally benign heterogeneous catalytic processes in the chemical industry. It remains a continuous challenge to find highly active solid Brønsted-type basic catalysts that are able to bring about C–C bond formation with good selectivity. Targeted transformations are various types of self- or cross-condensation reactions between aldehydes and ketones. The uncalcined CaFe-LDHs were found to be useful and efficient catalysts in an epoxidation reaction – they were significantly more active than the calcined derivatives. The epoxidation of 2-cyclohexen-1-one over uncalcined CaFe-LDHs were performed in various solvents (formamide, n-hexane, cyclohexene, methanol, ethanol, 2-methyl-2-propanol, acetone and 1,4-dioxane) and temperatures. Formamide and 313 K were the most advantageous solvent and temperature mix, however, the reactions could be conducted with high activities in n-hexane, cyclohexane as well as in methanol and ethanol. The uncalcined MgAl-hydrotalcite, MgFe-hydrotalcite and CaAl-hydrocalumite were less active than CaFe-hydrocalumite, but still more efficient than the calcined derivatives (mixed oxides) or another oxide like titania.

L-proline has for many years been widely used as a chiral organocatalyst for bond forming organic reactions. It efficiently catalyses the aldol reaction with a range of ketones and aldehydes, resulting in good yields and appreciable enantiomeric excesses. A great deal of research has also been dedicated to catalyst immobilization, with desire to achieve easy product isolation and efficient recycling protocols. Covalently functionalised silica gel could be prepared by immobilising N- or C-protected L-proline on chloropropylated silica gel. After deprotection L-proline anchored only at the C-terminal was active in cross-aldol dimerisation of acetone and benzaldehyde with moderate and 2-nitrobenzaldehyde with high conversion rates, and with high selectivities. Moderate enantioselectivity was achieved in the reaction with benzaldehyde. The commercially available L-prolinol anchored on polystyrene resulted in dimers of moderate enantioselectivities in a similar reaction, but with a larger variety of aldehydes. So it has been found experimentally that for the catalytic activities of covalently immobilised N-containing heterocycles freely available secondary nitrogens are inevitable.

The above-listed results clearly attest that layered double hydroxides are versatile materials. They can be functionalised in various ways with relative ease and, among many possible applications, they can be tailored to reactions that can be useful to laboratory use as well as in the fine chemical industry.

7. REFERENCES

- ¹ W. Feitknecht, G. Fischer, *Helv. Chim. Acta* 18 (1935) 555-569.
- ² M. Catti, G. Ferraris, S. Hull, A. Pavese, *Phys. Chem. Miner.* 22 (1995) 200-206.
- ³ D. Srankó, M. Sipiczki, É.G. Bajnóczy, M. Darányi, Á. Kukovecz, Z. Kónya, S.E. Canton, K. Norén, P. Sipos, I. Pálinkó, *J. Mol. Struct.* 993 (2011) 62-66.
- ⁴ S. Velu, K. Suzuki, M. Okazaki, T. Osaki, S. Tomura, F. Ohashi, *Chemistry of Materials* 11 (1999) 2163-2172.
- ⁵ A.I. Khan, D. O'Hare, *J. Mater. Chem.* 12 (2002) 3191-3198.
- ⁶ G. Alberti, U. Costantino: Solid state supramolecular chemistry: Two- and three-dimensional inorganic networks, In: G. Alberti, T. Bein (Eds.), *Comprehensive Supramolecular Chemistry*, vol. 7, Pergamon and Elsevier Science, Oxford, (1996)
- ⁷ J.T. Klopogge, D. Wharton, L. Hickey, R.L. Frost, *Am. Mineral.* 87 (2002) 623-629.
- ⁸ F. Cavani, F. Trifiró, A. Vaccari, *Catal. Today* 11 (1991) 173-301.
- ⁹ A.V. Radha, P.V. Kamath, C. Shivakumara, *Acta Cryst. B* 63 (2007) 243-250.
- ¹⁰ M. Vucelic, W. Jones, G.D. Moggridge, *Clays Clay Miner.* 45 (1997) 803-813.
- ¹¹ V. Rives, In: *Layered double Hydroxides: Present and future*, Nova Science Publisher, New York (2001).
- ¹² R.C. Peterson, R.J. Hill, G.V. Gibbs, *Can. Mineral.* 17 (1979) 703-711.
- ¹³ G.W. Brindley, C.C. Kao, *Phys. Chem. Miner.* 10 (1984) 187-191.
- ¹⁴ K. Shinoda, N. Aikawa, *Phys. Chem. Miner.* 25 (1998) 197-202.
- ¹⁵ A.S. Bookin, V.A. Drits, *Clays Clay Miner.* 41 (1993) 551-557.
- ¹⁶ A.S. Bookin, V.I. Cherkashin, V.A. Drits, *Clays Clay Miner.* 41 (1993) 558-564.
- ¹⁷ V. Fernon, A. Vichot, P. Colombet, H. van Damme, F. Bégin, *Mater. Sci. Forums* 152-153 (1994) 335-338.
- ¹⁸ M. Ecker, H. Pöllmann, *Mater. Sci. Forums* 166-169 (1994) 565-570.
- ¹⁹ M. Sacerdoti, E. Passaglia, *N. Jb. Miner. Mh.* (1988) 462-475.
- ²⁰ M. Belloto, B. Rebours, O. Clause, J. Lynch, D. Bazin, E. Elkaim, *J. Phys. Chem.* 20 (1996) 8527-8534.
- ²¹ I. Rousselot, C. Taviot-Guého, F. Leroux, P. Léone, P. Palvadeu, J.-P. Besse, *J. Solid State Chem.* 167 (2002) 137-144.
- ²² T.-H. Kim, I. Heo, S.-M. Paek, C.-B. Park, A.-J. Choi, S.-H. Lee, J.-H. Choy, J.-M. Oh, *Bull. Korean Chem. Soc.* 33-36 (2012) 1845-1850.
- ²³ O.P. Ferreira, O.L. Alves, D.X. Gouveia, A.G. Souza, J.A.C. de Paiva, J. Mendes, *J. Solid State Chem.* 177 (2004) 3058-3069.
- ²⁴ H.C. Hansen, C.B. Koch, *Appl. Clay Sci.* 10 (1995) 5-19.
- ²⁵ M.R. Schütz, A.E Schedl, F.E. Wagner, J. Breu *Appl. Clay Sci.* 54 (2011) 281-286.
- ²⁶ Ph. Refait, J.-M.R. Génin, *Clay Miner.* 32 (1997) 597-613.
- ²⁷ H.C.B. Hansen, C.B. Koch, *Clays Clay Miner.* 42 (1994) 170-179.
- ²⁸ S. Morlat-Thérias, C. Mousty, P. Palvadeau, P. Molinié, P. Léone, J. Rouxel, C. Taviot-Guého, A. Ennaoui, A. de Roy, J.P. Besse, *J. Solid State Chem.* 144 (1999) 143-151.
- ²⁹ J.-M.R. Génin, C. Ruby, *Solid State Sci.* 10 (2008) 244-259.
- ³⁰ B. Rusch, J.-M.R. Génin, C. Ruby, M. Abdelmoula, P. Bonville, *Solid State Sci.* 10 (2008) 40-49.
- ³¹ K.B. Ayala-Luis, C.B. Koch, H.C.B. Hansen, *Appl. Clay Sci.* 48 (2010) 334-341.

- ³² D.X. Gouveia, O.P. Ferreira, A.G. Souza, M.G. da Silva, J.A.C. de Paiva, O.L. Alves, J.M. Filho, *J. Mater. Sci.* 42 (2007) 534–538.
- ³³ A. Mendiboure, R. Schöllhorn, *Chim. Miner.* 23 (1987) 819–827.
- ³⁴ J.C. Schon, D. Alder, G. Dresselhaus, *J. Phys. C* 21 (1988) 5595–5614.
- ³⁵ A. Fogg, M. Dunn, J.S.D. O'Hare, *Chem. Mater.* 10 (1998) 356–360.
- ³⁶ M. Kaneyoshi, W. Jones, *Phys. Lett.* 296 (1998) 183–186.
- ³⁷ P.S. Braterman, Z.P. Xu, F. Yarberry, *Layered double hydroxides. In: S.M. Auerbach, K.A. Carrado, P.K. Dutta (Eds), Handbook of Layered Materials*, New York (2004) Taylor & Francis, pp. 373–474.
- ³⁸ M. Meyn, K. Beneke, G. Lagaly, *Inorg. Chem.* 29 (1990) 5201–5207.
- ³⁹ C. Ruby, R. Aïssa, A. Géhin, J. Cortot, M. Abdelmoula, J.-M.R. Génin, *C. R. Geosci.* 338 (2006) 420–432.
- ⁴⁰ J.J. Bravo-Suárez, E.A. Pérez-Mozo, S.T. Oyama, *Quim. Nova* 27 (2004) 601–614.
- ⁴¹ M. Adachi-Pagano, C. Forano, J.P. Besse, *J. Mater. Chem.* 13 (2003) 1988–1993.
- ⁴² M. Ogawa, H. Kaiho, *Langmuir* 18 (2002) 4240–4242.
- ⁴³ N. Morel-Desrosiers, J. Pisson, Y. Israeli, C. Taviot-Guého, J.P. Besse, J.P. Morel, *J. Mater. Chem.* 13 (2003) 2582–2585.
- ⁴⁴ Y. Israeli, C. Taviot-Guého, J.P. Besse, J.P. Morel, N. Morel-Desrosiers, *J. Chem. Soc., Dalton Trans.* (2000) 791–796.
- ⁴⁵ S. Miyata, *Clays Clay Miner.* 31 (1983) 305–311.
- ⁴⁶ R.P. Bontchev, S. Liu, J.L. Krumhansl, J. Voigt, T.M. Nenoff, *Chem. Mater.* 15 (2003) 3669–3675.
- ⁴⁷ S.P. Newman, W. Jones, *New J. Chem.* (1998) 105–115.
- ⁴⁸ K.K. Ravi, S.W. Marc, E.A. James, *Chem. Mater.* 9 (1997) 417–419.
- ⁴⁹ S. Xing, D.Q. Li, L.L. Ren, D.G. Evans, X. Duan, *Huaxue Xuebao* 61 (2003) 267–272.
- ⁵⁰ S. Miyata, *Clays Clay Miner.* 28 (1980) 50–56.
- ⁵¹ T. Hibino, A. Tsunashima, *Chem. Mater.* 10 (1998) 4055–4061.
- ⁵² J.S. Valente, G. Rodriguez-Gattorno, M. Valle-Orta, E. Torres-Garcia, *Mater. Chem. Phys.* 133 (2012) 621–629.
- ⁵³ C.O. Oriakhi, I.V. Farr, M.M. Lerner, *Clays Clay Miner.* 45 (1997) 194–202.
- ⁵⁴ H. Nakayama, N. Wada, M. Tsuhako, *Int. J. Pharm.* 269 (2004) 469–478.
- ⁵⁵ M. Ogawa, S. Asai, *Chem Mater* 12 (2000) 3253–3255.
- ⁵⁶ M.A. Aramendia, V. Borau, C. Jimenez, J.M. Marinas, J.R. Ruiz, F.J. Urbano, *J Solid State Chem* 168 (2002) 156–161.
- ⁵⁷ Y. Zhao, F. Li, R. Zhang, D.G. Evans, X. Duan, *Chem Mater* 14 (2002) 4286–4291.
- ⁵⁸ H.P. Boehn, J. Steinle, C. Vieweger *Angew Chem Int Ed Engl* 16 (1977) 265–266.
- ⁵⁹ L. Indira, M. Dixit, P.V. Kamath, *J Power Sources* 52 (1994) 93–97.
- ⁶⁰ G. Hu, D. O'Hare, *J. Am. Chem. Soc.* 127 (2005) 17808–17813.
- ⁶¹ V.R.L. Constantino, T. Pinnavaia, *Inorg. Chem.* 34 (1995) 883–892.
- ⁶² R. Tessier, D. Tichit, F. Figueras, J. Kervennal, FR Patent, 95 00094 (1995).
- ⁶³ K.K. Rao, M. Gravelle, J. Sanchez Valente, F. Figueras, *J. Catal.* 173 (1998) 115–121.
- ⁶⁴ S. Ueno, K. Yamaguchi, K. Yoshida, K. Ebitani, K. Kaneda, *Chem. Commun.* (1998) 295–296.
- ⁶⁵ E. Suzuki, M. Okamoto, Y. Ono, *J. Mol. Catal.* 61 (1990) 283–294.
- ⁶⁶ K. Zhu, C. Liu, X. Ye, Y. Wu, *Appl. Catal. A* 168 (1998) 365–372.

- ⁶⁷ B.M. Choudary, M.L. Kantam, C.R.V. Reddy, K.K. Rao, F. Figuéras, *J. Mol. Catal. A* 146 (1999) 279–284.
- ⁶⁸ B.M. Choudary, M.L. Kantam, C.R.V. Reddy, S. Aranganathan, P.L. Santhi, F. Figuéras, *J. Mol. Catal. A* 159 (2000) 411–416.
- ⁶⁹ B.F. Sels, D.E. De Vos, P. A. Jacobs, *Catal. Rev.* 43 (2001) 443–488.
- ⁷⁰ E. Iglesia, D.G. Barton, J.A. Biscardi, M.J.L. Gines, S.L. Soled, *Catal. Today* 38 (1997) 339–360.
- ⁷¹ D. Tichit, B. Coq, *CATTECH* 7 (2003) 206–217.
- ⁷² Z.P. Xu, J. Zhang, M.O. Adebajo, H. Zhang, C. Zhou, *Appl. Clay Sci.* 53 (2011) 139–150.
- ⁷³ T.H. Bennur, A. Ramani, R. Bal, B.M. Chanda, S. Sivasanker, *Catal. Commun.* 3 (2002) 493–496.
- ⁷⁴ Y.Z. Chen, C.M. Hwang, C.W. Liaw, *Appl. Catal. A* 169 (1998) 207–214.
- ⁷⁵ N. Das, D. Tichit, R. Durand, P. Graffin, *Catal. Lett.* 71 (2001) 181–185.
- ⁷⁶ B.M. Choudary, S. Madhi, N.S. Chowdari, L.M. Kantam, B. Sreedhar, *J. Am. Chem. Soc.* 124 (2002) 14127–14136.
- ⁷⁷ P. Levecque, H. Poelman, P. Jacobs, D. De Vos, B. Sels, *Phys. Chem. Chem. Phys.* 11 (2009) 2964–2975.
- ⁷⁸ S. Bhattacharjee, T.J. Dines, J.A. Anderson, *J. Catal.* 225 (2004) 398–407.
- ⁷⁹ B.M. Choudary, C.R.V. Reddy, B.V. Prakash, B. Bharathi, M.L. Kantam, *J. Mol. Catal. A* 217 (2004) 81–85.
- ⁸⁰ B.M. Choudary, B. Bharathi, C.R.V. Reddy, M.L. Kantam, K.V. Raghavan, *Chem. Commun.* (2001) 1736–1737.
- ⁸¹ L. Li, Y.J. Feng, Y.S. Li, W.R. Zhao, J.L. Shi, *Angew. Chem. Int. Edit.* 48 (2009) 5888–5892.
- ⁸² Y.S.D Yoo, A.A. Bhattacharyya, C.A. Radlowski, J.A. Karch, *Appl. Catal. B* 1 (1992) 169–189.
- ⁸³ A. Corma, A.E. Palomares, F. Rey, *Appl. Catal. B* 4 (1994) 29–43.
- ⁸⁴ H.-S. Shin, M.-J. Kim, S.-Y. Nam, H.-C. Moon, *Water Sci. Techn.* 34 (1996) 161–168.
- ⁸⁵ A. Legrouri, M. Badreddine, A. Barroug, A. de Roy, J.-P. Besse, *J. Mater. Sci. Lett.* 18 (1999) 1077–1079.
- ⁸⁶ M. Lakraimi, A. Legrouri, A. Barroug, A. De Roy, J.P. Besse, *J. Mater. Chem.* 10 (2000) 1007–1011.
- ⁸⁷ J. Olanrewaju, B.L. Newalkar, C. Mancino, S. Komarneni, *Mater. Lett.* 45 (2000) 307–310.
- ⁸⁸ M. Park, C.I. Lee, Y.J. Seo, S.R. Woo, D. Shin, J. Choi, *Environ. Sci. Pollut. Res.* 17 (2010) 203–209.
- ⁸⁹ Y. Seida, Y. Nakano, *Water Res.* 34 (2000) 1487–1494.
- ⁹⁰ T. Yamamoto, T. Kodama, N. Hasegawa, M. Tsuji, Y. Tamaura, *Energy Convers. Manag.* 36 (1995) 637–640.
- ⁹¹ Y. Ding, E. Alpay, *Proc. Safety & Environ. Protect.* 79 (2001) 45–51.
- ⁹² F. Leroux, J.-P. Besse, *Chem. Mater.* 13 (2001) 3507–3515.
- ⁹³ S. O’Leary, D. O’Hare, G. Seeley, *Chem. Commun.* (2002) 1506–1507.
- ⁹⁴ T. Challier, R.C.T. Slade, *J. Mater. Chem.* 4 (1994) 367–371.
- ⁹⁵ N.T. Whilton, P.J. Vickers, S. Mann, *J. Mater. Chem.* 7 (1997) 1623–1629.
- ⁹⁶ G. Camino, A. Maffezzoli, M. Braglia, M. de Lazzaro, M. Zammarano, *Polymer Degrad. Stabil.* 74 (2001) 457–464.
- ⁹⁷ C. Taviot-Guého, F. Leroux, *Struct. Bond.* 119 (2006) 121–159.

-
- ⁹⁸ J. Zhu, P. Yuan, H. He, R. Frost, Q. Tao, W. Shen, T. Bostrom, *J. Coll. Int. Sci.* 319 (2008) 498–504.
- ⁹⁹ A. Khan, D. O'Hare, *J. Mater. Chem.* 12 (2002) 3191–3198.
- ¹⁰⁰ K. Mori, Y. Nakamura, I. Kikuchi, *J. Polymer Sci.: Polymer Lett.* 19 (1981) 623–628.
- ¹⁰¹ A.P. Kumar, D. Depan, N. Singh Tomer, R.P. Singh, *Prog. Polymer Sci.* 34 (2009) 479–515.
- ¹⁰² U. Costantino, V. Ambroggi, M. Nocchetti, L. Perioli, *Mic. Mes. Mater.* 107 (2008) 149–160.
- ¹⁰³ A.I. Khan, A.J. Norquist, D. O'Hare, *Chem. Commun.* 22 (2001) 2342–2343.
- ¹⁰⁴ J.H. Choy, J.Jung, S.J.M. Oh, M. Park, J. Jeong, Y.K. Kang, O.J. Han, *Biomater.* 25 (2004) 3059–3064.
- ¹⁰⁵ J.H. Choy, E.Y. Jung, Y.H. Son, M. Park, *J. Phys. Chem. Solids* 65 (2004) 509–512.
- ¹⁰⁶ J.H. Choy, S.Y. Kwak, J.S. Park, Y. J. Jeong, *J. Mater. Chem.* 11 (2001) 1671–1674.
- ¹⁰⁷ J.H. Choy, S.Y. Kwak, J.S. Park, Y.J. Jeong, J. Portier, *J. Am. Chem. Soc.* 121 (1999) 1399–1400.
- ¹⁰⁸ J.H. Choy, Y.H. Son, *Bull. Korean Chem. Soc.* 25 (2004) 122–126.
- ¹⁰⁹ S.Y. Kwak, W.M. Kriven, M.A. Wallig, J.H. Choy, *Biomater.* 25 (2004) 5995–6001.
- ¹¹⁰ S.H. Hwang, Y.S. Han, J.H. Choy, *Bull. Korean Chem. Soc.* 22 (2001) 1019–1022.
- ¹¹¹ J.H. Yang, S.Y. Lee, Y.S. Han, K.C. Park, J.H. Choy, *Bull. Korean Chem. Soc.* 24 (2003) 499–503.
- ¹¹² M.Z. bin Hussein, Z. Zainal, A.H. Yahaya, D.W.V. Foo, *J. Control. Release* 82 (2002) 417–427.
- ¹¹³ P. Sipos, G. Hefter, P.M. May, *The Analyst* 125 (2000) 955–958.
- ¹¹⁴ P. Sipos, G. Hefter, P.M. May, *J. Chem. Eng. Data* 45 (2000) 613–617.
- ¹¹⁵ S.-H. Yang, A.X. Gray, A.M. Kaiser, B.S. Mun, B.C. Sell, J.B. Kortright, C. S. Fadley, *J. Appl. Phys.* 113 (2013) 073513.
- ¹¹⁶ G. Hahner, *Chem. Soc. Rev.* 35 (2006) 12, 1244–1255.
- ¹¹⁷ M.A. Woo, T.W. Kim, M.-J. Paek, H.-W. Ha, J.-H. Choy, S.-J. Hwang, *J. Solid State Chem.* 184 (2011) 171–176.
- ¹¹⁸ W. Meng, F. Li, D.G. Evans, X. Duan, X., *Mater. Res. Bull.* 39 (2004) 1185–1193.
- ¹¹⁹ D. Evans, R. Slade, *Struct. Bond.* 119 (2006) 1–87.
- ¹²⁰ J. Zhou, Z. P. Xu, S. Qiao, Q. Liu, Y. Xu, G. Qian *J. Hazard. Mater.* 189 (2011) 586–594.
- ¹²¹ F. Millange, R.I. Walton, L.X. Lei, D. O'Hare, *Chem. Mater.* 12 (2000) 1990–1994.
- ¹²² V. Rives, S. Kannan, *J Mater Chem* 10 (2000) 489–495.
- ¹²³ H.C.B. Hansen, C.B. Koch, R.M. Taylor, *J. Solid State Chem.* 113 (1994) 46–53.
- ¹²⁴ G. Hu, D. O'Hare, *D. J. Am. Chem. Soc.* 127 (2005) 17808–17813.
- ¹²⁵ Y. Zubavichus, A. Shaporenko, M. Grunze, M. Zharnikov, *J. Phys. Chem. A* 109 (2005) 6998–7000.
- ¹²⁶ A. Clearfield, M. Kieke, J. Kwan, J.L. Colon, R.C. Wang, *J. Inclusion Phenom. Mol. Recognit. Chem.* 11 (1991) 361–378.
- ¹²⁷ Z.P. Xu, P.S. Braterman, *J. Mater. Chem.* 13 (2003) 268–273.
- ¹²⁸ K. Yamaguchi, K. Mori, T. Mizugaki, K. Ebitani and K. Kaneda, *J. Org. Chem.* 65 (2000) 6897–6903.
- ¹²⁹ F. Wypych, G.A. Bubniak, M. Halma, S. Nakagaki, *J. Coll. Int. Sci.* 264 (2003) 203–207.
- ¹³⁰ M. Gruttadauria, F. Giacalone, R. Noto, *Chem. Soc. Rev.* 37 (2008) 1666–1688.
- ¹³¹ S.-E. Park, E.A. Prasetyanto, *Top. Catal.* 52 (2009) 91–100.

-
- ¹³² C. Aprile, F. Giacalone, M. Gruttadauria, A.M. Marculescu, R. Noto, J.D. Revell, H. Helma Wennemers, *Green Chem.* 9 (2007) 1328–1334.
- ¹³³ E.A. Prasetyanto, S.-C. Lee, S.-M. Jeong, S-E. Park, *Chem. Commun.* (2008) 1995–1997.
- ¹³⁴ Z. An, W. Zhang, H. Shi, J. He, *J. Catal.* 241 (2006) 319–327.
- ¹³⁵ B.M. Choudary, B. Kavita, N.S. Chowdari, B. Sreedhar, M.L. Kantam, *Catal. Lett.* 78. (2002) 373–377.
- ¹³⁶ R. Bruckner, In: *Harmata M (ed) Organic reaction mechanisms. Reactions, stereo-chemistry and synthesis.* Springer-Verlag, Berlin, 2010, p. 530.

MAGYAR NYELVŰ ÖSSZEFOGLALÓ (HUNGARIAN SUMMARY)

A réteges kettős hidroxidok (LDH-k) anioncserélő tulajdonságuknak köszönhetően különleges csoportot alkotnak a réteges szerkezetű anyagok között. A nagyszámú kationcserélő anyaggal szemben az anioncserélő ásványok ritkábban fordulnak elő. A réteges kettős hidroxidok alapképviselője a hidrotalcit, amely $\text{Mg}(\text{OH})_2$ (brucit) alapú. Itt a $\text{Mg}(\text{II})$ -ionok egy részét $\text{Al}(\text{III})$ -ionok helyettesítik. A réteg szerkezete ettől nem sérül, de pozitív töltésű lesz. Ezt a rétegek között elhelyezkedő (interkalált), teljesen vagy részlegesen hidratált egyszerű anionok kompenzálják.

Munkám során hidrotalcit- (MgFe) és hidrokalamit- (CaFe) típusú réteges kettős hidroxidok szintézisét optimalizáltam, az együttes lecsapás módszerét alkalmazva. Az előállított anyagok szerkezetvizsgálatát (por)röntgendiffraktometria (XRD), Mössbauer spektroszkópia, röntgenabszorpciós spektroszkópia (XAS), termogravimetria (TG/DTG), induktív csatolású plazma optikai emissziós spektrometria (ICP-OES), infravörös spektroszkópia (FTIR), pásztázó elektronmikroszkópia (SEM), energiadiszperzív fluoreszcenciás mikroanalízis (EDX) és transzmissziós elektronmikroszkópia (TEM) segítségével végeztem el. Az előállított LDH-k röntgendiffraktogramjai igazolták a réteges szerkezetet, és lehtëvé tették a rácsparaméterek meghatározását. Az optimális szintéziskörülmények kialakításakor fontos szempont volt az, hogyha a réteges kettős hidroxidok anioncserélő tulajdonságának kihasználása a cél, a szintézist N_2 atmoszféra alatt kell végrehajtani, és a pH növeléséhez használt NaOH koncentrációjának 3 M alatt kell lennie. Azt találtam, hogy a $\text{Ca}(\text{II}) : \text{Fe}(\text{III})$ arány növelésével a $\text{Ca}(\text{OH})_2$ mennyisége közel lineárisan nő 0 tömeg%-ról ~60 tömeg%.-ig. Ezzel egyidejűleg az anyagok stabilitása is növekszik – a melléktermékektől mentes hidrokalamit szerkezetű LDH ($\text{Ca}(\text{II}) : \text{Fe}(\text{III}) = 2$) a legkevésbé stabilis. Az ^{57}Fe Mössbauer spektroszkópiás mérések szerint a $\text{Fe}(\text{III})$ nagyspinű, némileg torzult oktaéderes környezetben van mind a CaFe -, mind a MgFe -LDH esetén az összes kiindulási fémarány esetén.

A rétegvastagságot, ami elengedhetetlen a térbeli elrendeződés megadásához, a TEM dark-field felvételekből becsültem meg. A kapott 0.2 nm jó egyezést mutat az irodalomban megtalálható, nagyfelbontású XRD-ből nyert 0.178 nm-rel.

A N-tartalmú heterociklusos karboxilsavak interkalálása a dehidratációs-rehidratációs módszerrel történt, ami lényegében abból áll, hogy a kiindulási Ca_3Fe -LDH-t 500 °C-on, N_2 atmoszférában 5 órán keresztül hőkezeljük, ezáltal a szerkezet összeomlik és egy sok hibahellyel rendelkező keverék fémoxid jön létre. Ezt (N_2 atmoszférában) enyhén lúgos, az

aniont is tartalmazó aceton/víz ill. etanol/víz elegyben kevertetjük, ezáltal a szerkezet az LDH tulajdonságainak köszönhetően visszaáll, közben pedig az interkaláció is lejátszódik. Az így előállított szerves-szervetlen hibrid anyagok szerkezetét és morfológiáját a már felsorolt vizsgálati módszerekkel jellemeztem, kiegészítve UV-Vis spektroszkópiás mérésekkel és molekulamodellezéssel. A szintézis során használt oldószerkelegy az interkaláció módját nagymértékben befolyásolta. Az interkalált anionok az oldószerrel függően eltérő térbeli elrendezésben épültek be a rétegek közé. Az interkalált anionok méretét a PM3 szemiempirikus kvantumkémiai módszerrel számolt paralelepipedonok dimenziójából számoltam ki. Mindezek alapján közelítő becslés tehető az anionok térbeli elhelyezkedését illetően a rétegek között. Az etanol:H₂O:NaOH és az aceton:H₂O:NaOH oldószerkelegyek lehetővé tették a N-tartalmú aromás, részlegesen vagy teljesen telített heterociklusok interkalálását vízszintes vagy függőleges elrendezésben a rétegekhez képest, megőrizve a réteges kettős hidroxid szerkezetét.

Az utóbbi időben a kémiai iparágak érdeklődése egyre nagyobb mértékben fordult a környezetbarát, heterogén katalízist alkalmazó folyamatok felé. Továbbra is különösen nagy kihívást jelent aktív szilárdfázisú Brønsted-típusú bázisos katalizátorok kifejlesztése, melyek jó szelektivitással katalizálják a C–C kötések kialakulását, például aldehidek és ketonok közötti kondenzációs reakciókban, melyeket a gyógyszeripari alapanyagok és a finomkémikáliák gyártása során használnak. A hőkezelés nélküli CaFe-LDH-k hatékony katalizátornak bizonyultak egy epoxidációs reakcióban – sokkal aktívabbak voltak, mint a kalcinált származékok. A 2-ciklohexén-1-on epoxidációja végbement hőkezelés nélküli CaFe-LDH-katalizátoron, különböző oldószerkelegyekben (formamid, n-hexán, ciklohexén, metanol, etanol, 2-metil-2-propanol, aceton és 1,4-dioxan) és hőmérsékleteken. A legjobb eredményeket formamidban és 313 K-en értem el, de a reakció jó aktivitással ment n-hexánban, ciklohexénben és metanolban is. A hőkezelés nélküli MgAl-hidrotalcit, MgFe-hidrotalcit és CaAl-hidrokalumit kevésbé volt aktív, mint a CaFe-hidrokalumit, de jobb katalizátornak bizonyultak a hőkezelt származékoknál (kevert fém-oxidok) vagy egyéb fém-oxidoknál, pl. titándioxidnál.

Az L-prolint már évek óta használják, mint királis organokatalizátort szerves kémiai reakciókban C–C kötések létrehozására. Sikeresen alkalmazták aszimmetrikus intermolekuláris aldol dimerizáció katalizátoraként sokféle keton és aldehid esetében, jó hozamokat és nagy enantioszelektivitást elérve. Sok figyelmet szenteltek a katalizátor immobilizálására, amivel egyrészt ezzel könnyítjük a reakcióelegy feldolgozását, másrészt a katalizátor visszanyeré-

sével és újraalkalmazásával kevésbé terheljük a környezetet. Kovalens kötésen keresztül funkcionizált szilikagél állítható elő N- vagy C-védett L-prolin immobilizálásával klórpropilezett szilikagél felületére. A védőcsoportok eltávolítása után csak a C-terminálison keresztül kötött L-prolin mutatott katalitikus aktivitást az acetone és 2-nitrobenzaldehyde közötti aldol dimerizációs reakcióban, kiváló szelektivitással, de enantioszelektivitás nélkül, illetve a benzaldehyddel kis konverzió mellett, de elfogadható szelektivitás, enantioszelektivitás értékekkel. A kereskedelmi forgalomban kapható polisztirolon kötött L-prolinol hasonló reakciókban, változatos aldehidekkel dimereket eredményezett közepes enantioszelektivitás értékekkel. Mindezek alapján megállapítottam, hogy a kovalensen immobilizált N-tartalmú heterociklusok szekunder nitrogénjének szabadnak kell maradnia a katalitikus aktivitás biztosításához.

Az eddig felsorolt eredmények egyértelműen igazolják a réteges kettős hidroxidok sokoldalúságát. Különböző szerves anionokkal funkcionizálhatók, és a sokféle területen alkalmazhatók, többek között finomvegyipari reakciók katalizátoraként.

ACKNOWLEDGEMENT

Firstly, let me gratefully acknowledge the immense support and help of Drs István Pálinkó and Pál Sipos. My grateful thanks go to them for both the theoretical and practical encouragement and teaching that I have received from them during the years I have spent in their unique research group.

Let me also gratefully acknowledge the efforts of Dr. Ernő Kuzmann for his valuable insights and suggestions regarding Mössbauer spectroscopy. I wish to express my sincere thanks to Dr. Gábor Peintler for his detailed review and excellent advices during the preparation of this thesis. Many thanks are due, too, to all members of the Material and Solution Structure Research Group.

I thank to all who helped me in any aspects in- and outside of the University of Szeged.

Many thanks to my family and friends for the tremendous support they gave me in the last years. Finally, I would like to acknowledge the most important person in my life – my husband. He has been a constant source of strength and inspiration.